HOKKAIDO UNIVERSITY

| | |
|---|---|
| Title | Study on a practical frost heave estimation with a combined thermal-hydraulic and mechanical simulation |
| Author(s) | 鄭, 好 |
| Degree Grantor | 北海道大学 |
| Degree Name | 博士(工学) |
| Dissertation Number | 甲第11617号 |
| Issue Date | 2014-12-25 |
| DOI | https://doi.org/10.14943/doctoral.k11617 |
| Doc URL | https://hdl.handle.net/2115/57722 |
| Type | doctoral thesis |
| File Information | Zheng_Hao.pdf |

Hokkaido University Collection of Scholarly and Academic Papers : HUSCAP

# STUDY ON A PRACTICAL FROST HEAVE ESTIMATION WITH A COMBINED THERMAL-HYDRAULIC AND MECHANICAL SIMULATION

# 温度・流体および力学連成シミュレーションによる実用的な凍上評価法に関する研究

**Hao ZHENG**

A thesis submitted in partial fulfilment of the requirements for the degree of Doctor of Engineering

Examination Committee: Prof Shunji KANIE
Prof Hiroshi YOKOTA
Prof Tatsuya ISHIKAWA

Doctoral Thesis No. EG-M…
Division of Engineering and Policy for Sustainable Environment
Graduate School of Engineering, Hokkaido University
December 25.

# Acknowledgements

I would like to take this chance to express my sincere gratitude to my supervisors, Professor Shunji KANIE, for his patience, guidance and help for my study and life in Japan. And in this five years, I learn from KANIE Sensei both knowledge and thinking methods. Sensei teaches me how to behave methodically and logically for a complicated task with optimistic attitude. And I believe that this will benefit me for a lifetime. His personal charisma does affect my opinions and ideas too. Sensei sets a good example for me to learn. In fact, I imitate Sensei's behaviors unconsciously. I believe that this five years' experience will affect my life deeply and forever.

I want to extend special thanks to Professor Satoshi AKAGAWA. During my research, Sensei always is ready to discuss with me and provide good suggestions based on his extensive experience in frost heave. AKAGAWA Sensei and I went to Russia for a conference and field trip together. During that half month, I learned industry, endurance and gentleman from Sensei. In addition, I really appreciate that AKAGAWA Sensei taught me so much in his frost heave experiment. In that time I realize my weakness and what is the right attitude for research.

For Professor MIKAMI and SATO Sensei, thanks for their help for my graduation. SATO Sensei is really a nice Sensei who is always smiling. He taught me how to ski in NISEKO, however I was so stupid and rolled down the slope. My scream could be heard all over the ski resort. I am really for that.

Also thanks go to Dr. Werawan, Mifue san, Yuki san Natalya san and KAWAMURA san. They are the persons who help me to deal with the complicated procedures and support me for the campus life. I really appreciate Dr. Werawan who supported me when I am in E cube. Before I came to here, I sent a lot of Emails to disturb Werawan Sensei and asked numerous questions. Thanks for your patience for me. Without your help, I cannot image what my life would be. And I will remember the joys and happiness from E cube, the big family for all international students.

I am very grateful of my classmates, Yokoi san, Nakano san, Makimura san and Takahashi san, for their instant help for my laboratory life. And also Mr. Fukugawa and Mr. Gochou, thanks for their sincere help in my master course. Here, thanks for all laboratory members. You make my life in Japan colorful and meaningful. I will never forget.

Thanks for my parents and my wife who are always behind me and encourage me in this five years.

At last I want to say, it has been a great experience to study in Hokkaido University. I enjoy the beautiful campus and love the nice people here. This five year's study will be the most precious memory of my life. THANKS.

# Abstract

For the developing of cold regions, frost heave related issues are critical challenges to engineers. The objective of this research is to build a numerical model of frost heave estimation in order to solve the engineering issues in cold areas. With such purpose, this model is designed to achieve the following requirements: with this model, thermal analysis, hydraulic analysis and mechanical analysis are supposed to be considered simultaneously. Only with such comprehensive analysis, frost heave and its related issues could be discussed, evaluated and predicted properly, such as the frozen and thawing area estimation, the amount of frost heave and thermal erosion brought by water flow, frost heave stress and other issues. Further, this model should be simple and practical enough. Parameters used in this model can be easily available and there are some standard regulations for these parameters. It should be easy to understand and apply. Only satisfied with such requirements, this model could be applied in engineering conveniently and widely. These ideas are the fundamental principles obeyed throughout this paper.

In the first chapter, the research significance of frost heave is explained. As the population increases continually and the high energy consumption life style, the demand for energy would increase further. Under such background, the developing of cold regions is an urgent task for more energy and other resources. Therefore, the frost heave related issues which are the most serious engineering obstacle in cold region development attract our attentions.

In the second chapter, frost heave research history is reviewed and summarized. Various theories have been proposed in the research history of frost heave in order to explain the mechanism of frost heave process in detail. These theories provides us a better understanding of frost heave, however there are still some obscure points that cannot be explained clearly at the current stage. Several outstanding theories and famous large scale experiment are introduced in this chapter. Without a perfect theoretical method, we adopt a widely accepted and well-performed practical equation, Takashi's equation, to predict frost heave ratio in this study.

As freezing rate is required by Takashi's equation, in the third chapter, thermal analysis is explained in detail. The derivations of heat transfer equation with and without convection are provided. In addition, Equivalent Heat Capacity Method is adopted to evaluate the latent heat influence caused by phase change. Freezing rate and direction are carefully discussed based on the thermal analysis result. Further the author also presents some basic skills of Finite Element Method used in this paper and its related issues. Based on this thermal analysis section, the author provides some simple examples to verify the transfer calculation and latent heat influence which can prove the reliability of this calculation program.

Constraining stress, the other parameter that Takashi's equation needs, is provided by the fourth chapter. In this section, the mechanical analysis is described from the basic governing equation. Meanwhile, the mechanical analysis combines the frost heave ratio calculated by Takashi's equation. The main purpose of mechanical analysis is: first, calculate the constraining stress in freezing direction; second, evaluate the stress influence brought by frost heave. Until now, the basic frost heave prediction model has been built and then experiment comparison is provided to confirm the simulation accuracy of our model. Comparison result indicates that our basic frost heave estimation model can predict frost heave amount with a satisfied accuracy and this model can be applied for real engineering. In addition, concerning the 3D frost heave, a preliminary study of a 3D frost heave experiment is introduced which is aiming to improve the existing Takashi's equation into 3D situation and then a temporary 3D frost heave equation is proposed.

Since soil mechanical property changes drastically as the stress and temperature condition varies. Nonlinear property of unfrozen soil is introduced in the fifth chapter. We adopt Duncan and Chang's equation to expresses the relationship between Young's modulus of unfrozen soil and differential stress. For frozen soil, the strength is dominated by temperature. However, for simplification, we assume a constant value for frozen soil Young's modulus. After adding this supplement to mechanical analysis, the nonlinear influence to frost heave and stress is evaluated by comparisons between elastic and nonlinear examples.

In the sixth chapter, thermal influence brought by water flow and unsaturated frost heave are discussed. According to this purpose, water flow governing equation considering both saturated and unsaturated conditions is derived. Then empirical equations for specific capacity of soil and pressure dependent water content are introduced. Further we assume that the unsaturated hydraulic conductivity for unfrozen soil is related to water pressure. For frozen situation, we assume this value to be zero to represent the low hydraulic conductivity. Based on this hydraulic analysis, simple example is used to verify our calculation first and then examples are provided to state the unsaturated frost heave and thermal influence brought by water flow.

Finally, in the conclusion chapter (chapter 7), some useful conclusions are presented and this practical numerical model is demonstrated to be reliable and promising. At the same time, the author also points out the future research directions which can enhance and improve this practical frost heave estimation model.

And compared with the existing model, our thermal-hydraulic and mechanical model based on Takashi's equation owns the following advantages: first, comparing to the segregation potential model, Takashi's model has some strong points. For example, Takashi's equation takes the freezing rate which is a very critical parameter in the evaluation of frost heave into account, however, segregation

potential method dose not; for the parameters used in Takashi's equation, there are a series of standard tests regulated by the Japanese Geotechnical Society which can guarantee the uniformity and reliability of this model. Second, comparing to the existing model which also adopted Takashi's equation our model takes the water flow process into consideration during unfrozen situation. Meanwhile, water content is also evaluated by empirical formula. Such analyses are the basic foundations for further research of thawing settlement estimation. We believe that our model is a significant improvement to the existing numerical models.

# TABLE OF CONTENTS

**1. INTRODUCTION ..... 1**

1.1 THE BACKGROUND OF STUDY ..... 1

1.2 RESEARCH AIM ..... 4

**2. THE BACKGROUDN OF FROST HEAVE ..... 7**

2.1 THE MECHANISM OF FROST HEAVE ..... 7

2.2 LITERATURE SURVEY ..... 8

*2.2.1 Taber, Stephen ..... 9*

*2.2.2 Beskow, Gunnar. ..... 9*

*2.2.3 The Generalized Clausius–Clapeyron Equation ..... 10*

*2.2.4 The Capillary Theory (Primarily Frost Heave) ..... 14*

*2.2.5 Frozen Fringe Models ..... 15*

2.3 EXPERIMENTAL METHODS ..... 17

*2.3.1 Segregation Potential Method ..... 17*

*2.3.2 Takashi's Model ..... 19*

2.4 LARGE SIZE FROST HEAVE TEST ..... 27

*2.4.1 The Calgary Frost Heave Test ..... 27*

*2.4.2 The First Fairbanks Frost Heave Test ..... 30*

*2.4.3 The Caen Frost Heave Test ..... 32*

*2.4.4 The Second Fairbanks Frost Heave Test ..... 33*

**3. THERMAL ANALYSIS ISSUES ..... 36**

3.1 HEAT TRANSFER (WITHOUT WATER FLOW) ..... 36

*3.1.1 The Application of FEM to Heat Transfer Equation ..... 38*

*3.1.2 The Application of Numerical Integration ..... 42*

*3.1.3 Finite Difference Method for Time Domain ..... 44*

3.2 HEAT TRANSFER WITH CONVECTION (WITH WATER FLOW) ..... 46

3.3 INFLUENCE OF LATENT HEAT ..... 48

3.4 FREEZING DIRECTION AND RATE ..... 49

3.5 VALIDATION EXAMPLES ..... 51

**4. MECHANICAL ANALYSIS ..... 55**

4.1 2D EQUILIBRIUM EQUATION ..... 55

4.2 THE APPLICATION OF FEM TO MECHANICAL ANALYSIS ..... 56

4.3 FROST HEAVE AMOUNT VALIDATION ..... 62

4.4 THREE-DIMENSIONAL FROST HEAVE ESTIMATION ..... 66

*4.4.1 VOLUMETRIC CHANGE DUE TO FROST HEAVE ..... 68*

**5. THE NONLINEAR PROPERTY OF UNFROZEN SOIL ..... 75**

5.1 NONLINEAR PROPERTY ASSUMPTIONS ..... 75

5.2 DISCUSSION OF NONLINEAR INFLUENCE ..... 80

*5.2.1 1D Nonlinear Example ..... 80*

*5.2.2 2D Nonlinear Example ..... 82*

*5.2.3 2D Application Nonlinear Example ..... 86*

**6. HYDRAULIC ANALYSIS ..... 93**

6.1 GOVERNING EQUATION OF WATER FLOW ..... 93

6.2 THE APPLICATION OF FEM TO WATER FLOW EQUATION ..... 96

6.3 DISCUSSION OF HYDRAULIC INFLUENCE ..... 99

*6.3.1 Validation Examples ..... 99*

*6.3.2 Influence of Hydraulic Condition ..... 104*

*6.3.3 Influence of Water Flow ..... 108*

*6.3.4 Sewage Tank Example ..... 111*

**7. CONCLUSIONS ..... 114**

# 1. INTRODUCTION

In this section, the research significance of frost heave is explained. As the population increases continually and the high energy consumption life style, the demand for energy would increase further. Under such background, the developing of cold regions is an urgent task for more energy and other resources. Therefore, the frost heave related issues which are the most serious engineering obstacle in cold region development attract our attentions.

## 1.1 THE BACKGROUND OF STUDY

Before the real story, let us review the history of energy consumption (Figure 1-1), a terrible fact could not be ignored: we consume energy too much and too fast. As the population increases continually and the high energy consumption life style, the demand for energy would increase even further. One urgent and critical issue for human being in the following 50 years is that where we can find enough energy to feed our greed. Referred to the population density map (Figure 1-2), we can find that only the arctic area covered by permafrost and deep oceans are still uncultured and has the ability of providing adequate space, food and energy for human. If we turn our eyes to the vast universe, the out space may also provide us energy and space for live. It even can provide us a new planet. However, it requires a high technology and long time. Thus, the promising locations for huge amount of energy are arctic area, deep oceans and out space. Only such uncultured places may provide enough space and energy for the crazy consumption of human. However, compared with the oceans and out space, the development of arctic area is the most promising and practical option for us in the near 50 years due to the low cost of transportation and requirement for technology. To the development of deep oceans and out space, the cost performance is really low and the requirement of technology is extremely high.

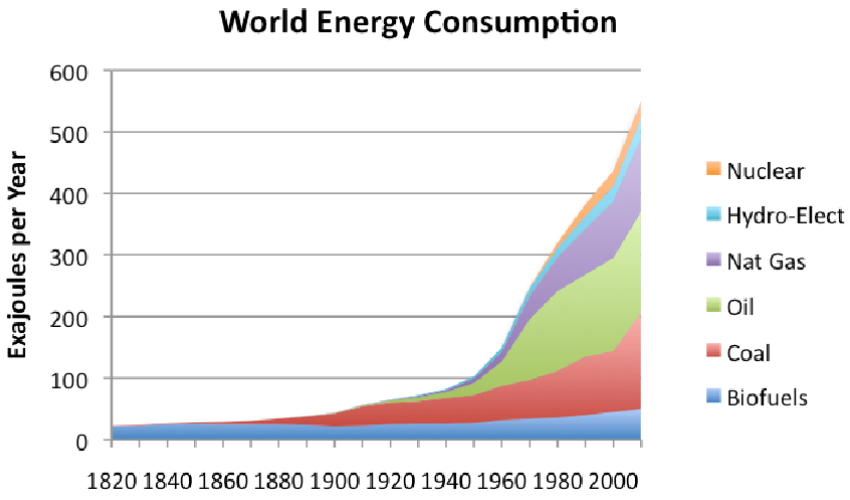



Figure 1-1 World energy consumption history

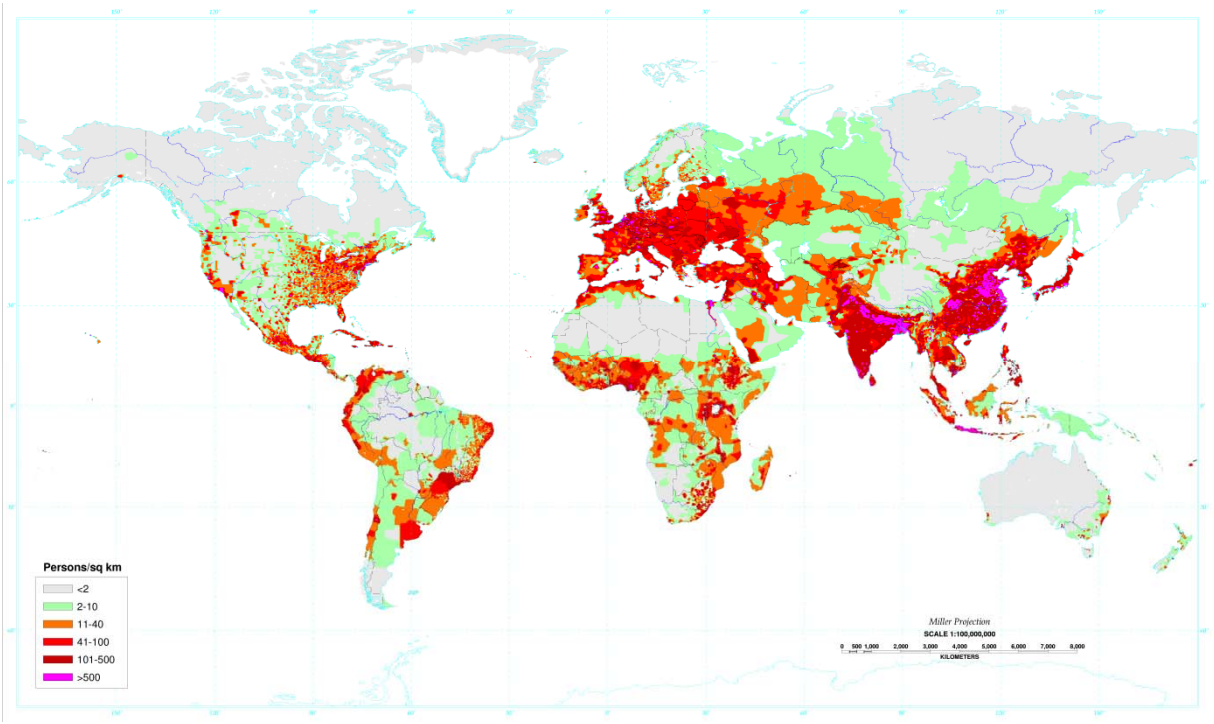



Figure 1-2 Population density (people per $km^2$) map of the world in 1994.

Compared with deep oceans and out space, the development of arctic area covered by permafrost is the easiest option. However, that does not mean there is no obstacle for the exploit of arctic zone. One of the main issues when we are planning to exploit the resources in cold regions, is the basic civil engineering problem caused by frost heave, such as the uneven heave to highway, airport; the damage to the gas or oil pipeline, the thawing of permafrost. Based on such background, the basic objective of this paper, is aiming to solve the frost heave and its related issues in cold regions by numerical simulations. As the foundation, we need an analysis model that includes all issues to evaluate the frost heave related situations and then by this model, try to solve the problems met in the civil infrastructures in cold regions.



Figure 1-3 The damaged building by differential thawing settlement in cold regions



Figure 1-4 The subsidence pool caused by thawing

On the other hand, frost heave related issues do not only occurs in the cold regions. As the urban constructions, freezing technology and its related issues are the new challenges to engineers. Many underground excavations such as those for subway tunnels, pump pits, and tunnels near or below lakes

or rivers, are difficult to conduct because flow-sand and water seepage frequently occur and shields cannot easily be constructed. For these diverse geotechnical construction problems, ground freezing technology is effective because it can address seepage problems as well as improve the strength of the soil. However, ground freezing may also cause some serious compressing pressure to affect the surrounding structures. Changing of the stress field and frost heave caused by freezing technology have to be evaluated carefully before construction.

Ground freezing, both in cold regions and urban areas, may be an effective technology, but owing to frost heave-related concerns, it may also be a serious challenge to structures. Therefore, predicting and controlling frost heave and stress caused by freezing are critical challenges for engineering construction in these fields.

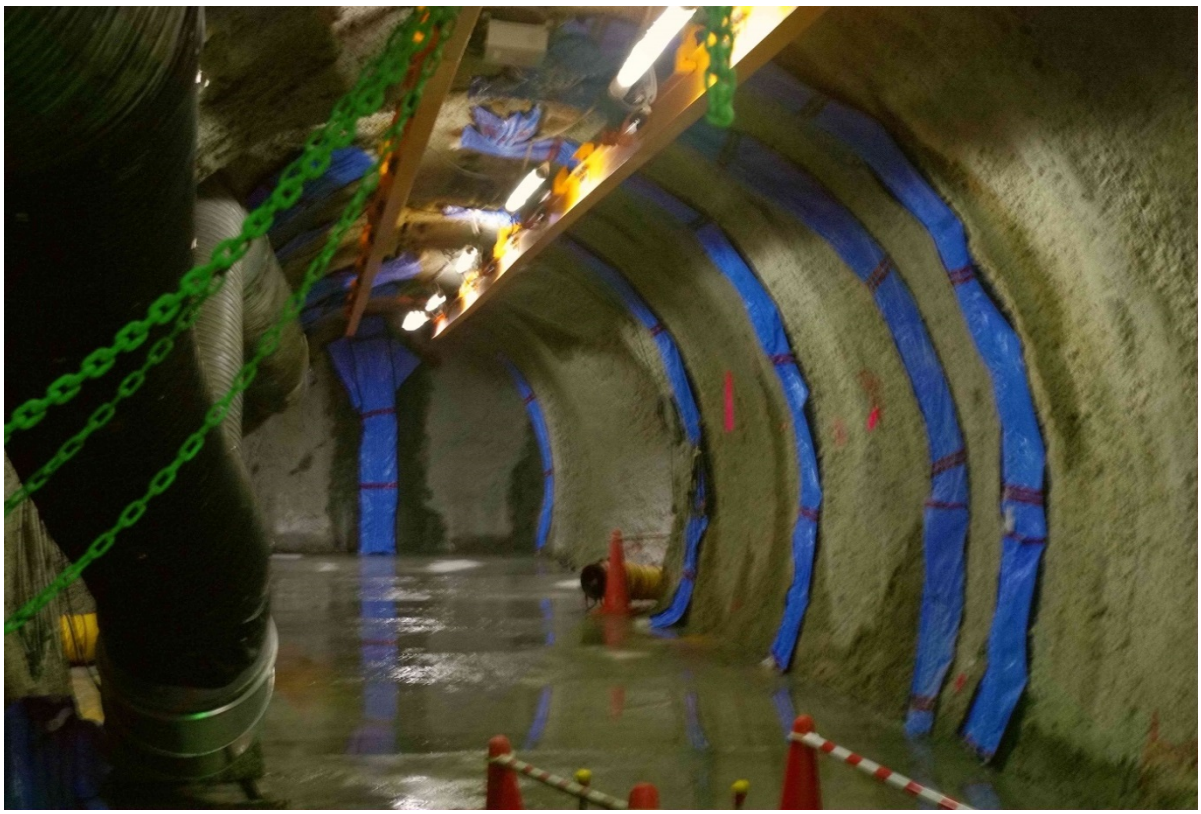


Figure 1-5 The underground tunnels

## 1.2 RESEARCH AIM

In this research, our ultimate aim it to build a complete and comprehensive model to estimate the frost heave and its related issues. With this purpose, a wide literature survey is made in order to find an approving theory. Based on this survey, a one-dimensional frost heave model is adopted as the theoretical foundation to estimate the frost heave ratio. Further, thermal hydraulic and mechanical

analysis are also combined together to provide adequate information for analysis. We believe that such comprehensive model is necessary and only after such model is built, more detail and examples in cold regions could be discussed.

In this research, Takashi's equation is adopted as the theory foundation to predict frost heave ratio. This equation compared to other models, own some inherent merits. It is a practical equation applied widely in Japan and performs well. Further, this equation is very simple and the parameters used for this equation are easily obtained according to the Japanese Geotechnical Society (JGS) regulated experiments. Therefore, Takashi's equation is adopted as the theoretical foundation of this model.

In addition, the interactions among thermal, hydraulic and mechanical analysis are considered in this research because the following aspects: for example, freezing and thawing depth; frost heave amount and stress distribution; and water head and content are supposed to be considered in this model. Meanwhile, freezing range affects the water flow and content; water content influences the latent heat and frost heave amount, and further frost heave amount will impact the stress distribution. All these interactions should be considered simultaneously. Furthermore, concerning the mechanical analysis process, nonlinear property of unfrozen soil is evaluated by Duncan and Chang's equation. This equation describes the relationship between Young's modulus of unfrozen soil and differential stress, which is convenient for numerical application. The structure of this research could be understood by Figure 1-6.

At the same time, three-dimensional frost heave estimation model is discussed. We are planning to propose an original three-dimensional equation to calculate the frost heave ratio. At this stage, one preliminary 3D equation is advanced based on the limited 3D indoor frost heave test. However, better experiment is necessary for a good equation.

Another aim of this paper is to evaluate the possibility for thawing settlement. In this research, the water flow during unfrozen situation is calculated. And this is one option for the thawing settlement estimation. The other one is practical equation similar with Takashi's equation to predict thawing settlement ratio. Further research is desired before the final decision.

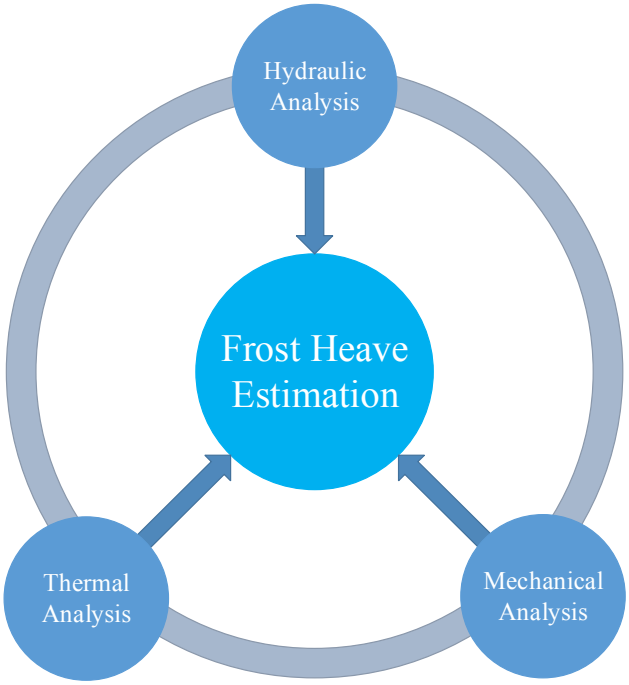



Figure 1-6 The framework of thermal-hydraulic-mechanical frost heave model

## 2. THE BACKGROUDN OF FROST HEAVE

In this chapter, frost heave research history is reviewed and summarized. Various theories have been proposed in the research history of frost heave in order to explain the mechanism of frost heave process in detail. These theories provides us a better understanding of frost heave, however there are still some obscure points that cannot be explained clearly at the current stage. Several outstanding theories and famous large scale experiment are introduced in this chapter.

### 2.1 THE MECHANISM OF FROST HEAVE

Frost heave phenomenon widely occurs in cold regions. From the formation mechanism, frost heave is caused by a volume expansion of soil during freezing conditions when water contained in the soil becomes ice. As widely known, when water becomes ice, there is a 9% volume expansion with a density deduction. Further, for a continuous formation of frost heave, water supply is required that delivers water to the freezing front via capillary action in certain soils or through the unfrozen water adsorbed by the soil particles. If continuous water supply is guaranteed, frost heave may occurs continuously and the amount of heave maybe several meters (Figure 2-1). Take Pingo as an example, which is also called as hydrolaccolith, can reach up to 70 meters in height and up to 600 meters in diameter. This huge size is attributed to the continuous water supply to the freezing front.



Figure 2-1 Pingo in cold regions (Pingo is formed by ice core)

Except the water supply, there are still several factors that affect frost heave process. First, the soil

itself which is referred to as "frost susceptible" through which water passes to feed the formation of ice lenses must be sufficiently porous to allow capillary action, yet not so porous as to break capillary continuity. That means the soil particle could not be too large. Sand and gravel never produce a frost heave. And the growth of ice lenses continually consumes the rising water transferred to the freezing front.

Second, the freezing rate, which is defined as the speed of advancement of the freezing line into the unfrozen soil portion [1], influences the amount of frost heave. Usually, the slower the freezing rate is, the larger frost heave amount is. This can be simply explained by that: a slower freezing rate can provide adequate time for extra water to migrate into the freezing front for further ice lenses formation. If frost susceptible soil was frozen in a very short period which means a fast freezing rate, there may be not enough time for water flowing into the freezing front. Therefore, the amount of frost heave will be limited due to water lack.

Third, constraining stress in the freezing direction also affects the amount of frost heave. Take the weightlift as an example; we assume that someone wants to uplift a 100 kg box. Of course, a 200 kg box will be harder than that of 100 kg. Similar thing occurs for the frost heave process, larger constraining stress in frost heave direction would result in a smaller frost heave. To be more serious, a large constraining stress could also reduce or prevent the water flow into the freezing front, meanwhile provides a larger constraint and initial settlement. On the other hand, a larger stress may also broke the soil structures and then destroy the water migration route. Therefore, it is conjectured that there is a stress that can prevent the appearance of frost heave phenomenon.

According to the influence factors of frost heave mentioned above, usually, the following points should be taken into account when frost heave is estimated: soil porosity, freezing rate and constraining stress. Only such influences are taken into account, we can predict frost heave amount reasonably and then, further, aiming to prevent the presence of frost heave appropriately.

## 2.2 LITERATURE SURVEY

Frost heave may have been noted by human a long time ago. However, attentions from the scientists and engineers and then treated it as research topic is not a long period. In this section, the author tries to summarize the research history of frost heave and introduce various theories proposed by numerous researchers in this field in order to provide a clear and instructional foundation for further research.

In 1920, G.J. Bouyoucos observed that water contained in soils would not all freeze at the same temperature [2]. And as mostly mentioned, Taber and Beskow are the pioneers who thought clearly about the process of frost heave and conducted appropriate experiments, although, there were a few papers discussing frost heave published before them. Without any exaggeration, Taber and Beskow

proposed the reasonable explanations for frost heave phenomenon first time and then pointed out a right direction for further and deep research of frost heave. After Taber and Beskow, numerous scientists and engineers devoted themselves into the research of frost heave. The first boom of frost heave research occurred during the 1970-1980 periods. The direct reason for this boom of frost heave research was the great interests in arctic energy due to the first worldwide Oil Crisis. Several new theories were proposed in order to explain the specific phenomenon during frost heave process. In addition, with the development of modern computer, various numerical models based on different theories were advanced. At the same time, large size and long period frost heave experiments had been done in order to obverse and uncover the process of frost heave and then validate the existing theories. After 2000, there is also one large size and long term frost heave experiment. This experiment was founded by JTST and cooperated with University of Alaska Fairbanks (UAF) which was also the experiment location. In the following section, the author summarizes the research history of frost heave and several theories will be introduced briefly.

### 2.2.1 Taber, Stephen.

Taber is the person who discovered the basic mechanism of frost heave first time. Taber completely discredited the general assumption that frost heave was caused by expansion of in-situ freezing water and pointed the right direction for further research. He demonstrated that benzene or nitrobenzene in a porous medium could also cause frost expansion experimentally. This implied the fact that frost heave was caused by water migration, not only in-situ expansion, because benzene at low temperature shrinks rather than expand.

In addition, Taber confirmed that the main factors controlling segregation and excessive heaving are: size of soil particle, amount of water available, size and percentage of voids, and rate of cooling.

Experiments have shown that freezing tends to concentrate water near the surface, and that segregation is accentuated by a high water-content. Therefore, prompt refreezing after thawing should result in greater segregation than on the first freezing. This conclusion was confirmed by thawing and refreezing clays which contained too little water to form ice layers on the first freezing by Taber [2] [3].

### 2.2.2 Beskow, Gunnar.

Beskow (1935) reinforced and improved Taber's works further. He proposed that the process of soil freezing is very similar to the soil drying process due to phase change of water. Thus, water flow from above the water table to the zone where water is changing into ice is analogous to flow of water to a zone where it is evaporating. This deduction provided a novel method to consider the frost mechanism. In addition, Beskow also noted that the freezing point of soil water depresses due to solutes in water

and fine soil particles. He constructed freezing temperature curves, showing unfrozen water content vs. temperature and noted that, for saturated fine-grained soils, even the water in the center of the pores is considerably influenced by the particle surface. In addition, Beskow documented the influence of effective stress on frost heave. He argued that the total compressive force acting on soil particles during freezing was the sum of the actual load (overburden) pressure and the positive capillary pressure (soil moisture tension). He also noted that when the capillary rise of water in the soil is lower than the distance between the freezing front and the groundwater table, then the soil does not heave [2] [4].

Taber and Beskow may do not realize how important their works are, however, we should understand that they are the person who opened a new door for frost heave research.

### 2.2.3 The Generalized Clausius–Clapeyron Equation

The Clausius–Clapeyron equation, named after Rudolf Clausius and Benoît Paul Émile Clapeyron, who defined it sometime after 1834, is a way of characterizing a discontinuous phase transition between two phases of matter of a single constituent. After that in 1943, Edlefsen and Anderson [5] advanced the Generalized Clausius–Clapeyron Equation (GCCE) in order to describe complicated process occurred during freezing. It provided theoretical support for the understanding of the driving force of heave and after that this GCCE have been widely applied in the quantitative analysis of frost heave. In the following, this equation will be explained.

Here we assume a static water-ice coexist system, which means that this system is closed and water do not migrate. The free energy of water and ice should be the same due to the static phase equilibrium:

$$f_w = f_i \tag{2-1}$$

Here $f_w$ and $f_i$ are the water free energy and ice free energy respectively.

And in this system, if there is some small change, the water and ice should have the change amount of Gibbs free energy:

$$\Delta f_w = \Delta f_i \tag{2-2}$$

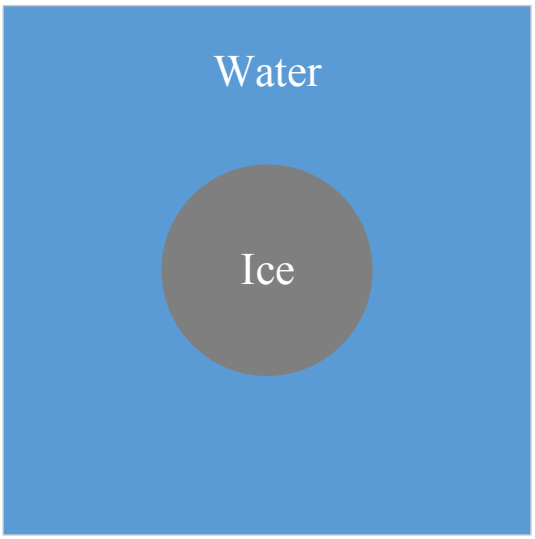



Figure 2-2 Water and ice system

And according to the definition of Gibbs free energy, the following equation could be obtained:

$$\Delta f = V\Delta P - S\Delta T - \Delta W_m \tag{2-3}$$

Here $W_{\mathrm{m}}$ means the internal energy and $V$ is the specific volume and $S$ is the entropy, $T$ is temperature. For the ice and water system, the change of Gibbs free energy is caused by pressure $P$ and temperature $T$. Substitute Equation (2-3) into Equation (2-2), we can get the following equation:

$$V_w\Delta P - S_w\Delta T = V_i\Delta P - S_i\Delta T \tag{2-4}$$

Where suffix $i$ and $w$ mean the ice and water status respectively. Equation (2-4) could be rewritten as:

$$\frac{\Delta P}{\Delta T} - - = \frac{S_w - S_i}{V_w - V_i} = \frac{L_w}{T\Delta V} \tag{2-5}$$

Here we assume that:

$$S_w - S_i = \frac{L_w}{T} \tag{2-6}$$

$L_w$ is the latent heat of water.

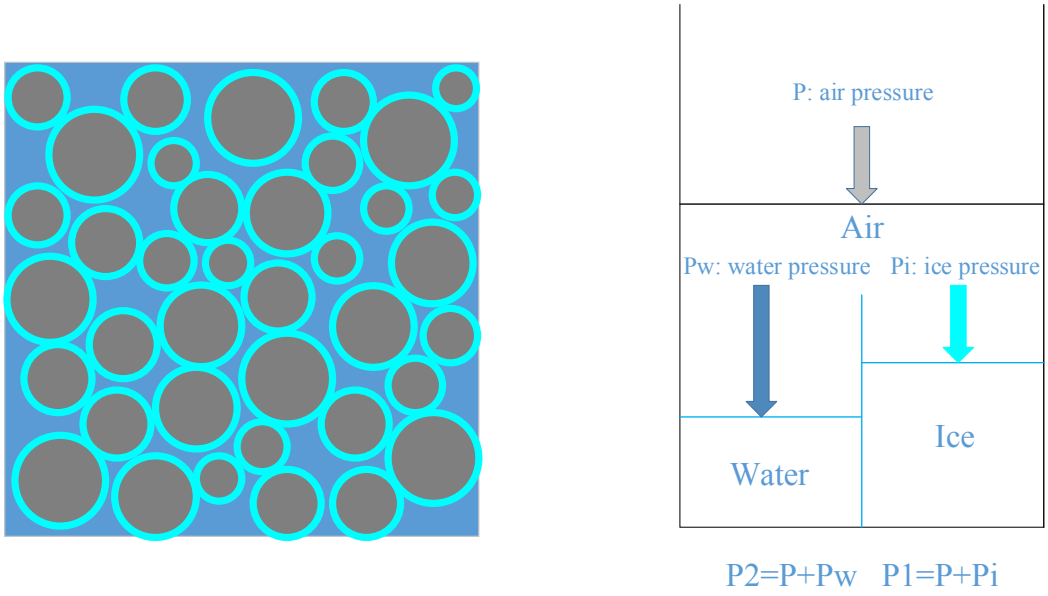



Figure 2-3 The illustration of GCCE

Equation (2-4) can be written as following according to the Figure 2-3:

$$V_w \Delta P_2 - S_w \Delta T_2 = V_i \Delta P_1 - S_i \Delta T_1 \tag{2-7}$$

And then substitute the relationship between $P$, $P_1$, $P_2$, $P_w$ and $P_i$, Equation (2-7) could be replaced as:

$$V_w \left(\Delta P + \Delta P_w\right) - S_w \Delta T_2 = V_i \left(\Delta P + \Delta P_i\right) - S_i \Delta T_1 \tag{2-8}$$

Divide Equation (2-8) by $\Delta T$, the following equation could be obtained:

$$V_w \left(\frac{\Delta P}{\Delta T} + \frac{\Delta P_w}{\Delta T}\right) - S_w = V_i \left(\frac{\Delta P}{\Delta T} + \frac{\Delta P_i}{\Delta T}\right) - S_i \tag{2-9}$$

Change the form of Equation (2-9):

$$V_w \frac{\Delta P_w}{\Delta T} - V_i \frac{\Delta P_i}{\Delta T} + \left(V_w - V_i\right) \frac{\Delta P}{\Delta T} = S_w - S_i \tag{2-10}$$

And then according to Equation (2-6), Equation (2-10) could be rewritten as:

$$V_w \frac{\Delta P_w}{\Delta T} - V_i \frac{\Delta P_i}{\Delta T} + \left(V_w - V_i\right) \frac{\Delta P}{\Delta T} = \frac{L_w}{T} \tag{2-11}$$

Because that in the water-ice system, there is no air pressure item, therefore Equation (2-11) could be expressed as following in the water-ice system:

$$V_w \Delta P_w - V_i \Delta P_i - \frac{L_w}{T} \Delta T = 0 \tag{2-12}$$

And this is the Generalized Clausius–Clapeyron Equation (GCCE). The third term of the left hand side of GCCE represents the total energy emanating when sub-cooled water changes to the ice phase, and the absolute value of the sum of the first and second terms of the left hand side represents the displacement work necessary for the phase change. Thus GCCE implies that the total energy produced due to the phase change is all consumed in the displacement work for the phase change [5].

The Generalized Clausius–Clapeyron Equation is used under static conditions when an ice lens exists but there is no water migration. It is an attempt to explain the mechanism of frost heave. However, typical analysis methods of frost heave are based on the assumption that frost heave accompanied by water migration can be approximated using a static equation of state, GCCE. These methods, therefore, have shown inherently poor accuracy when applied to predict frost heave. It was not until 1998 that Miyata improved GCCE by changing the function from static to dynamic equilibrium allowing water migration to be considered simultaneously [6]. This improved equation is shown as follow:

$$V_w \Delta P_w - V_i \Delta P_i - \frac{L_w}{T} \Delta T = \left(P_{ws} - P_w\right) V_w \tag{2-13}$$

The work that the system performs upon the surroundings is equal to the decrement of the Gibbs free energy. Two kinds of work are done by the system during frost heave in the steady state. They are the displacement work necessary for the phase change and the work necessary for water suction. As induced form the physical meaning of GCCE, the displacement work for the phase change is obviously included in the equation for the definition of the Gibbs free energy. Thus, this external work must be the work done in water suction. Therefore, the difference between the Gibbs free energy of water and ice should be equal to the work done in water suction $\left(P_{ws} - P_w\right) V_w$, where $P_{ws}$ means water supply pressure [7].

The physical meaning of this equation can be explained as follows. The mechanical energy generated by the solid-liquid phase change described on the left side of the Equation (2-13) is equal to the dissipation of mechanical energy due to the accompanying water migration described on the right side. This equation is consistent even when the process shifts from the dynamic condition to the static condition to the static condition, because it agrees with Equation (2-12) under the static condition of $P_{ws} = P_w$.

### 2.2.4 The Capillary Theory (Primarily Frost Heave)

Capillary Theory is one of the earliest frost heave theories aiming to describe frost heave pressure and ice-lens formation in porous medium. According to this theory, water migration to the freezing front is due to the pressure difference at the curved interface between the solid and liquid phases [8]. This relationship could be represented as:

$$P_i - P_w = \frac{2\sigma_{i-w}}{r_{i-w}} \tag{2-14}$$

Where $P_i$ is the ice pressure and $P_w$ is the pore water pressure, $\sigma_{i-w}$ is the surface tension of ice-water interface; and $r_{i-w}$ is the radius of ice-water interface. The ice pressure at a growing ice lens can be assumed to be equal to the overburden pressure in the system. When water migration stops ($P_w = 0$), the applied overburden pressure is determined to be the maximum frost-heave pressure. According to Equation (2-14), the maximum frost heave pressure is independent from the thermal conditions. The only factor that affects the value of frost heave pressure is the curvature radius of the ice-water interface.

Predictions of the maximum frost heaver pressure match well with experiments on idealized soils composed of mono disperse particles [9]. However, when soils containing a range of particle sizes were used, it was found that the calculated results did not agree with experimental results, as significantly larger heaving pressures were observed than were predicted. The reason for such underestimation is that the radius of ice-water interface is estimated based on air-entry measurements. Studies have shown that air entry values are determined by the largest pore sizes in a soil sample, which in turn are determined by the largest particle sizes in the sample. This would overestimate the soil particle sizes in the calculation.

In addition, a significant obstacle to the capillary theory is that this theory cannot explain mechanism for the initiation of new ice lenses. A significant feature of frost heave is the sudden appearance of a new lens a finite distance below a previously growing lens, leading to a rhythmic banding structure such as shown schematically in the following figure (Figure 2-4). No plausible mechanism within the capillary theory was offered to explain why ice lenses form such discrete bands and why new ice lenses form. This is an obvious defect of the existing capillary theory.

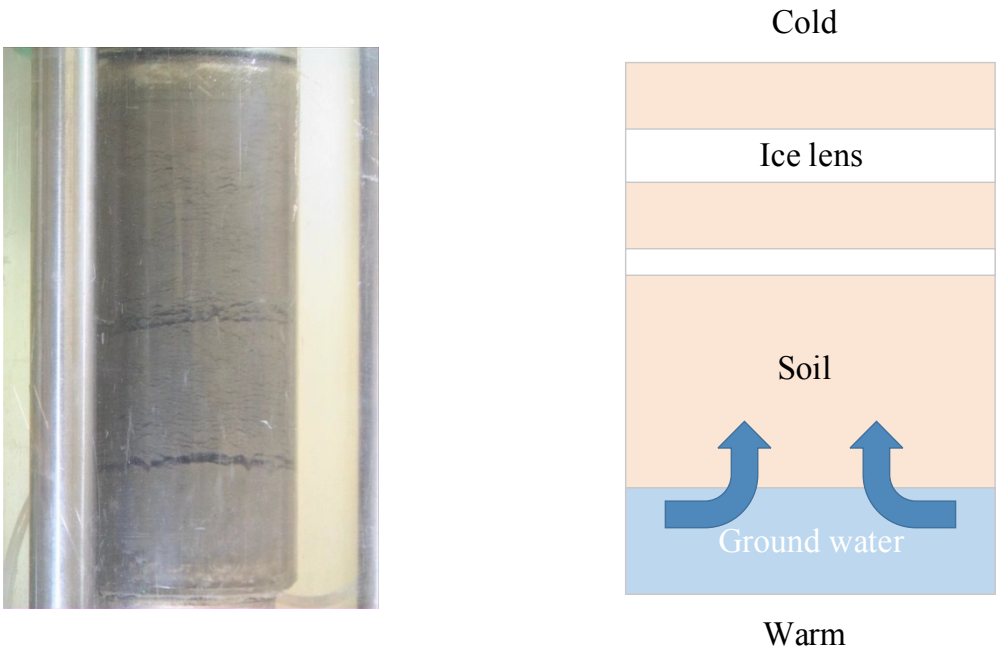



Figure 2-4 The ice structure in the indoor frost heave experiment

### 2.2.5 Frozen Fringe Models

The apparent defect of the capillary theory led some researchers to propose that frost heave can continue to occur after ice has formed a frozen fringe by growing into the pores of the soil [9].

Here frozen fringe is a very critical definition in frost heave research. It is widely accepted that not all of the pore water in a fine grained soil freezes at a unique temperature, but rather freezes over a certain range [10]. Experimental observations on frozen soil specimens under temperature gradients suggest that water migration still occurs beyond the freezing front in response to the temperature-induced unfrozen water content gradient and the pore-water pressure gradient. The migrating water freezes at the segregation temperature, which is slightly lower than the freezing temperature, and ice lenses continue to grow. Miller termed the partially-frozen zone between the freezing front and the segregation freezing frost as “frozen fringe” [11].

Miller’s theory, which he referred as secondary frost heaving (where the capillary theory was referred as the primary heaving), was the first to yield quantitative predictions of lens spacing. The frozen fringe concept has formed the basis of a large number of subsequent theories [12]. These works propose different physical explanations for the flow of premelted water in the frozen fringe, as well as various mechanisms to characterize the stress state leading to different ice-lens initiation criteria. Miller proposed that ice moves through a process of regelation around the soil particles during freezing. During the freezing process, pore ice is nucleated first and then the primary ice crystals propagate into the pore space based on the capillary theory. The ice is considered to exist as

continuous ice wedges, which extend within the frozen fringe. Miller defined this process as the "primary frost heave". The ice wedges are rigidly connected to the growing ice lens. The movement of ice through the pores is by a microscopic regelation process. The ice phase appears to move as a continuous rigid body at a velocity corresponding to the observed heave rate. This is why this model is also called "rigid ice model".

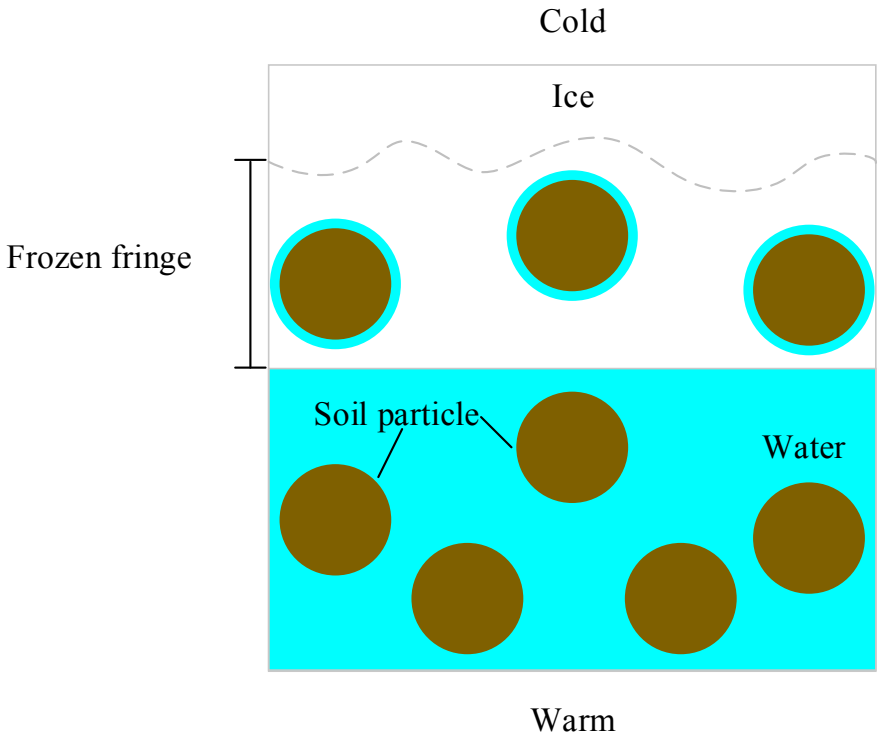



Figure 2-5 The soil water ice system with frozen fringe

In both primary and secondary frost heave, frozen fringe is a critical concept. Frozen fringe is the soil layer just below the bottommost ice lens and above the unfrozen soil where water and ice coexist in soil pores.

With primary frost heaving, only the rate of heat loss controls the rate of frost heave, while with secondary frost heaving, there is a component of hydraulic resistivity influencing frost heave rate. If the hydraulic conductivity of the soil limits the rate of water replenishment to the ice lens for the given rate of heat loss, soil water will freeze at increasing depths with associated changes in the depth and thickness of the frozen fringe. In addition, if there is a location in the frozen fringe at which the effective stress reaches zero, a new ice lens will begin to develop. The new ice lens will grow at a faster rate than the one above it because the hydraulic conductivity of soil immediately below is greater, although the ice lenses above the new one may continue to grow.

The frozen fringe thickness depends on the temperature gradient, overburden pressure, and the specific soil. High overburden pressure and low temperature gradients increase the thickness of the frozen fringe. The ice is a continuous body from the frozen fringe up through the ice lens, and it moves by regelation, or continuous ice-water phase change, accompanied by locally circulating liquid flow.

Miller's theory is one of the few theories that can describe discrete ice lens formation. And the rigid ice wedge assumption proposed by Miller also explained the increased strength of frozen soil.

## 2.3 EXPERIMENTAL METHODS

The complicated situation in the frozen fringe is still controversial in the academic circles. The ice structure in microscopic view is unclear and various assumptions have been proposed. The hydraulic conductivity of frozen fringe and the nonlinear property of soil should be well understood for a better simulation of frost heave process. However, there are numerous obstacles to discover the microscopic mechanism of frost heave. Due to the technical difficulty, an accurate measurement of hydraulic conductivity is a kind of impossible task at this stage. In addition, the measured hydraulic conductivity did not consider the stress and thermal dependency. Furthermore, most numerical frost heave estimation models adopt the Generalized Clausius-Chapeyron Equation as the theory foundation. It is noted that the Generalized Clausius-Chapeyron Equation is only valid in static phase [7]. Therefore, in order to overcome those unknowns, experimental estimation equations were developed in correct with laboratory frost heave tests. In the following section, two typical experimental models which are widely accepted and applied are introduced:

### 2.3.1 Segregation Potential Method

A detail model for one-dimensional frost heave without externally applied load was presented by Konrad and Morgenstern [13, 14] who suggested that after an ice lens is formed, the frozen soil behind the ice lens is passive with regard to mass transfer but that water is transported to the ice lens from the unfrozen soil through a thin zone of frozen soil refered to as the frozen fringe [13]. The driving force arises from suction generated as the ice-fringe interface and the fringe impedes the flow to the lens because of its low permeability.

In Segregation Potential method, a simple linear analysis of the conditions surrounding the frozen fringe was put forward based on the following assumpations:

1 the Clausius-Clapeyron equation is valid at the base of the ice lens;
2 water flow is continuous across the frozen fringe, and therefore accumulates at the base of the ice lens;

3 the fringe can be characterized by an overall permeability $\overline{K}_{fo}$;

4 the temperature conditions at the interface between the ice lens and the frozen fringe may be characterized by a particular segregation freezing temperature $T_{so}$.

Based on such assumptions, Konrad and Morgenstern developed a simplified and practical model for water migration in freezing soil in 1980s and showed that at the beginning of the final ice lens formation in step-freezing test, the velocity of the pore water coming into the unfrozen soil, $v_{u,}$ was proportional to the temperature gradient in the frozen fringe, grad $T_f$, provided the suction at the pore-freezing front was constant. And this relationship could be expressed as follow:

$$v_u = \frac{P_w - P_u}{d}\overline{K}_{fo} = \left(\frac{P_w - P_u}{T_s}\overline{K}_{fo}\right) grad\, T_f = SP\, grad\, T_f \tag{2-15}$$

Here $P_w$ is the suction at the ice lens; $P_u$ is the suction at the frost front; $\overline{K}_{fo}$ is the overall permeability of the frozen fringe. $d$ is the length of the frozen fringe; $T_S$ is the segregation-freezing temperature (temperature of freezing front of for an applied pressure $P_e$), the constant of proportionality, the slope of the linear relationship between $v_u$ and $T_f$, is defined as the segregation potential, SP [14].

They believed that, as for practical applications, it was accurate enough to use the simplified model based on frost heave characteristics near thermal steady state. The simplified model can be expressed:

$$SP = SP_0 e^{-aP_e} \tag{2-16}$$

$SP_0$ : the subscript 0 refer to freezing under no applied load.

$P_e$ : applied pressure at the freezing front.

$a$ : is a constant related to the soil frost heave sensitivity to $P_e$.

Finally, segregation frost heave is calculated as:

$$h_s = 1.09\int_0^t \left[ SP_0 e^{-aP_e} \times \mathrm{grad} T_f \right] dt \tag{2-17}$$

Where, ***t*** represents time and $h_S$ is the segregation frost heave.

However, for Segregation Potential method, one very critical parameter is not inclueded in this model, the freezing rate. As widely accepted, the freezing rate affects the frost heave amount a lot. Usually, a

slower freezing rate would result in a larger frost heave. Further, there is no standard test regulation for this mothod which may impede the widely application of this method due to the non-uniform. Besides that, the recent study of this method, also provide some improvements to this equation. Groenevelt and Grant (2013) [15] demonstrated that the driving force in segregation potential model should be the temperature gradient over the complete layer of soil at sub-zero (°C) temperature, that is, the combined frozen zone plus the frozen fringe, not the temperature gradient in the frozen fringe. This is a modification for the existing equation, in addition, some researchers are working to contain the freezing rate issue in this method.

### 2.3.2 Takashi's Model

Segregation Potential method is widely accepted in North America although there are some points could be better, however, in Japan, Takashi proposed a one-dimensional frost heave estimation equation [16, 17] which considers the constraining stress and freezing rate together; and further this model also includes three constants that can represent the soil properties.

Takashi has made repeated experiments on two kinds of saturated soil more than 170 times, and has succeeded in deriving an empirical formula which expresses the dependency of frost heave ratio on the penetration rate. It is demonstrated that the proposed model explains the empirical formula without conflicting with other phenomena accompanying frost action. And concerning the experiment process for Takashi's equation, the following section will provide a brief introduction.

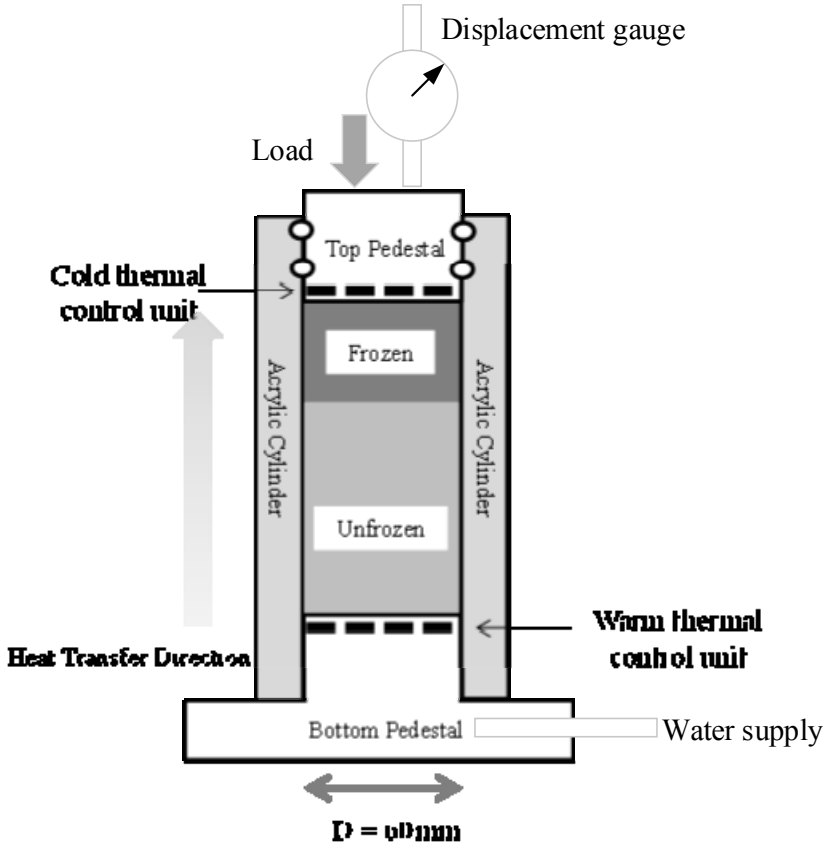



Figure 2-6 A conceptual image of frost heave test apparatus

First, the standard dimension of the specimen shall be 60 mm in diameter and 20-40 mm in height. The experiment apparatus is shown as Figure 2-6. Then use a cutter ring, straight knife, wire-saw trimmer to trim a specimen to the specified diameter. Then before experiment, the mass $m_0$ (g), the height $H_0$ (cm) and the diameter $D$ (cm) of the specimen shall be measured. The water content $w_0$ (%) is obtained using the extra sample cut from the specimen. One critical point should be noted that the specimen diameter is supposed to be roughly 1% smaller than the inner diameter of the mold to reduce the friction between the mold and the unfrozen part of the specimen. Furthermore, the model in which the specimen is inserted shall be placed on the bottom cooling plate. A filter paper shall be placed on the specimen top. The specimen shall intake water in order to achieve a greater degree of saturation. Volumetric change $\Delta V_d$ ($cm^3$) due to water intake or discharge or displacement magnitude $\Delta H_d$ (mm) during the saturation process shall be measured. And it is recommended to have a saturation degree over 90%.

The most critical stage in this experiment is the freezing process. The initial temperatures of the upper and lower ends of the specimen and a reading of the displacement gauge shall be recorded. It shall be confirmed that the temperatures of both ends of the specimen are between 0 and +1°C. And then form an ice nucleus at the bottom of the specimen by quickly lowering the temperature of the bottom

cooling plate. Usually -10 °C is applied in order to produce an ice nucleus. When the temperature decreases rapidly, obverse the temperature carefully until the temperature increases a little which is caused by the latent heat when ice lens forms. After that wait another 1 or minutes to make sure that ice lens exist then the real freezing process can be started. This process is called as "thermal shock". Then the temperature of the top cooling plate shall be kept at 0 °C and the temperature of the bottom cooling shall be lowered at a specified speed. Displacement of the specimen $\Delta H$ (mm), temperatures (top end temperature $T_W$ (°C) and bottom end temperature $T_C$ (°C) and water intake or discharge $\Delta V$ ($cm^3$)) shall be continuously recorded.

After the freezing process, based on the obtained data, we can plot the temperature versus elapsed time relationship by taking the temperatures of the specimen's upper and lower ends $T_W$ (°C) and $T_C$ (°C) in the vertical axis and elapsed time $t$ (h) in the horizontal axis. After that plot $\Delta H_W$ (mm) versus elapsed time curve by taking $\Delta H_W$ in the vertical axis and elapsed time $t$ (h) in the horizontal axis. The water intake or discharge per unit area $\Delta H_W$ is defined by the following equation.

$$\Delta H_W = \frac{\Delta V}{A} \times 10 \quad (mm) \tag{2-18}$$

$$A = \pi \frac{D^2}{4} \quad (cm^2) \tag{2-19}$$

Where $\Delta V$ is water intake or discharge during freezing ($cm^3$) and $A$ is cross sectional area of the specimen. And water intake or discharge ratio $\zeta_W$ (%) shall be determined from the following equation:

$$\xi_W = \frac{\Delta H_{wf}}{H_1} \times 10 \quad (\%) \tag{2-20}$$

$\Delta H_{wf}$ is the water intake or discharge during freezing divided by the initial cross sectional area of the specimen and $H_1$ is specimen height just before freezing (cm). And then plot the frost heave versus time curve by taking the frost heave $\Delta H$ (mm) in the vertical axis and time $t$ (h) in the horizontal axis. Freezing rate $U$ (mm/h) shall be calculated by the following formula:

$$U = \frac{10 H_1}{t_f} \quad (mm/h) \tag{2-21}$$

where $t_f$ is the duration time of freezing (h).

Frost heave ratio $\zeta$ (%) shall be calculated by the following formula:

$$\xi_W = \frac{\Delta H_f}{H_1} \times 10 \quad (\%) \tag{2-22}$$

where $\Delta H_f$ is the frost heave amount at the end of freezing period (mm). Then summarize the testing results with frost heave ratio $\zeta$ (%) in the vertical axis and the water intake or discharge ratio $\zeta_W$ (%) in the horizontal axis. Then approximate the test result by drawing the straight line in which the gradient of (frost heave ratio $\zeta$)/(water intake ratio $\zeta_W$) is equal to 1.09. This is shown as the following graph.

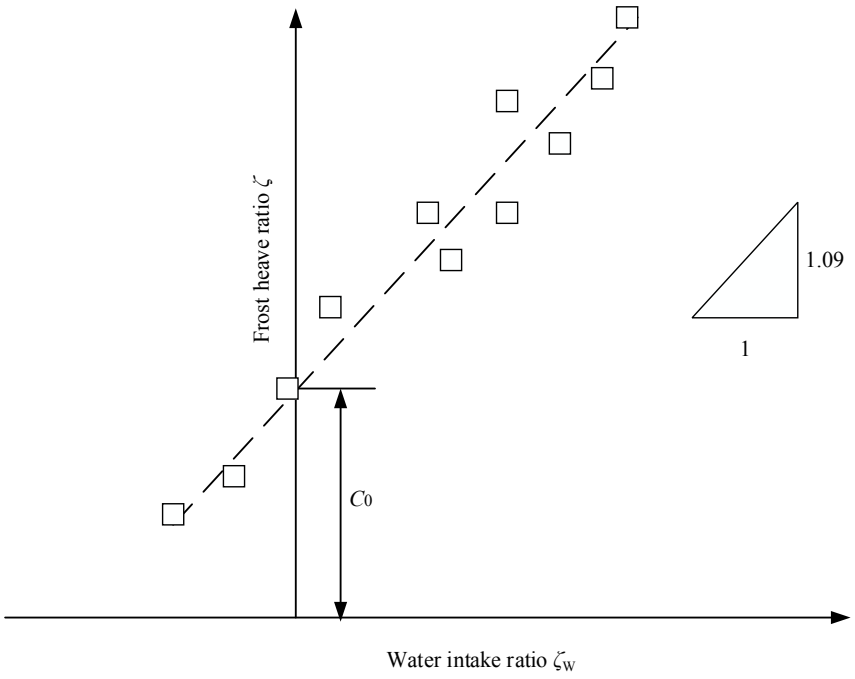



Figure 2-7 Determination of $C_0$

Read the value of the point at which the approximate straight line crosses the vertical axis (Figure 2-7). The value is defined as frost heave ratio without water intake or discharge $C_0$ (%). Then draw the relationship of frost heave ratio and the reciprocal of the applied stress by taking frost heave ratio in the vertical axis and the reciprocal of applied stress $\sigma$ (kN/m$^2$) in the horizontal axis. Similarly, by drawing an approximate straight line in the graph (Figure 2-8), the constant $C$, which is the gradient of the line divided by 100 and intersection point $\zeta_0$ (%), shall be obtained. With this line, the following equation that describes the relationship between $\zeta$ (%) and applied stress $\sigma$ (kN/m$^2$) shall be determined:

$$\xi = \xi_0 + \frac{100C}{\sigma} \tag{2-23}$$

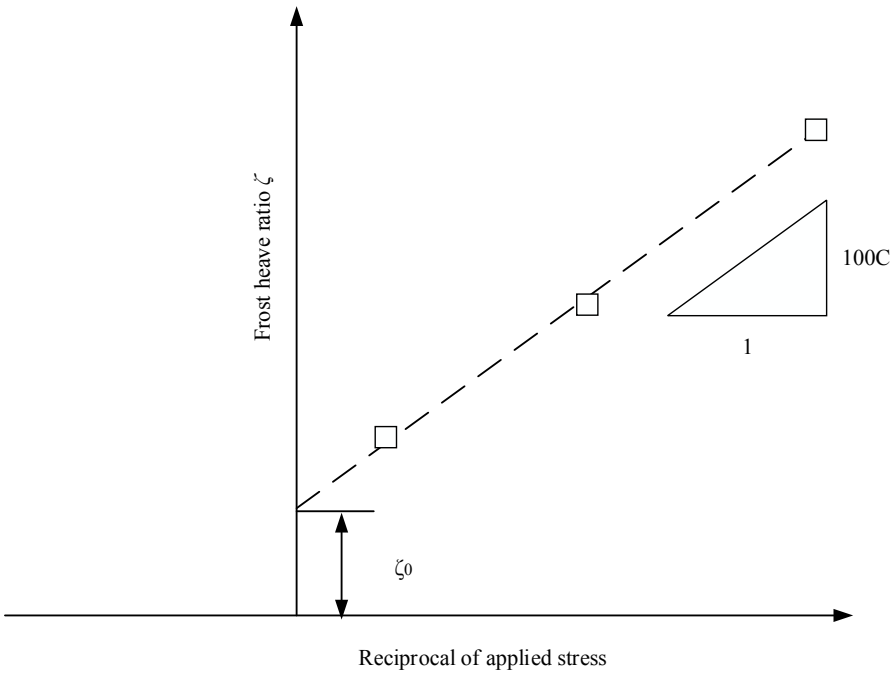



Figure 2-8 Relationship between $\zeta$ and $1/\sigma$

In order to evaluate the freezing rate dependency, plot the multiple of applied stress $\sigma$ (kN/m$^2$) and frost heave ratio $\zeta$ (%) minus $\zeta_0$ (%) in the vertical axis, and the reciprocal of square root of freezing rate $U$ (mm/h) in the horizontal axis as shown in Figure 2-9.

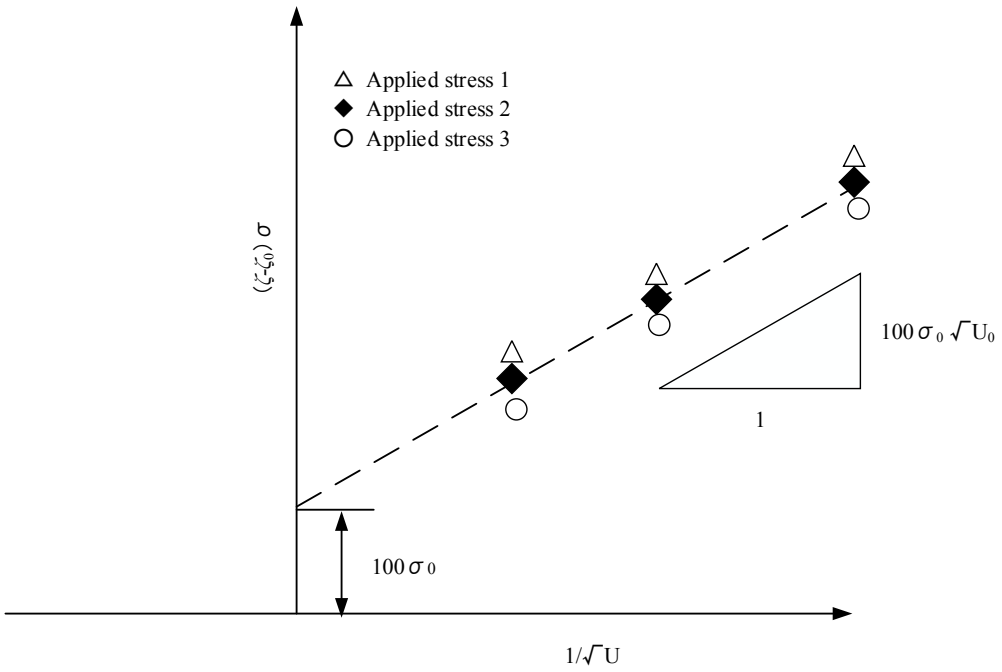



Figure 2-9 Relation between $(\zeta-\zeta_0)\,\sigma$ and $1/\sqrt{U}$

By drawing an approximate straight line in Figure 2-9, a frost heave constant $\sigma_0$ (kN/m$^2$) shall be

obtained from the intersection of the straight line with the vertical axis. Then, by dividing the gradient of the straight line by $\sigma_0$ (kN/m$^2$) and squaring the resulting quotient, the frost heave rate constant $U_0$ (mm/h) shall be obtained as shown in Figure 2-9. According to previous conclusions, the constants of the following equation (including the freezing rate dependency) shall be determined in order to describe the relationship between the frost heave ratio $\zeta$ (%), freezing rate $U$ (mm/h) and applied stress $\sigma$ (kN/m$^2$):

$$\xi = \xi_0 + 100\frac{\sigma_0}{\sigma}\left(1+\sqrt{\frac{U_0}{U}}\right) \tag{2-24}$$

And this is the derivation of Takashi's equation from experiment result. Please note the units used in this equation. Takashi's equation is adopted by the Japanese Geotechnical Society (JGS) [1] and has a complete set of experimental standard. Though it is originally applied only in one dimensional problem, these days, the applications in multi-dimensional problems are tried. Takashi's equation relates the frost heave ratio with the constraining stress and freezing rate as Equation (2-25) if we adopt the SI unit such as N/m$^2$ for stress and m/s for freezing rate.

$$\xi = \xi_0 + \frac{\sigma_0}{\sigma}\left(1+\sqrt{\frac{U_0}{U}}\right) \tag{2-25}$$

Here $\xi$ is frost heave ratio, which is defined as the ratio of a volume increase to the initial volume of the specimen; σ is the constraining effective stress in the freezing direction, and U is the freezing rate which is the speed of advancement of the freezing line into the unfrozen soil portion, and the unit of freezing rate $U$ is m/s. $\xi_0$, $\sigma_0$ and $U_0$ are constants for the soil material obtained by a JGS regulated experiment (JGS 0171-2003). It is obvious that U and σ are two critical variables for determining the frost heave ratio. Owing to the form of this equation, if the stress $\sigma$ is infinitesimally small, an infinite large value of frost heave ratio could be expected. Thus, there should be a limit for the stress where Takashi's equation performs well. According to Takashi's paper [16], this equation is valid when the stress is between 1–15 kg/cm$^2$ (98–1470 KPa). In our calculation, this stress range is used. And if water migration prevention in unfrozen soil is taken into account, the application of Takashi's equation could be expanded into relatively small stress, for example 30 kPa [18]. However, for a simple and practical multi-dimensional model, this point is not considered in our paper and this may lead to an overestimation of frost heave amount. But this overestimation is safe for engineering. Usually $U$ is obtained by observation for 1D indoor frost heave experiment. However, for multi-dimensional situation, it is not convenient to estimate freezing rate and freezing direction by observation directly. Hence, thermal conductivity analysis is necessary to evaluate the freezing rate and direction. $\sigma$ is obtained by mechanical analysis at each time-step.

From the microscopic point of view, frost heaving can be defined as a process in which, when soil is frozen, the distances between particles become larger than before freezing. Furthermore, frost heaving pressure can be defined as the pressure required to enlarge the distance between particles by freezing of soil. Since thus defined heaving pressure can be observed as a reaction against the overburden pressure during freezing, the heaving pressure increases corresponding to the overburden pressure as far as the latter does not exceed a certain limit. Observing from the unfroze soil side, consequently, Equation (2-25) means that heaving pressure will appear on the freezing front to heave the soil by ζ. In other words, since the amount of heave is inversely proportional to the heaving pressure, if no heave is allowed, the heaving pressure will tend to infinity [17].

Fundamentally, any prediction method of frost heave is the estimation of water flow volume into the freezing front. From this view, Takashi's equation could be explained in a different way. First, Takashi's equation is used to calculate the frost heave ratio which is defined as the volume expansion divided by the original volume or the increased height caused by frost heave divided by the original height:

$$\xi = \frac{V_f}{V} \tag{2-26}$$

And according to the mechanism of frost heave, we know that this $V_f$ is caused by the volume expansion of in-situ water becoming ice and also the migrated water becoming ice. Therefore:

$$V_f = W_o \times 0.09 + W_{ab} \times 1.09 \tag{2-27}$$

$W_{ab}$ is the volume of water absorbed to the freezing front and in experiment this $W_{ab}$ would be observed and recorded, and $W_0$ is the initial water contained in the soil simple before freezing. And based on Equation (2-26) and (2-27), the following relationship could be obtained:

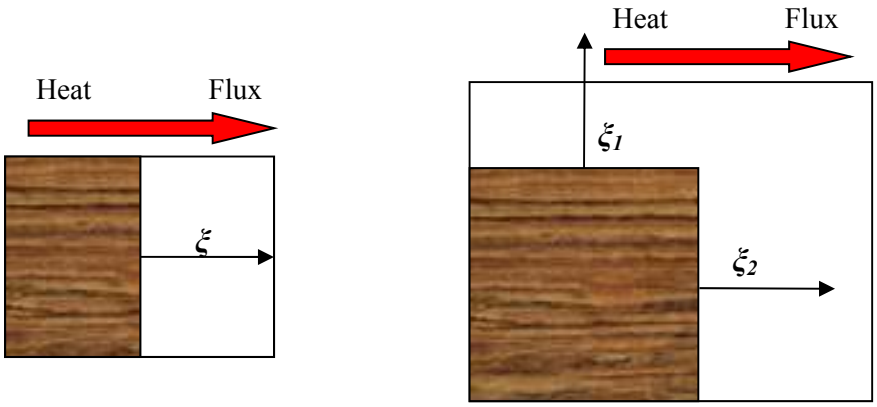
$$\xi = \frac{V_f}{V} = \frac{W_o \times 0.09 + W_{ab} \times 1.09}{V} \tag{2-28}$$

Through this Equation (2-28), we note that if we calculate the frost heave ratio $\zeta$ by Takashi's equation, we can predict the water volume flow into the freezing front in real engineering or numerical simulation:

$$W_{ab} = \frac{\xi \times V - W_o \times 0.09}{1.09} \tag{2-29}$$

However, there is one point worth paying special attention: for 1D situation, frost heave ratio never occurs in transverse direction and therefore there are no displacement and stress in that direction. But, in the multi-dimensional issues, displacement and stress caused by frost heave may happen in various directions. Hence, an anisotropic parameter $\beta$ is proposed to distribute frost heave ratio into different directions. Here we assume the problem as a two-dimensional anisotropic problem with a plain strain condition. $\beta$ is the anisotropic parameter that distributes the frost heave ratio in different directions. $\xi_1$ is the frost heave ratio in the freezing direction and $\xi_2$ is the frost heave ratio perpendicular to the freezing direction. Equation (2-30) shows the relationship between these parameters.

$$\xi_1 = \frac{1}{1+\beta}\xi, \quad \xi_2 = \frac{\beta}{1+\beta}\xi \tag{2-30}$$




One dimension frost heave ratio  Two dimension frost heave ratio

Figure 2-10 Expanding Takashi's equation into two dimension

According to Equation (2-30), when $\beta = 0$, all frost heave ratio is assigned to the freezing direction, which is called as anisotropic frost heave. When $\beta = 1$, half of the frost heave ratio is distributed into the freezing direction and the other half is allocated to the direction perpendicular to the freezing direction; we call this situation isotropic frost heave. The detail of how to expand one-dimensional originated Takashi's equation into multi-dimensional situation will be explained other chapter. Furthermore, three-dimensional experiments based modified Takashi's equation will be introduced.

From the equation itself, it includes constraining stress and freezing rate together, which are two critical factors which affects frost heave amount a lot. On the other hand, Takashi's equation is proved by practical engineering during the last several decades. In Japan, many liquid natural gas tanks have been built in the past several decades. After these tanks were built and operated, the soil surrounding these tanks occasionally froze, resulting in frost heave. Takashi's equation successfully solves such

engineering issues. Because of its satisfactory performance and simplicity, Takashi's equation has been widely applied in Japan; currently, it has become more popular internationally. For this reason, we adopt this equation as our theoretical foundation to estimate frost heave. Parameters used for Takashi's equation are simple and easily available. We believe that this equation can deal well with the complicated frost heave process in the engineering view. If we introduce water fluxes, hydrodynamic resistance and solute effects for the estimation of frost heave, various parameters are necessary. And more parameters and complicated models could not always guarantee a better simulation result. This is also contrary to our original intention. Additionally, we confirm that with suitable modifications, Takashi's equation may also successfully address multidimensional situations.

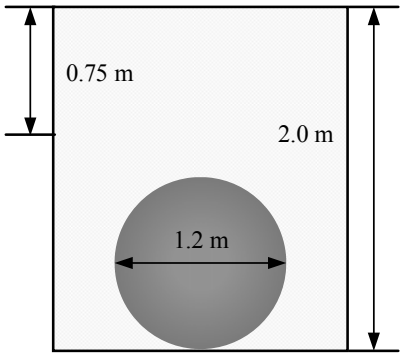
## 2.4 LARGE SIZE FROST HEAVE TEST

From the first Oil Crisis (1973), much more attentions were drawn to the huge energy deposited in arctic area. Various researches have been taken in order to solve the energy transportation dilemmas in permafrost area. Several famous large scale frost heave experiments were done since that time, and based on those researches several pipelines were constructed in cold regions, such as the Alaska, Canada and Siberia. These pipelines were used to transfer oil or liquid natural gas to the densely populated destination. For the oil pipelines, they need to be heat up in order to maintain the fluid status of viscous oil in cold regions. Such pipelines would break the heat balance in cold regions and then thaw the permafrost. The thawed permafrost would lose its strength and finally damage the pipeline system by the thawing settlement and thawing water. On the other hand, for the gas pipeline, usually natural gas is chilled into liquid status for high transportation efficiency. Chilled gas pipelines may cause some frost heave when go through the unfrozen frost susceptible area. To the discontinuous permafrost area, uneven frost heave is a serious challenge to the pipeline system. This uneven deformation probably brings much more damages to the pipeline system. In the following section, several representative large scale frost heave experiments are introduced. The information concerning to these experiments are quoted from the existing literatures.

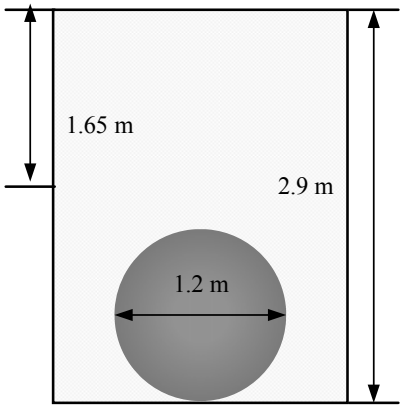
### 2.4.1 The Calgary Frost Heave Test

The Calgary Frost Heave Test Site sponsored by Foothills Pipe Lines Ltd. was constructed by Canadian Arctic Gas Study Ltd. in 1974. The operation of the test site was taken over by Foothills at the end of 1977. The facility consists of six full-size pipe sections. The first four are non-insulated pipe sections 1.2 m in diameter and approximately 12 m long. These sections were installed with the original construction of the site in 1974. In 1977, two pipe sections of identical diameter were installed, each insulated with a 15 mm thickness of polyurethane insulation. The ground around the pipes is frozen by circulating air at about -10°C through the system. For the control group (standard burial), the base of the pipe is buried at a depth of approximately 2 m from the original ground surface and there is a silt cover over the top of the pipe approximately 0.75 m thick. The deep burial section is similar to

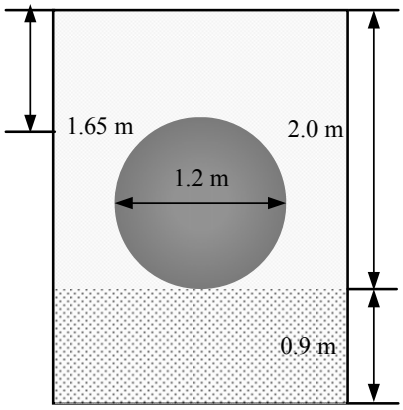
the control section except that the base of the pipe is buried to a depth of 2.9 m beneath the original ground surface. The gravel section is, again similar to the control section with the addition of 0.9 m of gravel placed underneath the pipe. The fourth section in this sequence is the restrained section. It again is similar to the control section but with the addition of restraining devices at each end which provide a constant hold-down pressure for this section. The insulated silt section has a geometry which is identical to the original control section. However, for the insulated gravel section, the base for the pipe is buried to a depth of 2 m from the surface and there is also a 1 m gravel layer under the pipe. The detail of this test sections are shown as Figure 2-11.



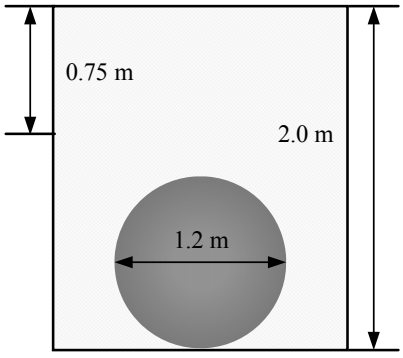

1: Cross section of section control



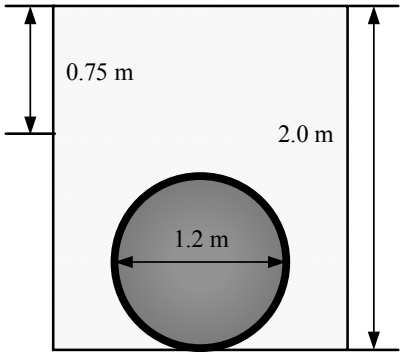

2: Cross section of deep burial section



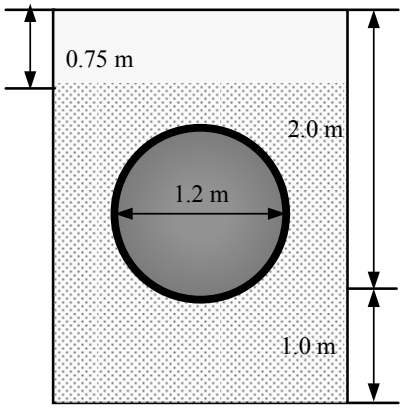

3: Cross section of gravel section




4: Cross section of restrained section




5: Cross section of insulated silt section




6: Cross section of insulated gravel section

Figure 2-11 Cross sections for the test sections at the Calgary frost heave test facility

The experiment process is omitted in this paper. Only some useful conclusions are provided. Based on the data from the insulated pipe sections, it could be noted: that the placement of insulation around the chilled pipe is very effective in limiting the frost penetration depth and related frost heave. And further, the summer warming effects negated the heave built up over the winter season. The non-insulated sections data have been compared to data from a laboratory test on soil from the test site. By the comparison, it was noticed that the general behavior was similar but with some differences [19]. More information concerning this full-size long term frost heave experiment could be referred to the paper by Slusarchuk *et al*. (1978) [20].

### 2.4.2 The First Fairbanks Frost Heave Test

This full-size frost heave test was taken by Northwest Alaskan Pipeline Ltd. in 1979. In fact this is a sister program with the Calgary Frost Heave Test. North Northwest Alaskan Pipeline Company NAPLINE and Foothills Pipe Lines (Yukon) Ltd were jointly sponsoring the Alaska Highway Gas Pipeline project and to address shared concerns regarding the possible adverse effects of frost heave they had undertaken these two full-size long term frost heave studies.

The Fairbanks Frost Heave Test Facility is comprised of eight 36.56 m sections, one 121.92 m section and one 21.37 m section. Refrigerated air at pressure of 4.62MPa has been continuously circulated through the pipe sections at flow rate of 25.78 $m^3$ per minute (velocity being 0.36 m/sec) since October 13 1979. The air inlet temperature is -13.33 °C and the outlet is -11.11 °C; however almost no drop in temperature occurs over the insulated test sections pipes No 8, 5, 7 and 2. At all the test section locations the pipes have 1.07 m of soil cover except for No.5 which has 0.91 m. The configuration of the test sections may be described as follows:

Table 2-1 Experiment descriptions of first Fairbanks frost heave test

| Section Number | Section Descriptions |
|---|---|
| 1 | The 18 inch diameter pipe at this test section is uninsulated and has no granular bedding. This test section is anticipated to serve as control of the heave mitigative effect of both the gravel bedding and insulation. |
| 2 | The pipe burial configuration is similar to test section No. 1; however the test pipe is wrapped with 5.08 cm of urethane insulation. |
| 3 | For test section No. 3, 0.15 m of gravel bedding support the test pipe In addition the trench is lined with six inches of styrofoam insulation. |
| 4 | The heave mitigative effect of gravel is evaluated at this test section: no insulation is utilized and 0.91 m thick gravel layer supports the pipe. |
| 5 | A slightly different burial configuration was utilized at this test location: the test pipe is wrapped with 5.08 cm of urethane insulation and 0.91 m high gravel berm constitutes the overburden. |
| 6 | The pipe burial configuration is the same as that of test section No. 1, however heat pipes were installed on both sides of the pipe at 2.44 m intervals. It is intended that this section will confirm that inducing frozen layer by the heat pipes below chilled pipeline; frost heave will greatly be reduced. The section is to investigate one of the possible mitigative measures for frost heave control. |
| 7 | 5.08 cm of urethane insulation in conjunction with 0.3 m of granular bedding are utilized for test pipe No. 7 |
| 8 | 10.16 cm of urethane insulation together with 0.91 m of gravel bedding were employed for test pipe No. 8. |
| 9 | Half of this 121.92 m test pipe is placed in permafrost and the other half in thawed silt. The test results will provide input for the evaluation of stresses and deformations which may develop at permafrost interfaces as a result of differential heave. |
| 10 | This test pipe is buried in permafrost to investigate the magnitude of secondary frost heave (frost heave in already frozen soils). |

Based on the above experiments, the following conclusions were obtained: At the depth of the pipe bottom, which is about 2.30 m below the ground surface, the effect of seasonal ground temperature variations on pipe surface temperature is insignificant. Further, by this experiment, they found that wrapping insulation around the pipe is more efficient than the board insulation along the trench sides in reducing the size of the frost bulb around the pipe. In addition, the effectiveness of the gravel berm in conducting heat during summer season so as to reduce the frost bulb beneath the chilled pipeline was confirmed. And also as expected, the thicker the insulation, the less frost depth and thus less frost heave will be.

All the above information is from the report from Northwest Alaskan Pipeline Company. Inc. [21].

### 2.4.3 The Caen Frost Heave Test

France and Canada conducted modeling experiments in Caen, France in the 1980s and 1990s. The public information concerning this large scale frost heave experiment is very limit, thus here the author cites the following information from Kim's dissertation. The Caen experimental facility consisted of a temperature-controlled hall, which was 18m long, 8m wide and 5m high. The test facility consisted of a container, which could be filled to a depth of 2m. The base of the container isolated the thermal and hydraulic regime within it from the natural ground conditions. The test container was filled with soil to a depth of 1.75m. The objective of the experiment was to observe pipe bending due to a sharp contrast in soils with different frost susceptibilities. To achieve this goal, two separate soils were used. The Caen silt was used to model the soil with higher frost-heave susceptibility. To model the soil with lower frost susceptibility, sand was used. The Caen silt and the sand each occupied one-half of the container. The pipeline consisted of a steel pipe 18m long and 0.273m diameter with a 5mm wall thickness. The instrumented pipeline was buried in a trench at a depth of 0.33m to the top of the pipeline. The entire 18m length of the pipeline was backfilled with the described soils. In order to model a relatively long-distance pipeline, both ends of the pipe were kept free of any constraints.

The Caen frost-heave experiment consisted of two major stages. The objective of the first series of experiments was to examine the behavior of a chilled pipeline located at the intersection between two initially unfrozen soils with widely different frost-heave susceptibilities. The second series of tests was designed to investigate the behavior of a chilled pipeline, which was located at the transition zone between pre-frozen and unfrozen frost-susceptible soil.

In the first series of experiments, the initially unfrozen soils were subjected to four periods of freezing between 1982 and 1989. Four freeze/thaw cycles were imposed. Pipe temperature ranged from -2 to -5°C. Air temperature was -0.75°C during freezing and 4°C during thawing. The groundwater table was maintained at a constant 0.3m below the base of the pipe.

The second stage of the experiment was carried out in the same facility between 1990 and 1993. In this experiment, a pipeline was embedded at a transition region between pre-frozen and unfrozen soil. The objective of the experiment was to examine the forces that would be generated on a pipeline, which was anchored by the pre-frozen soil. In order to allow comparison between this and the previous experiments, the silt composition, pipe size, and burial depth were kept the same. Two stress-relaxation cycles were imposed. The groundwater table was maintained at a constant 1.0m and 1.2m below the base of the pipe, in the first and the second cycle, respectively.

Prior to the start of the first stress-relaxation cycle as indicated by the commencement of pipeline cooling, the section with sand was pre-frozen for approximately 230 days. After the pre-freezing period, the operation started on June 26, 1991 (day 0). The ambient air temperature in the facility was maintained at -0.75oC and the cooling temperature in the pipeline was maintained at -5oC. This temperature specification was maintained from day 0 to day 214. From day 215 to day 256, the temperature in the pipe was lowered to approximately -8.5oC. A relaxation phase followed from day 257 to day 269. During this period, the pipe temperature was raised to 5 °C, while the ambient air temperature in the facility was maintained at -0.75 °C. This change generated thawing of soil local to the pipe. Resulting soil weakening allowed the pipe to straighten, thus reducing its internal stress.

Prior to the start of the second stress-relaxation cycle, a transitional phase followed from day 270 to day 370 to re-establish the pre-frozen sand and unfrozen silt sections. During this period, the ambient air temperature was held at -5°C and 5°C in the sand section and the silt section, respectively. The second stress-relaxation cycle was initiated on July 1, 1992 (day 371). From day 371 to day 769, the pipe temperature was held at -6 °C while the ambient air temperature was maintained at -4 °C. A relaxation phase was inserted from day 659 to day 672. During this phase, the pipe temperature was raised to 5 °C, while the ambient air temperature in the facility was maintained at -4 °C.

The Caen frost-heave experiment was a controlled-environment experiment with high-quality scientific instruments. Such a controlled-environment experiment was designed to remove the complicating aspects of natural climate and soils vagaries from the experiments so the essential factors in the phenomenon being investigated could be clearly distinguished. However, a real large diameter pipe was not used for this experiment [8].

### 2.4.4 The Second Fairbanks Frost Heave Test

The Second Fairbanks Frost Heave Test is different with the First Fairbanks Frost Heave Test. They were conducted by two different organizations. The Hokkaido University, Japan and the University of Alaska Fairbanks (UAF) conducted a full-scale field experiment to study the differential pipe heave effects near the frozen-unfrozne boundary from the end of 1999 to the August 2003. This project is operated and funded by the Japan Science and Technology Corporation (JST) in cooperation with the

UAF.

In December 1999, a 0.9-m-diam, 105-m-long chilled pipeline with X65 grade and 8.5 mm wall thickness was constructed and activated near 3.8 km Chena Hot Springs Road, Fairbanks, Alaska. To the north of the facility, the terrain is dominated by low, gently rolling hills, and to the south the terrain changes into the Chena River flood plain. The facility itself lies within the gently sloping transition between the two terrains and the construction site picture is shown by Figure 2-12.

The experimental pipeline is placed about 1.8 m below the surface with back-fill consisting of dry sand placed around and to the top of the pipe, with an additional 0.9 m thickness of crushed in situ soil and a thin crown of uncrushed in situ soil. The first 30 m of the pipeline are in shallow permafrost and the remaining section is in unfrozen ground. The detail could be found at Figure 2-13.

The instrumentation plan included the installation of thermistors, 40 strain gauges at 11 locations along the pipeline, 28 heave rods welded to the top of the pipeline, five heave gauges installed below the pipeline, and several other types of soil settlement devices. Heave rods for measuring pipeline movement and groundwater measurements were monitored manually once every two weeks using a rotating laser leveling device. Temperature measurements were recorded twice daily by three automated HP data acquisition systems. The field monitoring program was initiated in December 1999.



Figure 2-12 Construction site of second Fairbanks frost heave test

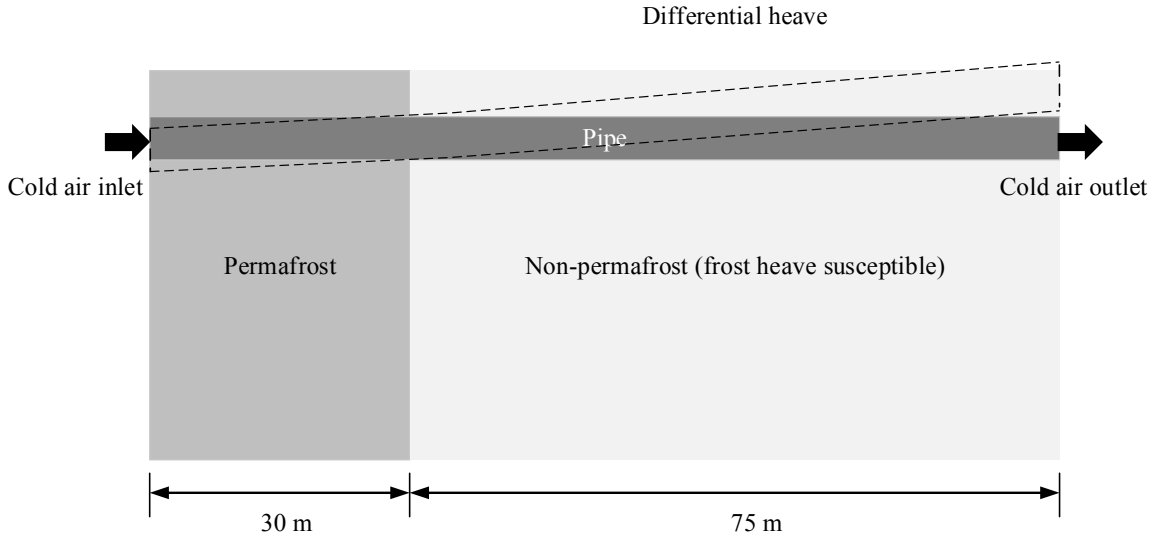



Figure 2-13 A conceptual image of second Fairbanks frost heave test

Based on such monitor data, the following conclusions were obtained: The maximum heave occured next to the permafrost-unfrozen transition and not solely in the deep permafrost zone. And also the movement of the pipeline within the unfrozen zone was characterized by three main heave phase according to the frost heave rate. The above information concering the Second Fairbanks Frost Heave Test are cited from Huang *et al*. 2004 [22] and Kim [8, 23, 24]

## 3. THERMAL ANALYSIS ISSUES

In this chapter we focus on heat transfer analysis, including basic governing equation derivation and Finite Element Method application to thermal analysis. Equivalent Heat Capacity Method is adopted to evaluate the latent heat influence caused by phase change. Freezing rate and direction are carefully discussed based on the thermal analysis result. Further the author also presents some basic skills of Finite Element Method used in this paper and its related issues. Based on this thermal analysis section, the author provides some simple examples to verify the transfer calculation and latent heat influence which can prove the reliability of this calculation program.

### 3.1 HEAT TRANSFER (WITHOUT WATER FLOW)

Now we consider the derivation of the basic differential equation for the two-dimensional problem of heat conduction without convection. The purpose of this derivation is to present a physical insight into the heat-transfer phenomena, which must be understood so that the frost heave process can be fully discussed. We begin with the control area shown in Figure 3-1. By the conservation rule of energy, we have:

$$E_{\text{in}}+E_{\text{generated}} = \triangle U+E_{\text{out}} \tag{3-1}$$

$E_{\text{in}}$ is the energy entering the control area, $\triangle U$ is the change in stored energy. $E_{\text{generated}}$ is the energy generated inside the control area and in our analysis this item is not considered and is assumed as 0.

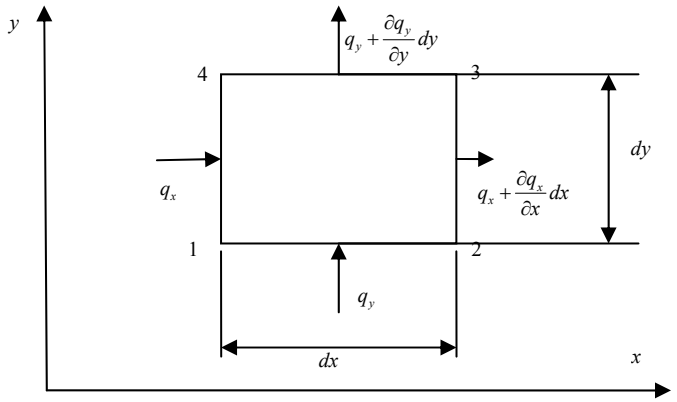



Figure 3-1 The control area for two-dimensional heat conduction

The heat transfer in x direction:

$$\left\{q_x-\left(q_x+\frac{\partial q_x}{\partial x}dx\right)\right\}dydt=-\frac{\partial q_x}{\partial x}dxdydt \tag{3-2}$$

$q_x$ is the (heat conducted) heat flux into the control area in $x$ direction, $q_x + \frac{\partial q_x}{\partial x} dx$ is the heat conducted out of the control area at $x$ direction, and $\theta$ is temperature. And the time interval is *dt.*

By Fourier's law of heat conduction,

$$q_x = -k_x \frac{\partial \theta}{\partial x} \tag{3-3}$$

where $k_x$ is the thermal conductivity in $x$ direction and $\frac{\partial \theta}{\partial x}$ is the temperature gradient. And Equation (3-3) states that the heat flux in the x direction is proportional to the gradient of temperature in the x direction. The minus sign in this equation implies that, by convention, heat flow is positive in the direction opposite the direction of temperature increase

Thus Equation (3-2) can be rewritten as follows:

$$-\frac{\partial q_x}{\partial x} dxdydt = k_x \frac{\partial^2 \theta}{\partial x^2} dxdydt \tag{3-4}$$

Similarly, heat transfer in $y$ direction can be written as follows:

$$k_y \frac{\partial^2 \theta}{\partial y^2} dxdydt \tag{3-5}$$

The sum of heat flow into the element is:

$$k_x \frac{\partial^2 \theta}{\partial x^2} dxdydt + k_y \frac{\partial^2 \theta}{\partial y^2} dxdydt \tag{3-6}$$

During the same period, the change in stored energy can be expressed by

$$\triangle \text{U} = \text{specific heat} \times \text{mass} \times \text{change in temperature} = c(\rho dxdydt)\frac{\partial \theta}{\partial t} \tag{3-7}$$

Where $c$ is specific heat and $\rho$ is the mass density, $t$ is the time duration.

With Equation (3-6) and Equation (3-7), the following equation can be obtained:

$$\rho c \frac{\partial \theta}{\partial t} dxdydt = k_x \frac{\partial^2 \theta}{\partial x^2} dxdydt + k_y \frac{\partial^2 \theta}{\partial y^2} dxdydt \tag{3-8}$$

And if assume $k_x = k_y = k$, and then dividing Equation (3-8) by *dxdydt*, we have the two-dimensional heat conduction equation as:

$$\rho c \frac{\partial \theta}{\partial t} = k \left( \frac{\partial^2 \theta}{\partial x^2} + \frac{\partial^2 \theta}{\partial y^2} \right) \tag{3-9}$$

### 3.1.1 The Application of FEM to Heat Transfer Equation

Based on the Equation (3-9), we assume a $\overline{\theta}$ ($\overline{\theta}$ is an approximation of the accurate $\theta$) first and then take it into Equation (3-9), we can get the error or residual *R* as follow:

$$\begin{aligned} R &= \left\{ \rho c \frac{\partial \overline{\theta}}{\partial t} - k \left( \frac{\partial^2 \overline{\theta}}{\partial x^2} + \frac{\partial^2 \overline{\theta}}{\partial y^2} \right) \right\} - \left\{ \rho c \frac{\partial \theta}{\partial t} - k \left( \frac{\partial^2 \theta}{\partial x^2} + \frac{\partial^2 \theta}{\partial y^2} \right) \right\} \\ &= \rho c \frac{\partial \overline{\theta}}{\partial t} - k \left( \frac{\partial^2 \overline{\theta}}{\partial x^2} + \frac{\partial^2 \overline{\theta}}{\partial y^2} \right) \end{aligned} \tag{3-10}$$

In an attempt to reduce this error in some overall manner over the whole domain, we attempt to make such an integral:

$$\iint \left\{ \rho c \frac{\partial \overline{\theta}}{\partial t} - k \left( \frac{\partial^2 \overline{\theta}}{\partial x^2} + \frac{\partial^2 \overline{\theta}}{\partial y^2} \right) \right\} \delta\theta dxdy = 0 \tag{3-11}$$

This can be rearranged as:

$$\iint \rho c \frac{\partial \overline{\theta}}{\partial t} \delta\theta dxdy - \iint k \left( \frac{\partial^2 \overline{\theta}}{\partial x^2} + \frac{\partial^2 \overline{\theta}}{\partial y^2} \right) \delta\theta dxdy = 0 \tag{3-12}$$

where $\delta\theta$ is a weighting function, and in this paper, Galerkin method is adopted. Then apply the Green's theorem to second term of Equation (3-12), we can see that:

$$\iint k\left(\frac{\partial^2\bar{\theta}}{\partial x^2}+\frac{\partial^2\bar{\theta}}{\partial y^2}\right)\delta\theta\,dxdy$$

$$=\oint_s k\frac{\partial\bar{\theta}}{\partial x}n_x\delta\theta ds-\iint k\frac{\partial\delta\bar{\theta}}{\partial x}\frac{\partial\bar{\theta}}{\partial x}dxdy+\oint_s k\frac{\partial\bar{\theta}}{\partial y}n_y\delta\theta ds-\iint k\frac{\partial\delta\bar{\theta}}{\partial y}\frac{\partial\bar{\theta}}{\partial y}dxdy$$

$$=-\oint_s q_x n_x\delta\theta ds-\iint k\frac{\partial\delta\bar{\theta}}{\partial x}\frac{\partial\bar{\theta}}{\partial x}dxdy-\oint_s q_y n_y\delta\theta ds-\iint k\frac{\partial\delta\bar{\theta}}{\partial y}\frac{\partial\bar{\theta}}{\partial y}dxdy \tag{3-13}$$

Here the derivation process of Green's Theorem is provided as follow:

First consider the integration by parts of the following two-dimensional expression:

$$\iint_\Omega \phi\frac{\partial\psi}{\partial x}dxdy \tag{3-14}$$

Integrating first with respect to $x$ and using the well-known relation for integration by parts in one-dimension:

$$\int_{x_L}^{x_R} ud\upsilon=-\int_{x_L}^{x_R}\upsilon du+(u\upsilon)_{x=x_R}-(u\upsilon)_{x=x_L} \tag{3-15}$$

And then apply this idea to Equation (3-14), we have:

$$\iint_\Omega \phi\frac{\partial\psi}{\partial x}dxdy=-\iint_\Omega\frac{\partial\phi}{\partial x}\psi dxdy+\int_{y_B}^{y_T}\left[(\phi\psi)_{x=x_R}-(\phi\psi)_{x=x_L}\right]dy \tag{3-16}$$

If now we consider a direct segment of the boundary $d\Gamma$ on the right-hand boundary, we note that

$$dy=n_x d\Gamma \tag{3-17}$$

where $n_x$ is the direction cosine between the outward normal and the $x$ direction. Similarly on the left-hand section we have

$$dy = -n_x d\Gamma \tag{3-18}$$

The final term of Equation (3-16) can thus be expressed as the integral taken around an anticlockwise direction of the complete closed boundary:

$$\oint_{\Gamma} \phi\psi n_x d\Gamma \tag{3-19}$$

The general expression in all case is

$$\iint_{\Omega} \phi \frac{\partial \psi}{\partial x} dxdy = -\iint_{\Omega} \psi \frac{\partial \phi}{\partial x} dxdy + \oint_{\Gamma} \phi\psi n_x d\Gamma \tag{3-20}$$

Similarly, if differentiation in the *y* direction arises we can write

$$\iint_{\Omega} \phi \frac{\partial \psi}{\partial y} dxdy = -\iint_{\Omega} \psi \frac{\partial \phi}{\partial y} dxdy + \oint_{\Gamma} \phi\psi n_y d\Gamma \tag{3-21}$$

Thus Equation (3-12) can be rewritten as:

$$\iint \rho c \frac{\partial \bar{\theta}}{\partial t} \delta\theta dxdy + \iint k \frac{\partial \delta\theta}{\partial x} \frac{\partial \bar{\theta}}{\partial x} dxdy + \iint k \frac{\partial \delta\theta}{\partial y} \frac{\partial \bar{\theta}}{\partial y} dxdy = -\oint_S q_x n_x \delta\theta ds - \oint_S q_y n_y \delta\theta ds \tag{3-22}$$

By introducing the concept of shape function, temperature can be expressed as follow:

$$\bar{\theta} = \begin{bmatrix} N_1 & N_2 & N_3 & N_4 \end{bmatrix} \begin{Bmatrix} T_1 \\ T_2 \\ T_3 \\ T_4 \end{Bmatrix} = [N]\{T\} \tag{3-23}$$

[*N*] is shape function and [*T*] is node temperature.

$$\delta\theta = [N]\{\delta T\} \qquad \frac{\partial \bar{\theta}}{\partial x} = \left[\frac{\partial N}{\partial x}\right]\{T\} \qquad \frac{\partial \bar{\theta}}{\partial t} = [N]\left\{\frac{\partial T}{\partial t}\right\} \tag{3-24}$$

Substituting Equation (3-23) and (3-24) into Equation (3-22), we have

$$\{\delta T\}^T \iint \rho c [N]^T [T] dxdy \left[\frac{\partial T}{\partial t}\right] + \{\delta T\}^T k \left\{ \iint \left( \left[\frac{\partial N}{\partial x}\right]^T \left[\frac{\partial N}{\partial x}\right] + \left[\frac{\partial N}{\partial y}\right]^T \left[\frac{\partial N}{\partial y}\right] \right) dxdy \right\} \{T\}$$

$$= -\{\delta T\}^T \left\{ \oint_S q_x n_x [N]^T ds + \oint_S q_y n_y [N]^T ds \right\} \tag{3-25}$$

Then dividing Equation (3-25) by $\{\delta T\}^T$, we have the heat conduction equation as:

$$\iint \rho c [N]^T [T] dxdy \left[\frac{\partial T}{\partial t}\right] + k \left\{ \iint \left( \left[\frac{\partial N}{\partial x}\right]^T \left[\frac{\partial N}{\partial x}\right] + \left[\frac{\partial N}{\partial y}\right]^T \left[\frac{\partial N}{\partial y}\right] \right) dxdy \right\} \{T\}$$

$$= -\oint_S q_x n_x [N]^T ds - \oint_S q_y n_y [N]^T ds \tag{3-26}$$

And here we assume that,

$$\left[\frac{\partial N}{\partial x}\right]^T \left[\frac{\partial N}{\partial x}\right] + \left[\frac{\partial N}{\partial y}\right]^T \left[\frac{\partial N}{\partial y}\right]$$

$$= \begin{bmatrix} \frac{\partial N_1}{\partial x} \\ \frac{\partial N_2}{\partial x} \\ \frac{\partial N_3}{\partial x} \\ \frac{\partial N_4}{\partial x} \end{bmatrix} \begin{bmatrix} \frac{\partial N_1}{\partial x} & \frac{\partial N_2}{\partial x} & \frac{\partial N_3}{\partial x} & \frac{\partial N_4}{\partial x} \end{bmatrix} + \begin{bmatrix} \frac{\partial N_1}{\partial y} \\ \frac{\partial N_2}{\partial y} \\ \frac{\partial N_3}{\partial y} \\ \frac{\partial N_4}{\partial y} \end{bmatrix} \begin{bmatrix} \frac{\partial N_1}{\partial y} & \frac{\partial N_2}{\partial y} & \frac{\partial N_3}{\partial y} & \frac{\partial N_4}{\partial y} \end{bmatrix}$$

$$= \begin{bmatrix} \frac{\partial N_1}{\partial x} & \frac{\partial N_1}{\partial y} \\ \frac{\partial N_2}{\partial x} & \frac{\partial N_2}{\partial y} \\ \frac{\partial N_3}{\partial x} & \frac{\partial N_3}{\partial y} \\ \frac{\partial N_4}{\partial x} & \frac{\partial N_4}{\partial y} \end{bmatrix} \begin{bmatrix} \frac{\partial N_1}{\partial x} & \frac{\partial N_2}{\partial x} & \frac{\partial N_3}{\partial x} & \frac{\partial N_4}{\partial x} \\ \frac{\partial N_1}{\partial y} & \frac{\partial N_2}{\partial y} & \frac{\partial N_3}{\partial y} & \frac{\partial N_4}{\partial y} \end{bmatrix} = [B]^T [B]$$

Finally Equation (3-26) can be simplified as below:

$$\iint \rho c\left[N\right]^T\left[N\right]dxdy\left[\frac{\partial T}{\partial t}\right]+k\left\{\iint\left[B\right]^T\left[B\right]dxdy\right\}\left\{T\right\}=\left\{f\right\} \tag{3-27}$$

Here $\left\{f\right\}=-\oint_S q_x n_x\left[N\right]^T ds-\oint_S q_y n_y\left[N\right]^T ds$

### 3.1.2 The Application of Numerical Integration

In the previous section, we obtain the FEM equation for heat transfer. However, there are some integration operations in that equation (Equation (3-27)); we need to transfer that integration operation into a simple and convenient form for numerical calculation. Numerical Integration is a good method to convert integration into arithmetic operation. And in this research, Gaussian Quadrature is adopted to realize our object. Details are provided in the following:

The range of integration is between -1 and +1, and the most obvious way of obtaining the integral for two dimensions

$$I=\int_{-1}^{1}\int_{-1}^{1} f(\xi,\eta)d\xi d\eta \tag{3-28}$$

is first to evaluate the inner integral keeping $\eta$ constant, i.e.,

$$\int_{-1}^{1} f(\xi,\eta)d\xi=\sum_{j=1}^{n} f\left(\xi_j,\eta\right)w_j=\psi(\eta) \tag{3-29}$$

Evaluating the outer integral in a similar manner, we have

$$I=\int_{-1}^{1}\psi(\eta)\,d\eta=\sum_{i=1}^{n}\psi(\eta_i)w_i=\sum_{i=1}^{n}w_i\sum_{j=1}^{n}f\left(\xi_j,\eta_i\right)w_j=\sum_{i=1}^{n}\sum_{j=1}^{n}f\left(\xi_j,\eta_i\right)w_i w_j \tag{3-30}$$

where $\xi$, $\eta$ are Gaussian quadrature abscissae and $w$ is the corresponding weights, $n$ is the number of calculation nodes.

Numerical integration is very helpful because you do not need to INTEGRATE the equations. Instead, you just need to sum up all the terms in the equations. But for numerical integration, the integral domain is defined from -1 to 1. This is totally different our original problem. Hence, here we need some skills to transfer it.

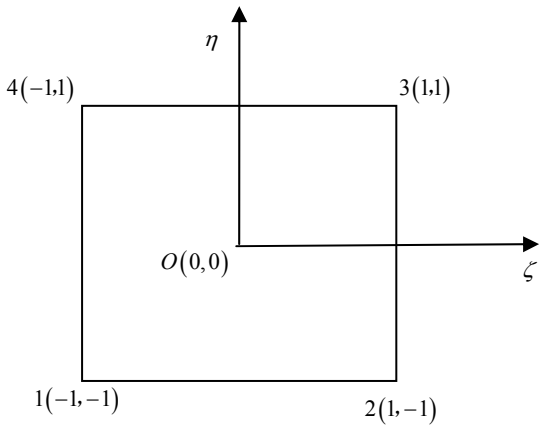



Figure 3-2 Linear square element in $\zeta$-$\eta$ coordinates

In Figure 3-2, the shape function could be expressed as follows:

$$N_1 = \frac{1}{4}(1-\zeta)(1-\eta) \qquad N_2 = \frac{1}{4}(1+\zeta)(1-\eta)$$
$$N_3 = \frac{1}{4}(1+\zeta)(1+\eta) \qquad N_4 = \frac{1}{4}(1-\zeta)(1+\eta)$$

And then,

$$\frac{\partial N}{\partial \zeta} = \frac{\partial N}{\partial x}\frac{\partial x}{\partial \zeta} + \frac{\partial N}{\partial y}\frac{\partial y}{\partial \zeta},\ \frac{\partial N}{\partial \eta} = \frac{\partial N}{\partial x}\frac{\partial x}{\partial \eta} + \frac{\partial N}{\partial y}\frac{\partial y}{\partial \eta}$$

The matrix form:

$$\begin{bmatrix} \frac{\partial N}{\partial \zeta} \\ \frac{\partial N}{\partial \eta} \end{bmatrix} = \begin{bmatrix} \frac{\partial x}{\partial \zeta} & \frac{\partial y}{\partial \zeta} \\ \frac{\partial x}{\partial \eta} & \frac{\partial y}{\partial \eta} \end{bmatrix} \begin{bmatrix} \frac{\partial N}{\partial x} \\ \frac{\partial N}{\partial y} \end{bmatrix}$$

Here $x = \sum_{i=1}^{4} N_i(\zeta,\eta)x_i, y = \sum_{i=1}^{4} N_i(\zeta,\eta)y_i$

$$B(x,y)=\begin{bmatrix}\dfrac{\partial N(\zeta,\ \eta)}{\partial x}\\ \dfrac{\partial N(\zeta,\ \eta)}{\partial y}\end{bmatrix}=\begin{bmatrix}\sum_{i=1}^{4}\dfrac{\partial N_i(\zeta,\ \eta)}{\partial \zeta}x_i & \sum_{i=1}^{4}\dfrac{\partial N_i(\zeta,\ \eta)}{\partial \zeta}y_i\\ \sum_{i=1}^{4}\dfrac{\partial N_i(\zeta,\ \eta)}{\partial \eta}x_i & \sum_{i=1}^{4}\dfrac{\partial N_i(\zeta,\ \eta)}{\partial \eta}y_i\end{bmatrix}^{-1}\begin{bmatrix}\dfrac{\partial N(\zeta,\ \eta)}{\partial \zeta}\\ \dfrac{\partial N(\zeta,\ \eta)}{\partial \eta}\end{bmatrix}=J^{-1}\begin{bmatrix}\dfrac{\partial N(\zeta,\ \eta)}{\partial \zeta}\\ \dfrac{\partial N(\zeta,\ \eta)}{\partial \eta}\end{bmatrix}$$

$$J=\begin{bmatrix}\sum_{i=1}^{4}\dfrac{\partial N_i(\zeta,\ \eta)}{\partial \zeta}x_i & \sum_{i=1}^{4}\dfrac{\partial N_i(\zeta,\ \eta)}{\partial \zeta}y_i\\ \sum_{i=1}^{4}\dfrac{\partial N_i(\zeta,\ \eta)}{\partial \eta}x_i & \sum_{i=1}^{4}\dfrac{\partial N_i(\zeta,\ \eta)}{\partial \eta}y_i\end{bmatrix}$$

And $dxdy=\det|J|\,d\zeta d\eta$ , then Equation (3-27) becomes,

$$\int_{-1}^{1}\int_{-1}^{1}\rho c\left[N(\zeta,\eta)\right]^T\left[N(\zeta,\eta)\right]\det|J|\,d\zeta d\eta\left\{\frac{\partial T}{\partial t}\right\}+\int_{-1}^{1}\int_{-1}^{1}k\left[J^{-1}B(\zeta,\eta)\right]^T\left[J^{-1}B(\zeta,\eta)\right]\det|J|\,d\zeta d\eta\{T\}=\{f\} \quad (3\text{-}31)$$

Now Equation (3-31) could be integrated by numerical integration because we have already transfer the integral domain to -1 and 1.

### 3.1.3 Finite Difference Method for Time Domain

Equation (3-31) can be expressed as:

$$\int_{-1}^{1}\int_{-1}^{1}\rho c\left[N(\zeta,\eta)\right]^T\left[N(\zeta,\eta)\right]\det|J|\,d\zeta d\eta\begin{Bmatrix}\dfrac{\partial T_1}{\partial t}\\ \vdots\\ \dfrac{\partial T_n}{\partial t}\end{Bmatrix}+\int_{-1}^{1}\int_{-1}^{1}k\left[J^{-1}B(\zeta,\eta)\right]^T\left[J^{-1}B(\zeta,\eta)\right]\det|J|\,d\zeta d\eta\begin{Bmatrix}T_1\\ \vdots\\ T_n\end{Bmatrix}=\begin{Bmatrix}f_1\\ \vdots\\ f_n\end{Bmatrix} \quad (3\text{-}32)$$

Here:

$$[M]=\rho c\int_{-1}^{1}\int_{-1}^{1}\left[N(\zeta,\eta)\right]^T\left[N(\zeta,\eta)\right]\det|J|\,d\zeta d\eta$$

$$[K]=\int_{-1}^{1}\int_{-1}^{1} k\left[J^{-1}B(\zeta,\eta)\right]^{T}\left[J^{-1}B(\zeta,\eta)\right]\det|J|\,d\zeta\,d\eta$$

Then Equation (3-32) can be expressed:

$$[M]\{\dot{T}\}+[K]\{T\}=\{f\} \tag{3-33}$$

We begin by assuming that two temperature states $T_i$ and $T_{i+1}$ at time $t_i$ and $t_{i+1}$ are related by

$$T_{i+1}=T_i+\left[(1-\beta)\dot{T}_i+\beta\dot{T}_{i+1}\right](\Delta t) \tag{3-34}$$

Equation (3-34) is known as the *generalized trapezoid rule*.

We now write Equation (3-33) for time $t_i$ and $t_{i+1}$. We then multiply the first of these two equations by $(1-\beta)$ and the second by $\beta$ to obtain:

$$(1-\beta)(KT_i+M\dot{T}_i)=(1-\beta)f_i$$
$$\beta(KT_{i+1}+M\dot{T}_{i+1})=\beta f_{i+1}$$

And then we add these equations together to obtain:

$$M\left[(1-\beta)\dot{T}_i+\beta\dot{T}_{i+1}\right]+K\left[(1-\beta)T_i+\beta T_{i+1}\right]=(1-\beta)f_i+\beta f_{i+1} \tag{3-35}$$

Apply the generalized trapezoid rule to replace the first item:

$$M\frac{T_{i+1}-T_i}{\Delta t}+K\left[(1-\beta)T_i+\beta T_{i+1}\right]=(1-\beta)f_i+\beta f_{i+1} \tag{3-36}$$

Rewriting Equation (3-36), we can get:

$$\left(\frac{1}{\Delta t}M+\beta K\right)T_{i+1}=\left[\frac{1}{\Delta t}M-(1-\beta)K\right]T_i+(1-\beta)f_i+\beta f_{i+1} \tag{3-37}$$

Here $\Delta t$ is the time increment, $\beta$ is a parameter controlling to different finite difference method for time domain. When $\beta$=0, it is forward difference method, when $\beta$=0.5, it is Crank-Nicolson method, when $\beta$=1, it is backward difference method. Here $0 \leq \beta \leq 1$. And in this paper the Crank-Nicolson method is adopted.

The following matrix is used to show the boundary condition for matrix. We assume that the displacement at node 2 is fixed as *b*. And then the matrix should be dealt as the following:

$$\begin{bmatrix} K_{11} & 0 & K_{13} & K_{14} & K_{15} & K_{16} \\ 0 & 1 & 0 & 0 & 0 & 0 \\ K_{31} & 0 & K_{33} & K_{34} & K_{35} & K_{36} \\ K_{41} & 0 & K_{43} & K_{44} & K_{45} & K_{46} \\ K_{51} & 0 & K_{53} & K_{54} & K_{55} & K_{56} \\ K_{61} & 0 & K_{63} & K_{64} & K_{65} & K_{66} \end{bmatrix} \begin{Bmatrix} u_1 \\ u_2 \\ u_3 \\ u_4 \\ u_5 \\ u_6 \end{Bmatrix} = \begin{Bmatrix} f_1 - bK_{12} \\ b \\ f_3 - bK_{32} \\ f_4 - bK_{42} \\ f_5 - bK_{52} \\ f_6 - bK_{62} \end{Bmatrix}$$

### 3.2 HEAT TRANSFER WITH CONVECTION (WITH WATER FLOW)

If the heat brought by water flow is considered, the governing equation should be like:

$$\rho c \frac{\partial \theta}{\partial t} = k\left( \frac{\partial^2 \theta}{\partial x^2} + \frac{\partial^2 \theta}{\partial y^2} \right) - \rho_w c_w \left( \nabla u \theta_w \right) \tag{3-38}$$

Here $u$ means the water flux and $\theta_w$ is the temperature of water. And according to the Partial derivative rule, we know that:

$$\nabla u \theta_w = u \nabla \theta_w + \theta_w \nabla u \tag{3-39}$$

And if we adopt the linear shape function for the hydraulic calculation, it is easy to know that $u = -k \frac{\partial h}{\partial x}$ and $\nabla u = 0$. Thus, $\nabla u \theta_w = u \nabla \theta_w$.

Here k is the coefficient of permeability or hydraulic conductivity, h is the total head (hydraulic head). However, in this equation, there are two different temperatures, soil mixture temperature and flow water temperature. The relationship between these two different temperatures is shown as the following figure. And we assume that when the water flow around the soil particle, the heat transfer between soil and flow water completes instantaneously. Therefore, we can regard $\theta_w = \theta$

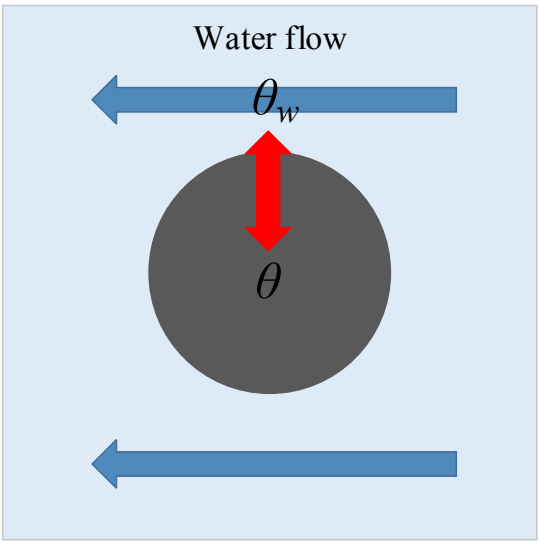



Figure 3-3 Heat transfer when water flow around soil particle

Then Equation (3-38) could be rewritten as:

$$\rho c\frac{\partial \theta}{\partial t}=k\left(\frac{\partial^2 \theta}{\partial x^2}+\frac{\partial^2 \theta}{\partial y^2}\right)-\rho_w c_w u\nabla\theta \tag{3-40}$$

Then apply the Galerkin method to each term in Equation (3-40):

$$\iint \rho_w c_w u\nabla\theta\,\delta\theta dxdy = k\rho_w c_w \iint u\nabla\theta\,\delta\theta dxdy$$

$$k\rho_w c_w \iint u\nabla\theta\,\delta\theta dxd = -k\rho_w c_w \iint \left[\frac{\partial N}{\partial x}\right][h]\left[\frac{\partial N}{\partial x}\right][T][N][\delta T]dxdy$$

$$k\rho_w c_w \iint \left[\frac{\partial N}{\partial x}\right][h]\left[\frac{\partial N}{\partial x}\right][T][N][\delta T]dxdy = k\rho_w c_w [\delta T]^T \iint [h]\left[\frac{\partial N}{\partial x}\right]\left[\frac{\partial N}{\partial x}\right]^T [N]dxdy[T]$$

$$K_c = k\rho_w c_w [\delta T]^T \iint [h]\left[\frac{\partial N}{\partial x}\right]\left[\frac{\partial N}{\partial x}\right]^T [N]dxdy[T]$$

Other part is the same with the calculation of heat transfer without water flow. The governing equation can be expressed as:

$$[M]\{\dot{T}\}+[K]\{T\}-[K_c]\{T\}=\{f\} \tag{3-41}$$

$$\left(\frac{1}{\Delta t}M+\beta(K-K_c)\right)T_{i+1}=\left(\frac{1}{\Delta t}M-(1-\beta)(K-K_c)\right)T_i+(1-\beta)f_i+\beta f_{i+1} \tag{3-42}$$

### 3.3 INFLUENCE OF LATENT HEAT

Latent heat is the name given to energy which is either lost or gained by a substance when it changes state, for example from water to ice. It is measured as an amount of energy, joules, rather than as a temperature. In the real situation, the influence of latent heat cannot be neglected. And in this paper we calculate latent heat by Equivalent Heat Capacity method. In some extent, latent heat slows the rate of temperature change. The basic idea is to establish the additional heat capacity equivalent to the influence of latent heat during the phase change.

We express the solid phase limit temperature as $T_S$ (if temperature is lower than $T_S$, soil could be considered as fully frozen) and the liquid phase limit temperature as $T_L$. In our paper, we consider the water as pure fresh water. It will be frozen at the temperature $T_L$ which is 0°C. And as widely known, in the finely porous material, unfrozen water exists even if the temperature is slightly lower than 0°C. As the temperature decreases, the content of unfrozen water also decreases. In this study, if the temperature is lower than $T_S$, we argue that unfrozen water content does not change anymore and this element could be regarded as totally frozen. Also between this two values $T_L$ and $T_S$, the latent heat is considered due to phase change of water. $T_S$ is usually decided by the experiment which can obverse the relationship between temperature and water content. As to the materials used in this paper, −0.5 °C is a widely accepted value[10]. In addition, the latent heat of the water is expressed as $L$ and the weight of the water in the unit volume soil is expressed as $m_w$. And $m_w=\theta\times\rho_w$ , $\rho_w$ is the density of water and $\theta$ is the volumetric water content at the beginning. The soil mixture heat capacity is $c_1\rho$ (without latent heat) is increased to the equivalent heat capacity, $\rho c_2$, owing to the influence of latent heat when the temperature is between $T_S$ and $T_L$. Here, $c_2$ is the equivalent characteristic heat of the soil mixture:

$$\int_{T_s}^{T_L} c_2\rho dT=Lm_w+\int_{T_s}^{T_L} c_1\rho dT \tag{3-43}$$

$$c_2\rho=\frac{Lm_w}{T_L-T_s}+c_1\rho \tag{3-44}$$

As a result, the equivalent heat capacity method defines the relation between the heat capacity of soil and its temperature as Figure 3-4.

$$\rho c_2 \left(T_L - T_{t+\Delta t}\right) = \rho c_1 \left(T_L - T'\right)$$
$$T_{t+\Delta t} = T_L - \frac{c_1}{c_2}\left(T_L - T'\right) \tag{3-45}$$

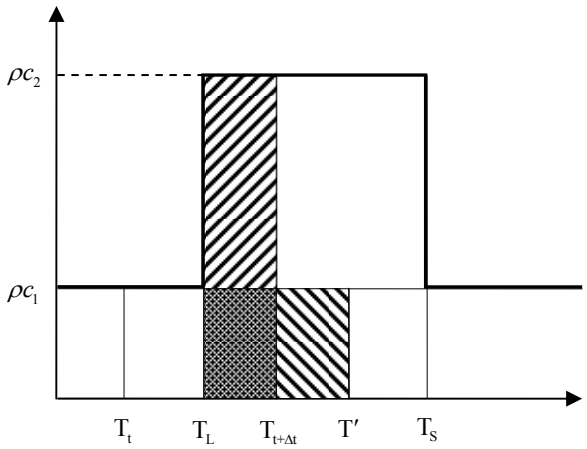



Figure 3-4 Equivalent heat capacity method

### 3.4 FREEZING DIRECTION AND RATE

As shown in Figure 3-5, if the temperature of the middle point of the element $\theta_t > T_S$(-0.5℃) and after $\Delta t$, $\theta_{t+\Delta t} \leqq T_S$(-0.5℃), we can consider this element is frozen. And the rate of temperature change in $x$ direction and $y$ direction are $\partial\theta/\partial x$ and $\partial\theta/\partial y$ respectively, therefore the freezing direction can be defined:

$$\alpha = \tan^{-1}\frac{\partial\theta/\partial y}{\partial\theta/\partial x} \tag{3-46}$$

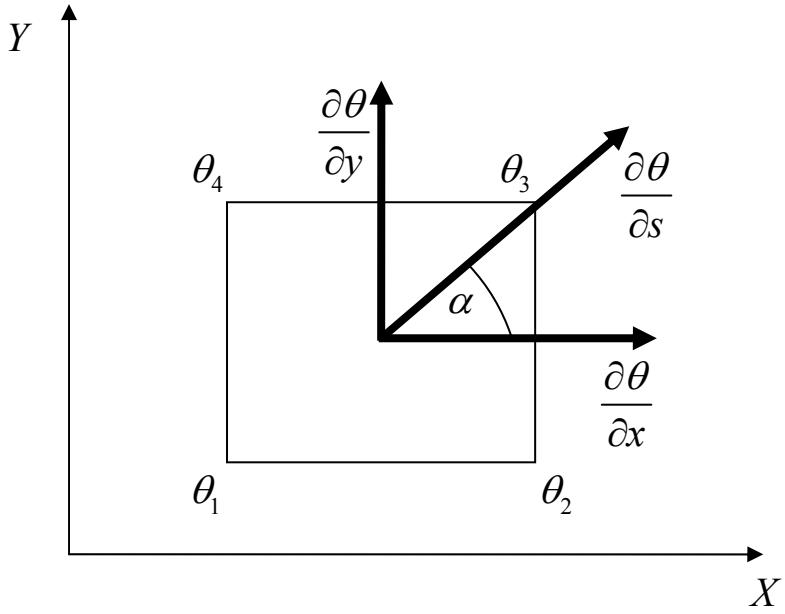



Figure 3-5 The freezing direction calculation diagram

As shown in Figure 3-6, the location change rate in freezing direction is given by the following:

$$\frac{\partial\theta}{\partial s}=\sqrt{\left(\frac{\partial\theta}{\partial x}\right)^2+\left(\frac{\partial\theta}{\partial y}\right)^2} \tag{3-47}$$

And the freezing distance is

$$\Delta s=\frac{\theta_t-\theta_{t+\Delta t}}{\frac{\partial\theta}{\partial s}} \tag{3-48}$$

And velocity equals to distance dived by time.

$$U=\frac{\Delta s}{\Delta t} \tag{3-49}$$

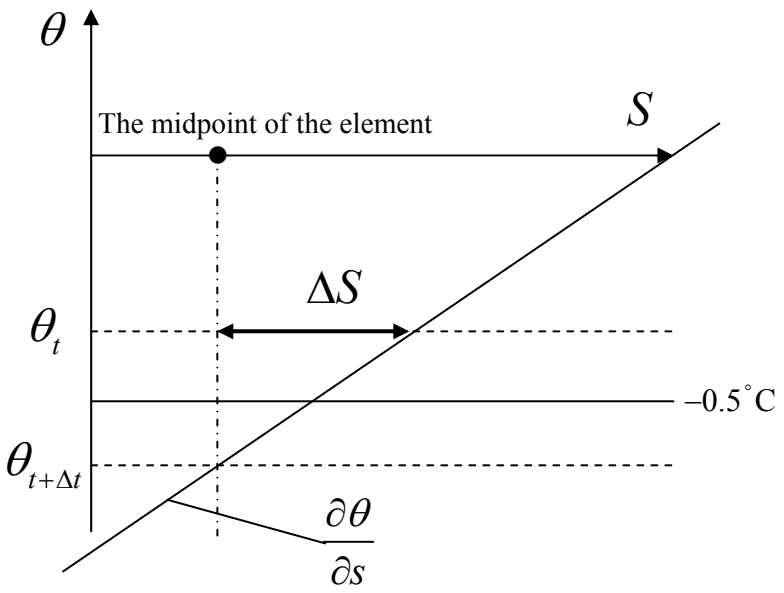



Figure 3-6 The freezing rate calculation diagram

### 3.5 VALIDATION EXAMPLES

In this section, the numerical calculation of heat transfer is given to validate our model and program. First a one element example is used. The calculations of FEM program and FEM Excel are compared. The size of this element is 1m×1m, the Crank-Nicolson method is applied for the time domain, and the time interval is 1 second. The material parameters are shown in the table:

Table 3-1 Parameters for one element model

| | |
|---|---|
| Thermal conductivity: $k$ | 1 [J/m.K.s] |
| Specific heat capacity: $c$ | 1 [J/kg.K] |
| Density: $\rho$ | 1 [kg/ $m^3$] |

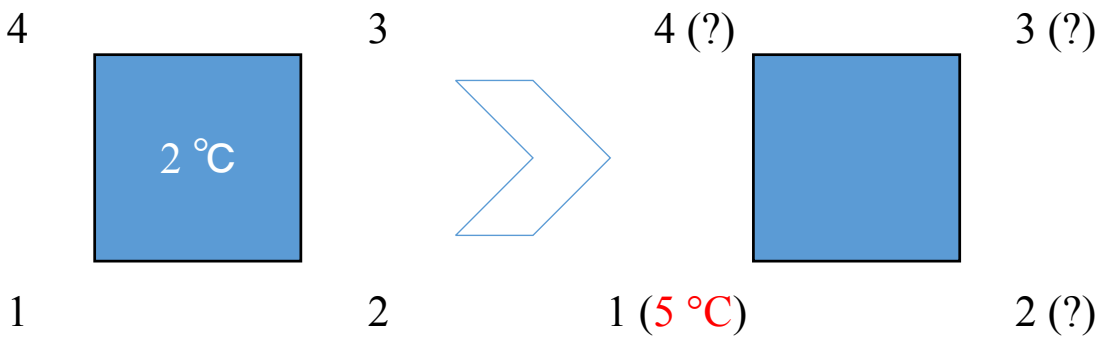



Figure 3-7 One element example for thermal validation

And then compare the temperature change at node 3. With the help of Excel, we do the same heat transfer calculation by hand. We find that result based on FORTRAN program is the same with Excel one. In fact, at the other nodes, node2 and node 4, the same situation happens.

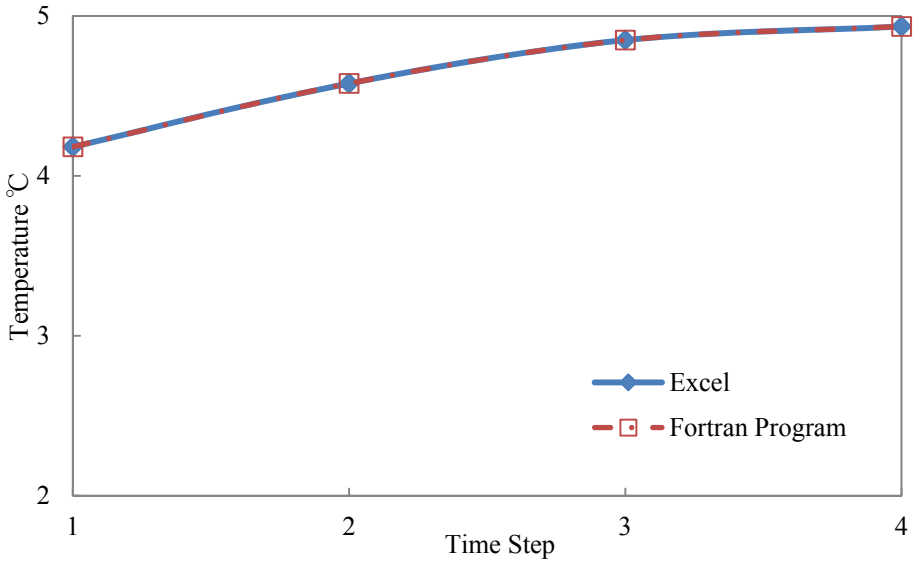



Figure 3-8 The comparison between program and excel results

Although, this example is very simple, it validates that our numerical calculation of heat transfer is reliable. The detail of Excel calculation process is not give here. It strictly follows the FEM idea and deals matrix by Excel. In addition, the temperature range of this example is between 2 and 5 degree. There is no phase change occurs during the whole calculation period. Thus, latent heat does not work under this situation. In the following, an example considering latent heat is illustrated.

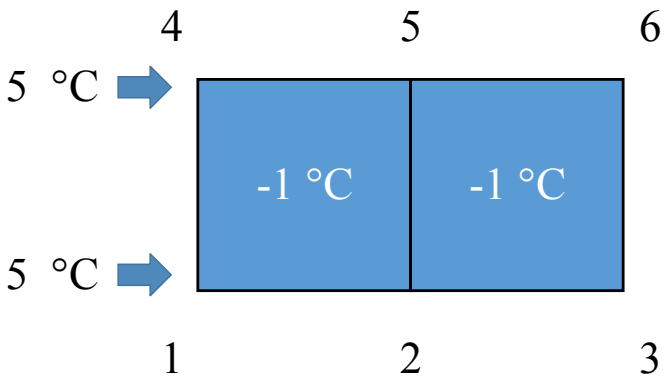



Figure 3-9 Two elements example for latent heat influence

The size of this example is 2cm × 1 cm and the initial temperature is -1 °C and then apply a warm temperature at the left side, what we are doing is to obverse the influence of latent heat to temperature change history. The detail thermal parameters are shown in the following Tables:

Table 3-2 Parameters for two elements model

| | |
|---|---|
| Thermal conductivity: $k$ | 1 [J/m.K.s] |
| Specific heat capacity: $c$ | 800 [J/kg.K] |
| Density: $\rho$ | 2000 [kg/ $m^3$] |
| Water content: | 0.3 |

The following figure (Figure 3-10) presents the time history of temperature change at node 6 and compares the influence of latent heat. According to this figure, we note that when latent heat is taken into account, the heat transfer process is delayed compared to the no latent heat situation. In addition, one interesting phenomenon is that if we check the temperature change curve with latent heat, we can find that the temperature change slope when temperature is between -1°C to -0.5 °C is different with that when temperature is between -0.5°C and 0°C. This is caused by the different heat capacity before and after phase change occurs. Further, the heat transfer speed increases a lot when the temperature is higher than 0°C. That indicates that after the node 6's temperature is higher than 0°C no phase change anymore, and therefore temperature changes faster. Please refer to the following equation:

$$c_2\rho = \frac{Lm_w}{T_L - T_s} + c_1\rho \tag{3-50}$$

This equation describes that when phase change occurs, the heat capacity would be increased to simulate the influence of latent heat. $\rho c$ will be increased to $\rho c_2$ by the amount of latent heat influence. Of course a larger heat capacity would slow the heat transfer speed. After temperature goes through

that phase, there is no phase change anymore; therefore latent heat influence will not be considered again.

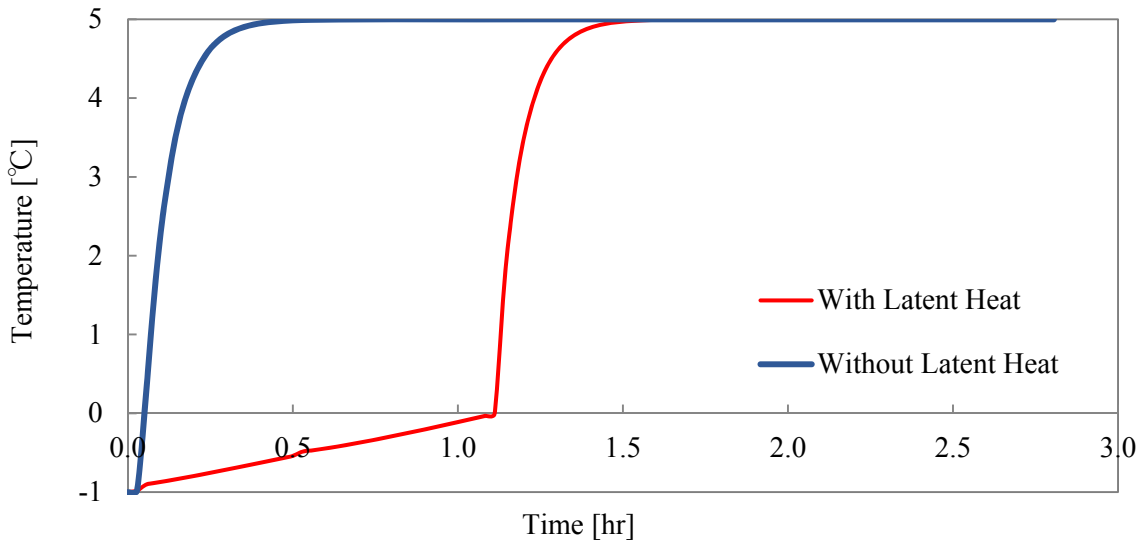



Figure 3-10 The temperature change history of two elements model

Based on these two simple but meaningful examples, we confirm that our numerical program performs well at the calculation of thermal analysis.

## 4. MECHANICAL ANALYSIS

In this section, the mechanical analysis is described from the basic governing equation. Meanwhile, the mechanical analysis combines the frost heave ratio calculated by Takashi's equation. The main purpose of mechanical analysis is: first, calculate the constraining stress in freezing direction; second, evaluate the stress influence brought by frost heave. Then experiment comparison is provided to confirm the simulation accuracy of our model. Finally, a preliminary study of 3D frost heave is introduced.

### 4.1 2D EQUILIBRIUM EQUATION

In Figure 4-1, the equilibrium condition of two dimension element is shown. In this small element 1234, the stresses in *x* direction are shown as solid lines and stresses in y direction are shown as dotted lines. The *X* in the element means the body force.

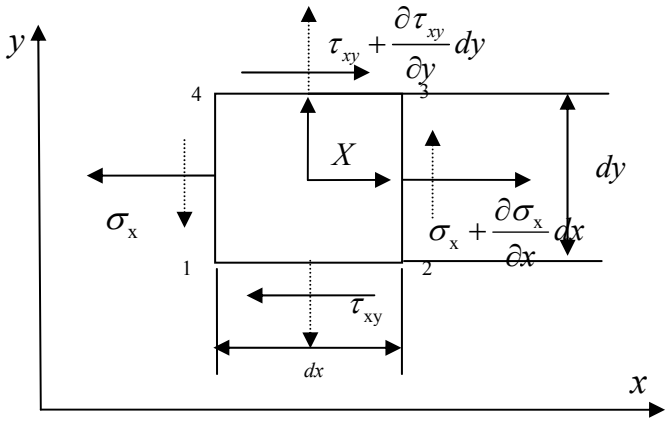



Figure 4-1 Two-dimensional state of stress

The balance in *x* direction is:

$$\left(\sigma_x+\frac{\partial \sigma_x}{\partial x}dx\right)dy-\sigma_x dy+\left(\tau_{xy}+\frac{\partial \tau_{xy}}{\partial y}dy\right)dx-\tau_{xy}dx+Xdxdy=0 \qquad (4\text{-}1)$$

And it can be simplified as:

$$\frac{\partial \sigma_x}{\partial x} + \frac{\partial \tau_{xy}}{\partial y} + X = 0 \tag{4-2}$$

Similarly,

$$\frac{\partial \sigma_y}{\partial y} + \frac{\partial \tau_{xy}}{\partial x} + Y = 0 \tag{4-3}$$

Those are called as Differential Equation of Equilibrium.

## 4.2 THE APPLICATION OF FEM TO MECHANICAL ANALYSIS

For the above equation, we assume a virtual displacement $(\delta u, \delta v)$ and then apply integration:

$$\int_A \left( \frac{\partial \sigma_x}{\partial x} + \frac{\partial \tau_{xy}}{\partial y} + X \right) \delta u dA + \int_A \left( \frac{\partial \sigma_y}{\partial y} + \frac{\partial \tau_{xy}}{\partial x} + Y \right) \delta v dA = 0 \tag{4-4}$$

Then expand this equation as the following form:

$$\int_A \frac{\partial \sigma_x}{\partial x} \delta u dA + \int_A \frac{\partial \tau_{xy}}{\partial y} \delta u dA + \int_A \frac{\partial \sigma_y}{\partial y} \delta v dA + \int_A \frac{\partial \tau_{xy}}{\partial x} \delta v dA + \int_A \left( X \delta u + Y \delta v \right) dA = 0 \tag{4-5}$$

Applying Green's Theorem for the first term of this equation:

$$\int_A \frac{\partial \sigma_x}{\partial x} \delta u dA = \oint_S \sigma_x \delta u \, l \, ds - \int_A \sigma_x \frac{\partial \delta u}{\partial x} dA \tag{4-6}$$

$$\int_A \frac{\partial \tau_{xy}}{\partial y} \delta u dA = \oint_S \tau_{xy} \delta u \, m \, ds - \int_A \tau_{xy} \frac{\partial \delta u}{\partial y} dA \tag{4-7}$$

$$\int_A \frac{\partial \sigma_y}{\partial y} \delta v dA = \oint_S \sigma_y \delta v \, m \, ds - \int_A \sigma_y \frac{\partial \delta v}{\partial y} dA \tag{4-8}$$

$$\int_A \frac{\partial \tau_{xy}}{\partial x} \delta v dA = \oint_S \tau_{xy} \delta v \, l \, ds - \int_A \tau_{xy} \frac{\partial \delta v}{\partial x} dA \tag{4-9}$$

And then substitute these four terms into the original equation:

$$\begin{aligned}&\int_S \left(\sigma_x l + \tau_{xy} m\right)\delta u\, dS + \int_S \left(\sigma_y m + \tau_{xy} l\right)\delta v\, dS + \int_A \left(X\delta u + Y\delta v\right)dA \\ &= \int_A \left[\sigma_x \frac{\partial \delta u}{\partial x} + \sigma_y \frac{\partial \delta v}{\partial y} + \tau_{xy}\left(\frac{\partial \delta v}{\partial x} + \frac{\partial \delta u}{\partial y}\right)\right]dA\end{aligned} \tag{4-10}$$

Here, the surface force could be expressed as:

$$\begin{aligned}\overline{X}_v &= \sigma_x l + \tau_{xy} m \\ \overline{Y}_v &= \sigma_y m + \tau_{xy} l\end{aligned} \tag{4-11}$$

$$\begin{aligned}\frac{\partial \delta u}{\partial x} &= \delta \frac{\partial u}{\partial x} = \delta\varepsilon_x \\ \frac{\partial \delta v}{\partial y} &= \delta \frac{\partial v}{\partial y} = \delta\varepsilon_y\end{aligned} \tag{4-12}$$

Therefore,

$$\frac{\partial \delta v}{\partial x} + \frac{\partial \delta u}{\partial y} = \delta\left(\frac{\partial v}{\partial x}\right) + \delta\left(\frac{\partial u}{\partial y}\right) = \delta\left(\frac{\partial v}{\partial x} + \frac{\partial u}{\partial y}\right) = \delta\gamma_{xy} \tag{4-13}$$

Then the equation could be rewritten as:

$$\begin{aligned}&\int_S \overline{X}_v \delta u\, dS + \int_S \overline{Y}_v \delta v\, dS + \int_A \left(X\delta u + Y\delta v\right)dA \\ &= \int_A \left[\sigma_x \delta\varepsilon_x + \sigma_y \delta\varepsilon_y + \tau_{xy}\delta\gamma_{xy}\right]dA\end{aligned} \tag{4-14}$$

And then,

$$\{\varepsilon\} = \left[\varepsilon_x \;\; \varepsilon_y \;\; \gamma_{xy}\right]^T \tag{4-15}$$

$$\{\sigma\} = \left[\sigma_x \;\; \sigma_y \;\; \tau_{xy}\right]^T \tag{4-16}$$

$$\{u\} = \left[u \;\; v\right]^T \tag{4-17}$$

$$\{X\} = \left[X \;\; Y\right]^T \tag{4-18}$$

$$\{\Phi\} = \left[\overline{X}_v \;\; \overline{Y}_v\right]^T \tag{4-19}$$

$$\int_S \{\Phi\}^T \delta\{u\} dS + \int_A \{X\}^T \delta\{u\} dA = \int_A \{\sigma\}^T \delta\{\varepsilon\} dA \tag{4-20}$$

$$\int_S \{\Phi\}^T \delta\{u(x,y)\} dS + \int_A \{X\}^T \delta\{u(x,y)\} dA = \int_A \{\sigma\}^T \delta\{\varepsilon(x,y)\} dA \tag{4-21}$$

And here,

$$\delta\{u(x,y)\} = [N]\{\delta u\} \tag{4-22}$$

$$\delta\{\varepsilon\} = \left[\frac{\partial N}{\partial x}\right]\{\delta u\} \tag{4-23}$$

$$\int_S \delta\{u\}^T [N]^T \{\Phi\} dS + \int_A \delta\{u\}^T [N]^T \{X\} dA = \int_A \delta\{\varepsilon\}^T \{\sigma\} dA = \int_A \delta\{u\}^T \left[\frac{\partial N}{\partial x}\right]^T \{\sigma\} dA \tag{4-24}$$

And in this equation, $\delta\{u\}^T$ is a constant, thus we can delete it. Therefore, the above equation could be summarized as:

$$\int_S [N]^T \{\Phi\} dS + \int_A [N]^T \{X\} dA = \int_A \left[\frac{\partial N}{\partial x}\right]^T \{\sigma\} dA \tag{4-25}$$

And $\{\sigma\} = [E]\{\varepsilon\} = [E]\left[\frac{\partial N}{\partial x}\right]\{u\}$, so the equation could be rewritten as:

$$\int_S [N]^T \{\Phi\} dS + \int_A [N]^T \{X\} dA = \int_A \left[\frac{\partial N}{\partial x}\right]^T [E]\left[\frac{\partial N}{\partial x}\right] dA\{u\} \tag{4-26}$$

And we assume that:

$$[K] = \int_A \left[\frac{\partial N}{\partial x}\right]^T [E]\left[\frac{\partial N}{\partial x}\right] dA \tag{4-27}$$

$$\{F_s\} = \int_S [N]^T \{\Phi\} dS \tag{4-28}$$

$$\{F_b\} = \int_A [N]^T \{X\} dA \tag{4-29}$$

Thus, the equation could be expressed as:

$$[K]\{u\} = \{F_s\} + \{F_b\} = \{F\} \tag{4-30}$$

In the following part, the detail of each matrix will be explained. The displacement vector in any point can be expressed as:

$$\{f(x,y)\} = \begin{Bmatrix} u(x,y) \\ v(x,y) \end{Bmatrix} = [N(x,y)]\{\delta(x,y)\} \tag{4-31}$$

Here $\delta$ is the node displacement, and $N$ is shape function.

$$\begin{Bmatrix} u(x,y) \\ v(x,y) \end{Bmatrix} = \begin{bmatrix} N_i & N_j & N_m & N_k \end{bmatrix} \begin{Bmatrix} \delta_i \\ \delta_j \\ \delta_m \\ \delta_k \end{Bmatrix} = \begin{bmatrix} N_i & 0 & N_j & 0 & N_m & 0 & N_k & 0 \\ 0 & N_i & 0 & N_j & 0 & N_m & 0 & N_k \end{bmatrix} \begin{Bmatrix} u_i \\ v_i \\ u_j \\ v_j \\ u_m \\ v_m \\ u_k \\ v_k \end{Bmatrix} \tag{4-32}$$

And the strain is expressed as:

$$\{\varepsilon\} = [B(x,y)]\{\delta(x,y)\} = \begin{bmatrix} \frac{\partial N_i}{\partial x} & 0 & \frac{\partial N_j}{\partial x} & 0 & \frac{\partial N_m}{\partial x} & 0 & \frac{\partial N_k}{\partial x} & 0 \\ 0 & \frac{\partial N_i}{\partial y} & 0 & \frac{\partial N_j}{\partial y} & 0 & \frac{\partial N_m}{\partial y} & 0 & \frac{\partial N_k}{\partial y} \end{bmatrix} \begin{Bmatrix} u_i \\ v_i \\ u_j \\ v_j \\ u_m \\ v_m \\ u_k \\ v_k \end{Bmatrix} \tag{4-33}$$

Next, the stress should be:

$$\{\sigma\} = [D](\{\varepsilon\} - \{\varepsilon_t\}) \tag{4-34}$$

Here $\varepsilon_t$ is the frost heave strain.

If it is plane stress condition assumption:

$$[D]=\frac{E}{1-v^2}\begin{bmatrix}1 & v & 0\\ v & 1 & 0\\ 0 & 0 & (1-v)/2\end{bmatrix} \tag{4-35}$$

If it is plane strain condition assumption:

$$[D]=\frac{E}{(1-v)(1-2v)}\begin{bmatrix}1-v & v & 0\\ v & 1-v & 0\\ 0 & 0 & (1-2v)/2\end{bmatrix} \tag{4-36}$$

In this research, the plain strain assumption is adopted in our FORTRAN program.

And then the node force is:

$$\{F\}=\begin{Bmatrix}F_i\\ F_j\\ F_m\\ F_k\end{Bmatrix}=\begin{Bmatrix}U_i\\ V_i\\ U_j\\ V_j\\ U_m\\ V_m\\ U_k\\ V_k\end{Bmatrix} \tag{4-37}$$

Virtual work equals to the virtual displacement multiplying force:

$$\left\{\delta^*\right\}^T\left\{F(x,y)\right\}=\begin{bmatrix}u_i^* & v_i^* & u_j^* & v_j^* & u_m^* & v_m^* & u_k^* & v_m^*\end{bmatrix}\begin{Bmatrix}U_i\\V_i\\U_j\\V_j\\U_m\\V_m\\U_k\\V_k\end{Bmatrix} \tag{4-38}$$

And

$$\left\{\varepsilon^*\right\}^T\left\{\sigma\right\}-\left\{f^*\right\}^T\left\{p\right\}=\left\{\delta^*\right\}^T\left[B\right]^T\left\{\sigma\right\}-\left\{\delta^*\right\}^T\left[N\right]^T\left\{p\right\}=\left\{\delta^*\right\}^T\left(\left[B\right]^T\left\{\sigma\right\}-\left[N\right]^T\left\{p\right\}\right) \tag{4-39}$$

Here $\left\{p\right\}=\begin{Bmatrix}p_x\\p_y\end{Bmatrix}=\rho\left[N(x,y)\right]\left\{\alpha\right\}$ is body force and $\rho$ is density and $\alpha$ is acceleration. And then make integration in the whole domain.

$$\left\{\delta^*\right\}^T\left(\int\left[B(x,y)\right]^T\left\{\sigma\right\}dV-\int\left[N(x,y)\right]^T\left\{p\right\}dV\right) \tag{4-40}$$

Based on the virtual work theory, we know that Equation (4-38) equals to Equation (4-40)

$$\left\{\delta^*\right\}^T\left\{F(x,y)\right\}=\left\{\delta^*\right\}^T\left(\int\left[B(x,y)\right]^T\left\{\sigma\right\}dV-\int\left[N(x,y)\right]^T\left\{p\right\}dV\right) \tag{4-41}$$

$$\begin{aligned}\left\{F(x,y)\right\}&=\int\left[B(x,y)\right]^T\left\{\sigma\right\}dV-\int\left[N(x,y)\right]^T\left\{p\right\}dV\\&=\int\left[B(x,y)\right]^T\left[D\right]\left(\left\{\varepsilon\right\}-\left\{\varepsilon_t\right\}\right)dV-\int\left[N(x,y)\right]^T\left\{p\right\}dV\\&=\int\left[B(x,y)\right]^T\left[D\right]\left[B(x,y)\right]dV\left\{\delta^*\right\}-\int\left[B(x,y)\right]^T\left[D\right]\left\{\varepsilon_t\right\}dV-\int\left[N(x,y)\right]^T\left\{p\right\}dV\end{aligned} \tag{4-42}$$

After the application of Numerical Integration, we can express Equation (4-42) as:

$$\begin{aligned}&\{F(x,y)\}\\&=\int_{-1}^{1}\int_{-1}^{1}\left[J^{-1}B(\varsigma,\eta)\right]^{T}[D]\left[J^{-1}B(\varsigma,\eta)\right]\det|J|\,d\varsigma d\eta\{\delta^{*}\}-\int_{-1}^{1}\int_{-1}^{1}\left[J^{-1}B(\varsigma,\eta)\right]^{T}[D]\{\varepsilon_t\}\det|J|\,d\varsigma d\eta\\&-\int_{-1}^{1}\int_{-1}^{1}\left[N(\varsigma,\eta)\right]^{T}\rho\left[N(\varsigma,\eta)\right]\det|J|\,d\varsigma d\eta\{\alpha\}\end{aligned}\tag{4-43}$$

Here

$$J=\begin{bmatrix}\sum_{i=1}^{4}\frac{\partial N_i(\varsigma,\eta)}{\partial\zeta}x_i & \sum_{i=1}^{4}\frac{\partial N_i(\varsigma,\eta)}{\partial\zeta}y_i\\ \sum_{i=1}^{4}\frac{\partial N_i(\varsigma,\eta)}{\partial\eta}x_i & \sum_{i=1}^{4}\frac{\partial N_i(\varsigma,\eta)}{\partial\eta}y_i\end{bmatrix}\tag{4-44}$$

Based on all these equations, the stress in any node should be:

$$\{\sigma\}=[D][B]\{\delta\}-[D]\{\varepsilon_t\}\tag{4-45}$$

The stress caused by frost heave should be:

$$\{\sigma_t\}=-[D]\{\varepsilon_t\}\tag{4-46}$$

## 4.3 FROST HEAVE AMOUNT VALIDATION

In this section, a 1D indoor frost heave experiment is simulated by our numerical model in order to demonstrate the accuracy of this numerical model.

The size of this soil sample is 150 mm × 60 mm. The sample is surrounded by an acrylic cylinder that can prevent horizontal expansion and also behaves as the insulation layer. The top pedestal is used as the cold side and the bottom pedestal is used as the warm side, a temperature control unit is installed in the pedestals. Water supply during the freezing process is provided from the bottom of the sample. At the top surface of the sample, a load applies a 62.5 kPa constraining stress to the sample; the frost heave displacement is measured from the top pedestal. The experimental equipment is shown in Figure 4-2. The initial temperature of the soil is maintained as 2°C. Temperature changes of both warm and cold sides are shown in Figure 4-3 ($T_W$ and $T_C$). In this experiment, the frost-susceptible soil Dotan is used as the soil sample. The meshing of the numerical model is shown in Figure 4-4 and the material parameters are listed in Table 4-1. The total number of nodes is 55 and the number of elements is 40;

hence, the size of each element is 15mm × 15mm. The total calculation period is 150 h and the time step is 10 s which are determined by the Courant number for time-step calculation. The initial temperature of the soil is 2°C, and the temperatures of the warm and cold sides are changed at each time step, as shown in Figure 4-3. The boundary conditions for this numerical model are shown in Figure 4-4. In the horizontal direction, displacement to the *X* direction is prevented and heat flow is forbidden at both sides. At the bottom boundary, displacement in the *Y* direction is fixed, and warm temperature is applied from the bottom. For the top surface of this model, displacement is free but a load is applied to simulate the constraining stress forced on the surface. In this model, 62.5 kPa is used as the limit for constraining stress. According to the boundary conditions, we can confirm that the freezing direction is from top to bottom, which would cause a frost heave on the top of this soil sample. Although a nonlinear Young's modulus is adopted in this paper, thermal analysis would not be affected by this nonlinear property. Because of the free boundary condition at the top surface, the stress condition is never changed; thus, the Young's modulus is never changed for unfrozen soil.

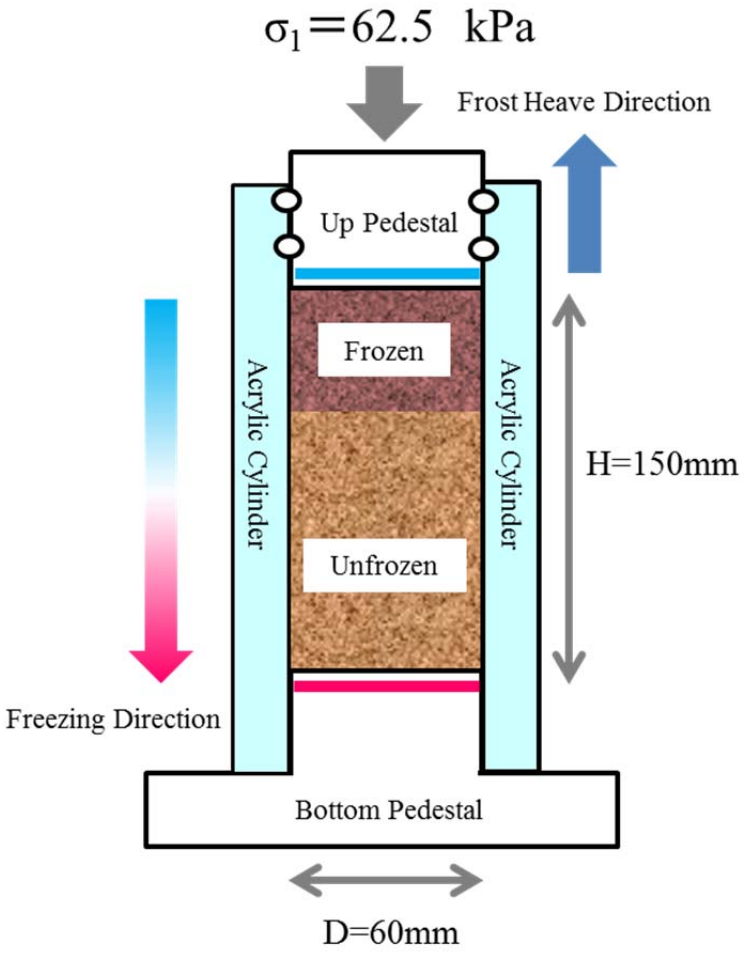



Figure 4-2 Schematic diagram of 1D indoor experiment.

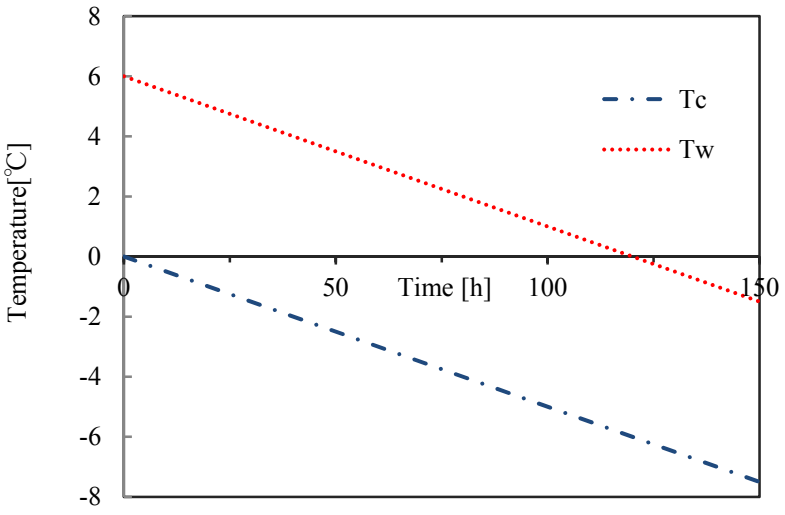



Figure 4-3 Temperature changes on warm ($T_W$) and cold ($T_C$) sides.

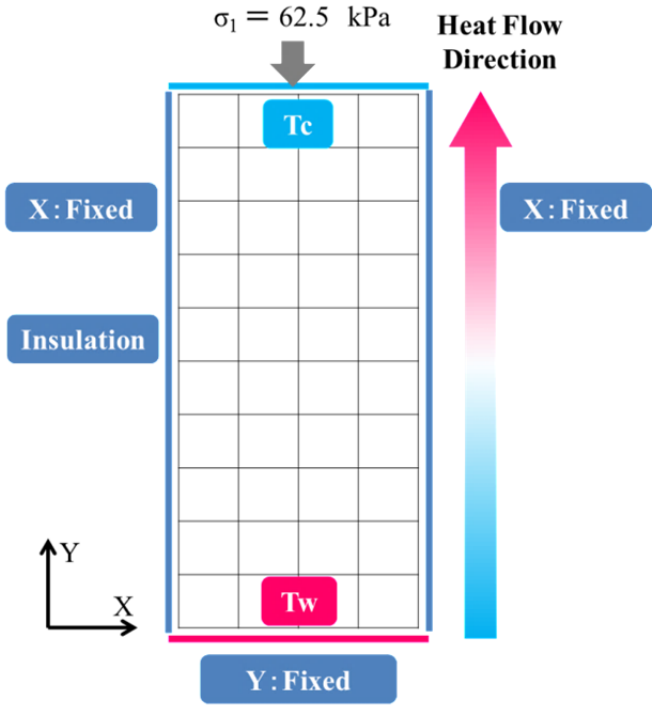



Figure 4-4 Meshing and boundary conditions for numerical model.

Table 4-1 Material parameters for 1D indoor experiment

| Name | Value | Name | Value |
|---|---|---|---|
| $E$ [N m$^{-2}$] | $1.26 \times 10^{7}$ | $\theta$ | 0.437 |
| ν | 0.3 | $\xi_0$ | $6.478 \times 10^{-3}$ |
| $\rho$ [kg m$^{-3}$] | 1790 | $U_0$ [m s$^{-1}$] | $4.431 \times 10^{-7}$ |
| $c$ [J kg$^{-1}$ K$^{-1}$] | 1790 | $\sigma_0$ [N m$^{-2}$] | 4563 |
| $\lambda$ [J s$^{-1}$ m$^{-1}$ K$^{-1}$] | 2.26 | $\beta$ | 0/0.5/1 |

After 150 h, we verify the temperature distribution of this sample, as shown in Figure 4-5. The frost heave development process of the linear model is shown in Figure 4-6. According to the frost heave development history, we can confirm that the whole soil sample is completely frozen, even on the warm side of the soil, after 129 h. By using this time period, we can estimate that the freezing rate is approximately $3.230 \times 10^{-7}$m s$^{-1}$ (150 mm / 129 h) and that the constraining stress is 62.5 kPa if we omit the very small influence of gravity in this example. According to this, we can predict frost heave by manual calculation and then compare this calculation with simulated and experimental results. Additionally, in the manual calculation, the same constants as in Takashi's equation are used, as listed in Table 4-1. The manual calculation result of the frost heave ratio is shown as follows:

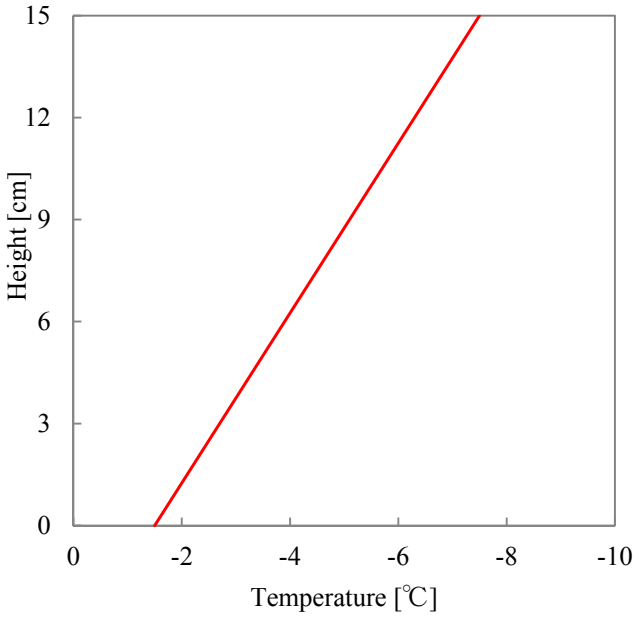



Figure 4-5 Temperature distribution of numerical simulation after 150 h.

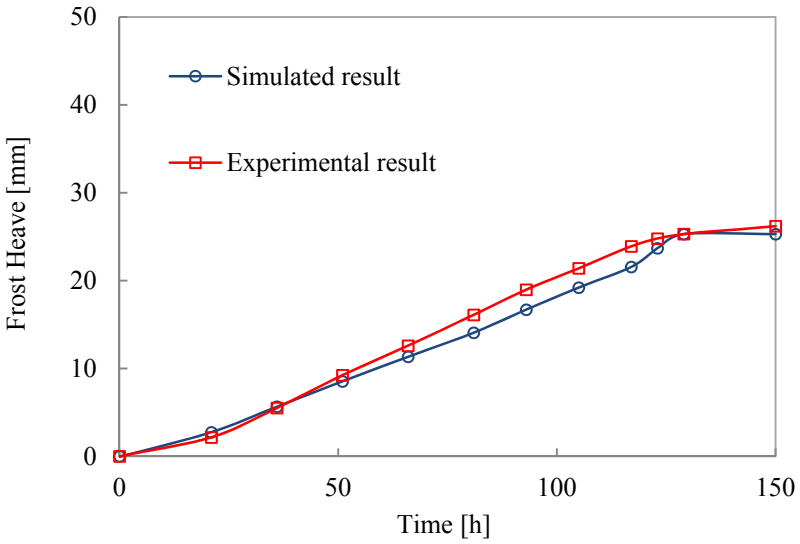



Figure 4-6 Frost heave development of experimental and simulated result.

After considering the height of the soil sample, frost heave = 0.1650 × 150 = 24.75 mm. If we consider the errors in our estimation of freezing rate and constraining stress during manual calculation, the accuracy of this calculation is highly satisfactory. The manual calculation result is very similar to the numerical simulation and experimental results. Additionally, the numerical simulation results display a development process and a final frost heave result that are very similar to experimental results. This demonstrates that the program calculation is reliable. The accuracy of the finite element formulation and encoding is validated by very satisfactory agreement among the analytical and numerical solutions and experimental results.

Until now, the validation of our program is completed. By this good agreement with experiment result, we confirm that this model and program meet the original requirements of our design. And it can be used to predict frost heave in engineering with a good accuracy. In the following chapters, more complicated models which are close to the real engineering field are presented to show the ability of our model.

## 4.4 THREE-DIMENSIONAL FROST HEAVE ESTIMATION

3D frost heave estimation equation is a promising direction for further research in this field. Frost heave is a complicated process which includes thermal, hydraulic and mechanical change in the microscopic view. From the macroscopic point, the stress condition, freezing rate and the drain condition would affect the amount of frost heave itself. For the thermal hydraulic and mechanical analysis, three dimensional is not difficult. In fact the process is the same. The only different point is about the numerical integration and direction issues. The difficult point for three-dimensional frost heave estimation is the Takashi's equation itself. As widely known, Takashi's equation is originally

derived from one dimensional indoor frost heave experiment. At that time, multi-dimensional issues were not considered at all.

And in this research, by introducing an anisotropic parameter $\beta$, we expand this equation into two-dimenisional situation. In that situation, we adopt such an assupation that the total frost heave ratio is kept constant no matter it is one-dimensional or two-dimensional problem. After that, in the two-dimensional situation, the frost heave ratio is distributed into two different, the freezing direction and the direction that perpendicular to the freezing direction.

$$\xi_1 = \frac{1}{1+\beta}\xi \quad , \quad \xi_2 = \frac{\beta}{1+\beta}\xi \tag{4-47}$$

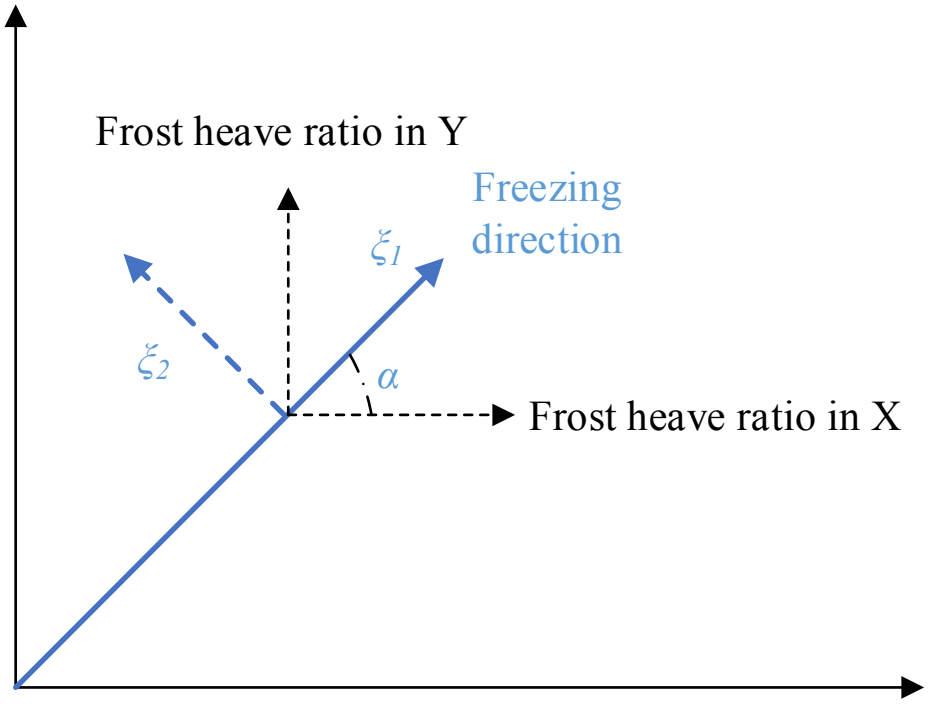



Figure 4-7 The distribution of frost heave ratio in two-dimensional coordinate

Just as shown in this figure, we distribute frost heave ratio calculated by Takashi's equation into two direction, freezing direction and the direction that perpendicular to the freezing direction. After that, we project these two frost heave ratio into $X$ and $Y$ axis. The relationship could be expressed by the following equation:

$$\text{Frost heave in X direction} = \xi_1 \cos\alpha + \xi_2 \sin\alpha \tag{4-48}$$

$$\text{Frost heave in Y direction} = \xi_1 \sin\alpha + \xi_2 \cos\alpha \tag{4-49}$$

In our calculation, α is assumed between 0 to 90 degree. And through the above equation, we ensure that frost heave happens in expansion way, never in a compression way. This is what we have done in the two-dimensional situation. However, when we expand this idea into three-dimensional situation, it becomes complicated.

Just based on this complicated situation, a modified Takashi's equation is desired to solve such problem. In such a modified or improved equation, we hope it is simple as the original Takashi's equation, at the same time, this new equation is supposed to consider the multi-dimensional issues appropriately.

Three-dimensional experiments were carried out using Fujinomori clay, which is frequently used in Japan as a frost-susceptible material. The specimens were consolidated under a pressure of 1MPa, and the freezing rate was set at almost 1 mm/h. The frost heave ratio in the heat flow direction is recorded using a dial gauge. The change in the radius direction is measured using a vernier scale after the experiment.

### 4.4.1 VOLUMETRIC CHANGE DUE TO FROST HEAVE

A preliminary study of the results showed that the volumetric change due to frost heave could be expressed by Equation (4-50) with a small modification to the original Takashi's equation.

$$\xi_v = \xi_0 + \frac{\sigma_0}{\sigma} + \frac{U_0}{U} \tag{4-50}$$

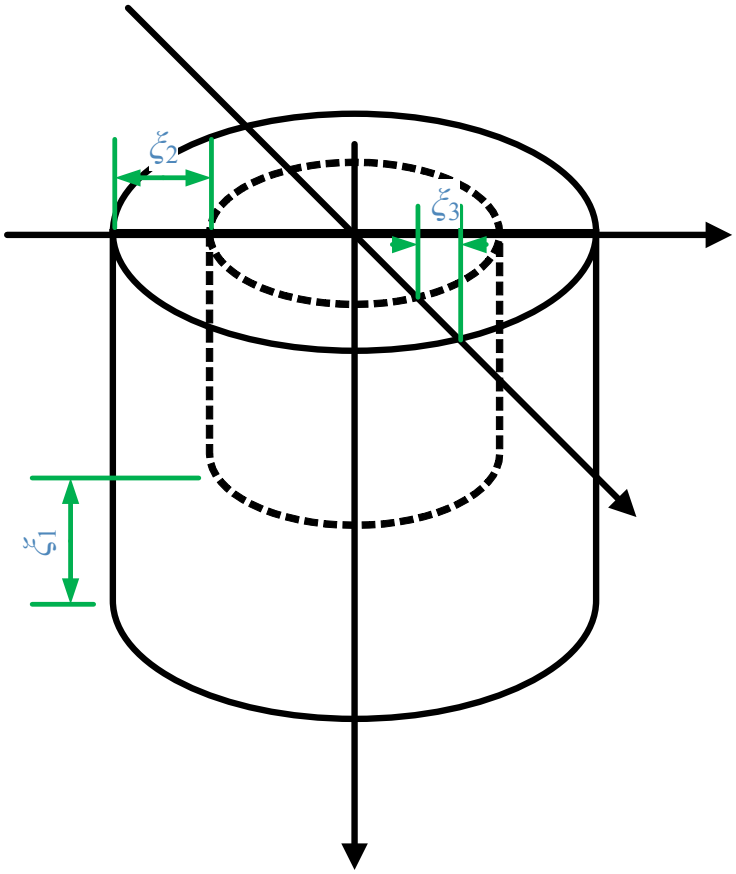



Figure 4-8 The measurement of three-dimensional frost heave test

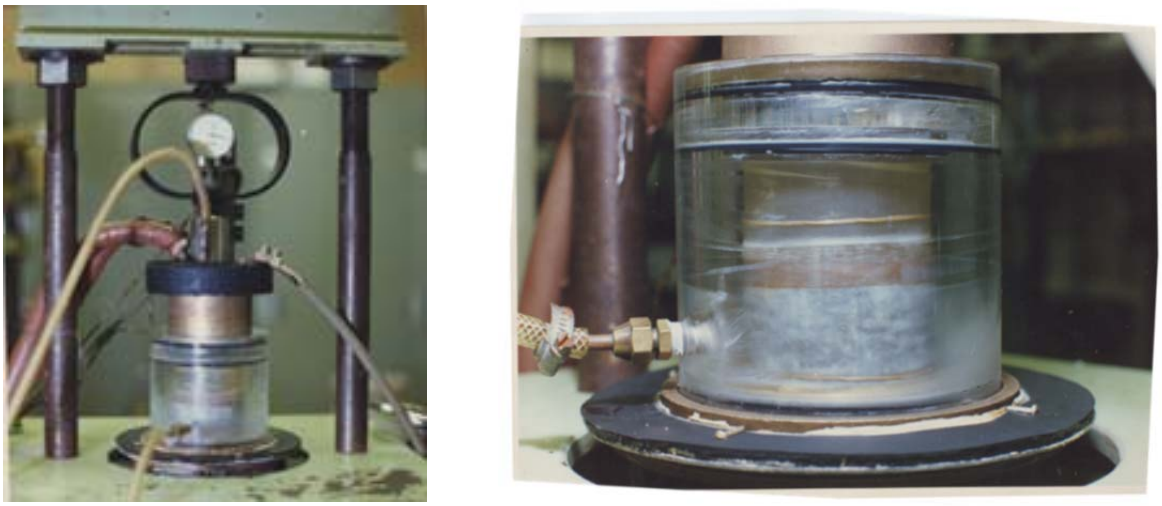


Figure 4-9 The three-dimensional frost heave experiment system

Here $\xi_v$ is total frost heave ratio, which is defined as the ratio of a volume increase to the initial volume of the specimen; σ is the constraining effective stress in the freezing direction, and $U$ is the

freezing rate which is the speed of advancement of the freezing line into the unfrozen soil portion, and the unit of freezing rate $U$ is m/s. $\xi_0$, $\sigma_0$ and $U_0$ are constants for the soil material obtained by three-dimensional experiment. This equation is very similar with the original Takashi's equation, and the parameters used in this new equation are also very close to that. However, they have totally different value and meaning.

As we have emphasized, original Takashi's equation is derived from 1D experiments, so if we want to apply the Takashi's equation into multi-dimensional problem, an anisotropic parameter is needed to distribute the frost heave in different directions. And this modified Takashi's equation is derived from 3D indoor frost heave experiment, we do not need to distribute frost heave ratio in each direction by ourselves. A preliminary study of some 3D frost heave experiments showed that the volumetric change due to frost heave could be expressed by this equation; and the linear regression coefficient was 0.788 which proves the accuracy of this equation (Figure 4-10).

The frost heave ratio in direction $i$ was assumed to be given by this equation with delivering coefficient $a_i$.

$$\xi_i = \alpha_i \left( \xi_0 + \frac{\sigma_0}{\sigma} + \frac{U_0}{U} \right) \tag{4-51}$$

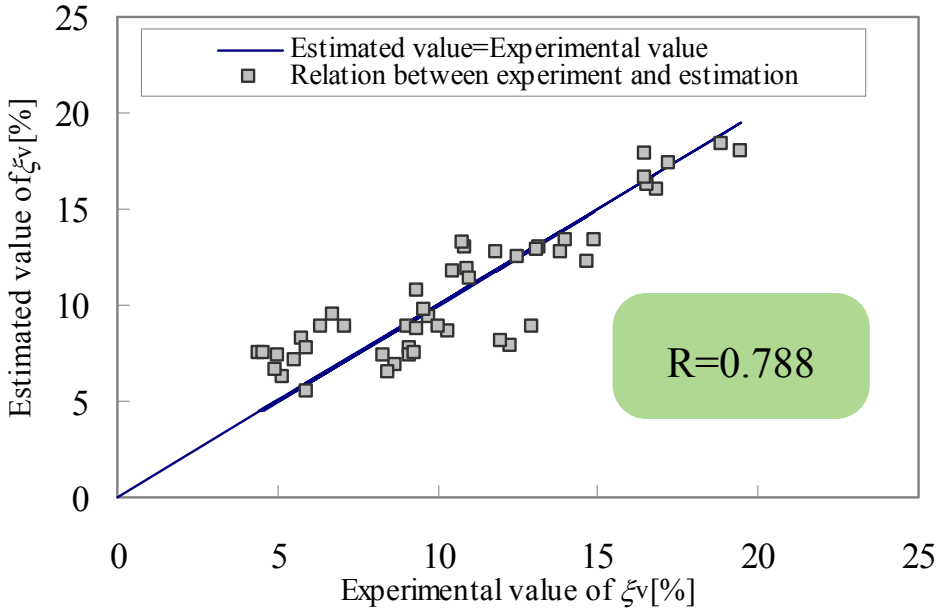



Figure 4-10 The comparison between estimated value and experimental value

$$\alpha_1 = \frac{\sigma_2 + \sigma_3 - \sigma_1 - 1/2|\sigma_2 - \sigma_3|}{\sigma_1 + \sigma_2 + \sigma_3} \quad \alpha_3 = \frac{\sigma_1 + \sigma_2 - \sigma_3 - 1/2|\sigma_1 - \sigma_2|}{\sigma_1 + \sigma_2 + \sigma_3} \qquad \text{(4-52) (a)}$$

$$\alpha_i = \frac{1}{2}\left(1 - \frac{\sigma_i}{\sigma_1 + \sigma_2 + \sigma_3}\right) \qquad \text{(4-52) (b)}$$

By applying the equations above, the frost heave ratio $\xi_1$ in the heat flow direction can be calculated; Figure 4-11 shows the comparison with the experimental results. As shown in the figure, if Equation (4-52) a is adopted as the delivering coefficient, the coefficient of determination becomes 0.796. When Equation (4-52) b is applied, the estimation shows better agreement with the experimental results, and the coefficient of determination becomes 0.927. Thus, the frost heave ratio in the heat flow direction was evaluated appropriately.

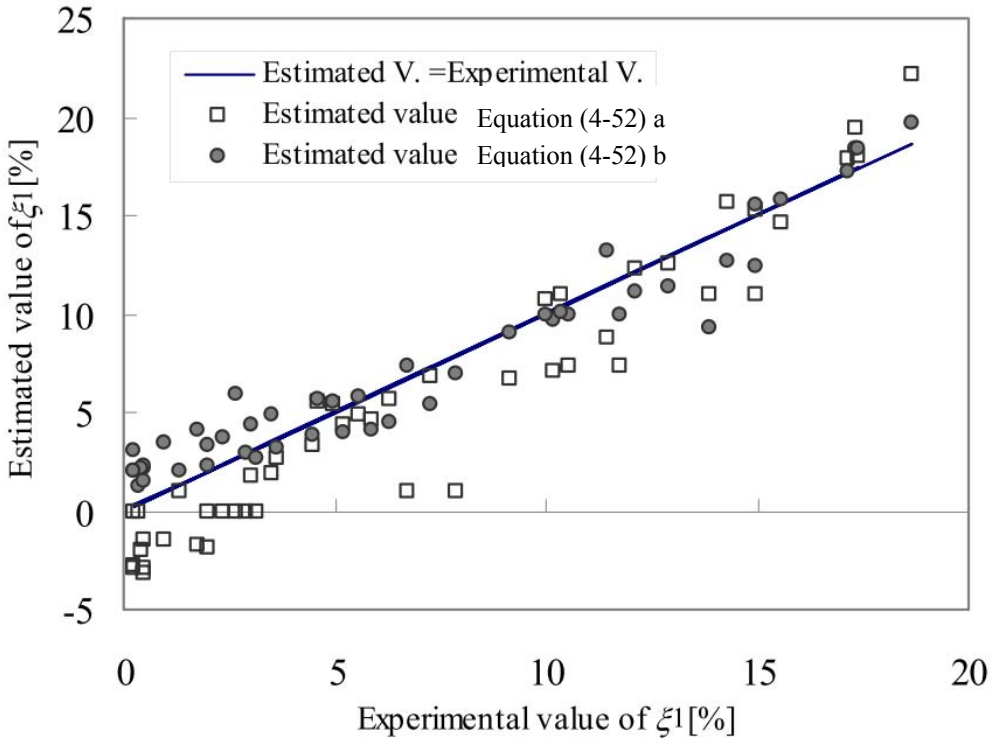



Figure 4-11 The comparison between estimated value and experimental value by two different equations. Comparison of frost heave ratio in the heat flow direction $\xi_1$ between experimental results and that estimated by Equation (4-50). The coefficients of determination for Equation (4-52) a and b were 0.796 and 0.927, respectively.

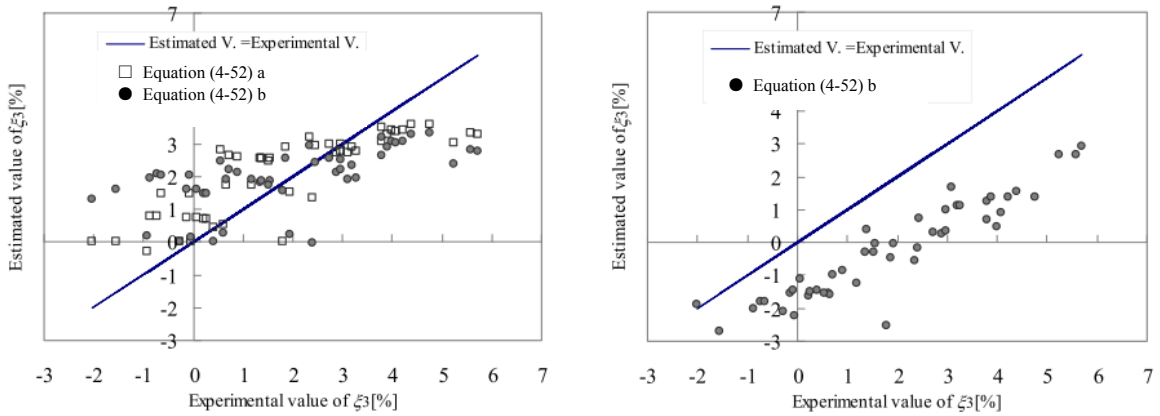
In contrast, it was a little difficult to evaluate the frost heave ratio $\xi_3$ in the normal direction to the heat flow. Figure 4-12 (a) shows a comparison of the experimental and estimated values of $\xi_3$. The coefficients of determination became worse: 0.635 for Equation (4-52) a and 0.352 for Equation (4-52) b. This inaccuracy may have been caused by the measuring method for the change in diameter of the

specimen. Unlike the frost heave in the heat flow direction $\xi_1$, the change in diameter of the specimen was measured using a Vernier scale after the experiment, and the observed values themselves were less reliable.

In the experiments, the original water content $W_c$ and amount of water absorbed into the specimen were recorded. If the frost heave in the heat flow direction $\xi_1$ is appropriately given, the frost heave ratio $\xi_3$ can be estimated by the following equation:

$$\xi_3 = \sqrt{\frac{w_c + (1+\Gamma)\cdot\xi_w + 1}{1+\xi_1}} - 1 \qquad (4\text{-}53)$$

where $W_c$ is the original water content of the specimen; $\Gamma$, the volumetric change ratio of water; and $\xi_w$, the ratio of absorbed water to the original volume of the specimen. Figure 4-12 b shows the relation between $\xi_3$ estimated by Equation (4-53) and the experimental results. The estimated values were relatively smaller than those observed, but the former had an almost linear relation with the latter. The frost heave $\xi_3$ can be estimated in a manner similar to that in Equation (4-51), although some additional modification maybe necessary.




(a) Comparison of frost heave ratio $\xi_3$ by Equation (4-51)

(b) Comparison of frost heave ratio $\xi_3$ by Equation(4-53)

Figure 4-12 (a): comparison of frost heave ratio $\xi_3$ between experimental results and that estimated by Equation (4-51). The coefficients of determination for Equation (4-52) a and b were 0.635 and 0.352, respectively. (b): comparison of frost heave ratio $\xi_3$ between the experimental results and that estimated by Equation (4-53).

This equation may be not the perfect one; maybe we will enhance it or modify it in future based on

more experiment data. But now this equation does improve the original one-dimensional equation into three-dimensional equation. And in future's 3D experiment, we may improve the experiment equipment and method. For example, concerning the volume measurement, in the existing method, Vernier was used to measure the deformation. However, due to the complexity of soil, frost heave deformation may be uneven. This situation brings serious challenge to our experiment data. Thus, an accurate method is desired to measure the volume change after frost heave occurs.

We are planning to adopt drainage method to measure the volume change caused by frost heave. The detail of this method is illustrated as following:

If we assume that the original volume of the soil sample is $V_0$ and after freezing, the volume becomes $V$:

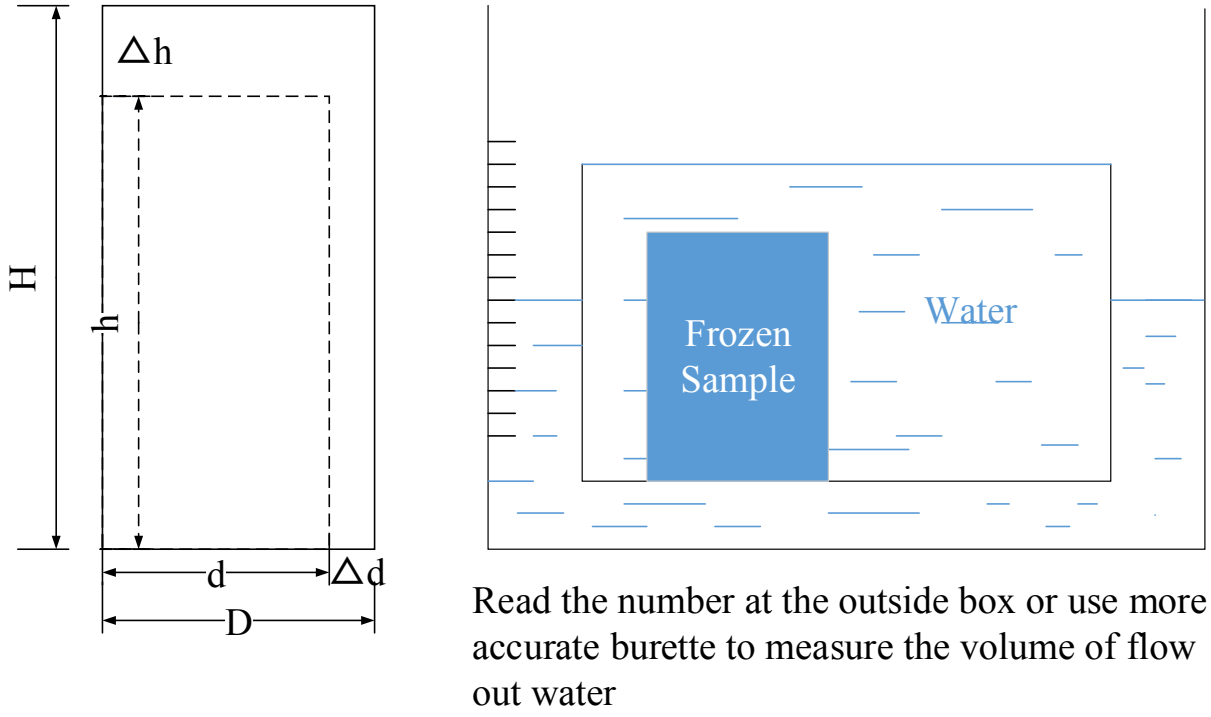



Figure 4-13 The drainage method to measure the volume change

According to the left figure of the soil sample, we can know that the initial volume before frost heave occurs is:

$$V_0 = \frac{\pi d^2}{4} \times h \tag{4-54}$$

And the volume after freezing is:

$$V = \frac{\pi D^2}{4} \times H = \frac{\pi (d + \Delta d)^2}{4} \times (h + \Delta h) \tag{4-55}$$

And by the drainage method, the volume of freezing sample V is known, d is measured carefully before freezing, and at the same time, the displacement at the top surface $\Delta$h is obtained by Linear Variable Differential Transformer (LVDT) which is accurate enough for our experiment. Based on these known values and the above equations, we can know that

$$\Delta d = 2\sqrt{\frac{V}{\pi (h + \Delta h)}} - d \tag{4-56}$$

And further, based on the definition of frost heave ratio, we can know that:

$$\xi_v = \frac{V - V_o}{V_o} \tag{4-57}$$

$$\xi_1 = \frac{\Delta h}{h} \quad \xi_3 = \frac{\Delta d}{d} \tag{4-58}$$

If during the experiment, the amount of water absorbed by the specimen $W_{ab}$ is observed and recorded, and $W_o$ is the initial water contained in the soil simple before freezing, the following relationship could be derived:

$$\xi_v = \frac{V - V_o}{V_o} = \frac{W_{ab} \times 1.09 + W_o \times 0.09}{V_o} = \xi_1 + \xi_2 + \xi_3 \tag{4-59}$$

This relationship should be right because that all frost heave is caused by the volume expansion when water becomes into ice. And in order to reduce the measurement error, $V_o$ is also should be measured with the same method as $V$ by drainage method. And of course, the soil sample should be surrounded by rubber membrane.

# 5. THE NONLINEAR PROPERTY OF UNFROZEN SOIL

Since soil mechanical property changes drastically as the stress and temperature condition varies, nonlinear property of unfrozen soil is introduced in this chapter. We adopt Duncan and Chang's equation to expresses the relationship between Young's modulus of unfrozen soil and differential stress. For frozen soil, the strength is dominated by temperature. However, for simplification, we assume a constant value for frozen soil Young's modulus. After adding this supplement to mechanical analysis, the nonlinear influence to frost heave and stress is evaluated by comparisons between elastic and nonlinear examples.

## 5.1 NONLINEAR PROPERTY ASSUMPTIONS

Traditionally, the elastic model has been used to evaluate stress caused by frost heave; however, in some situations, the elastic model overestimates the stress field caused by frost heave. This is a serious and critical concern for engineering because it increases the cost of a project. Therefore, a nonlinear model that considers the temperature and stress-dependent Young's modulus is necessary for the accurate estimation of frost heave and stress fields. To our knowledge, research concerning nonlinear frost heave is very limited. In Shen and Ladanyi's study (1987) [25] the Young's modulus of frozen soil was a function of temperature, but was not affected by strain rate and confining pressure. In their research, the Young's modulus of unfrozen soil was treated as a constant value; for frozen soil, the Young's modulus was an exponential function of temperature.

$$E_o = 4 \times 10^2 \left| T \right|^{0.636} \quad (MPa) \tag{5-1}$$

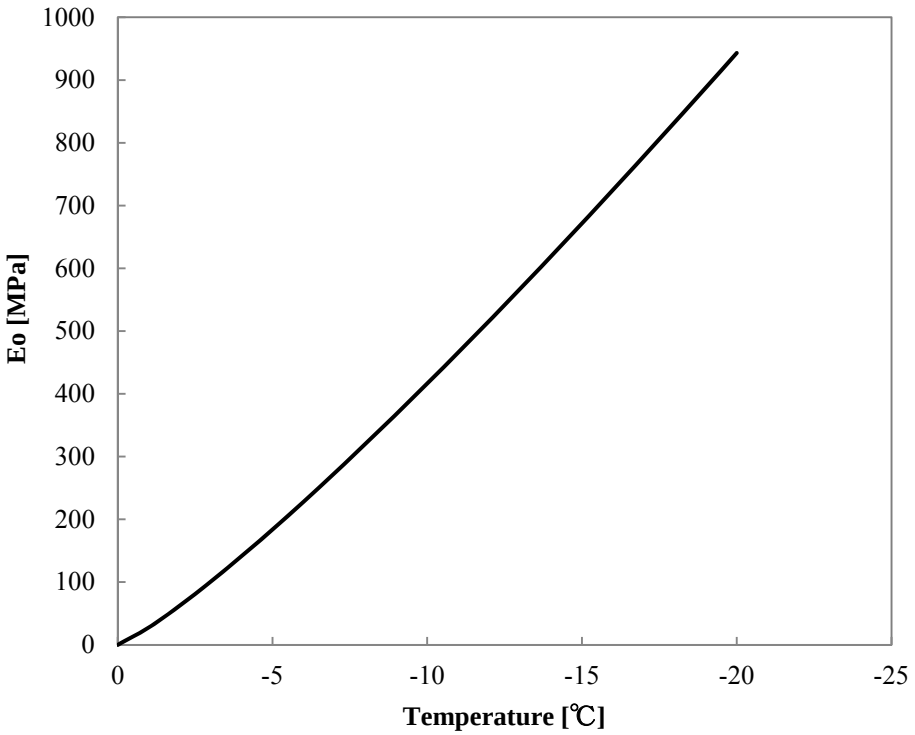



Figure 5-1 The relationship between temperature and frozen soil *E*

Ladanyi and Shen (1993) [26] and Konrad and Shen (1996) [27] also introduced the concept of temperature-dependent Young's modulus into a frost heave estimation model for frozen soil. In addition, they applied a bilinear model to justify the plastic situation of soil. In their studies, the plastic status of soil was considered through a reduction of the Young's modulus. The Young's modulus of frozen soil is considered by the following equation:

$$E_o = 13.75|T|^{1.18} \quad (MPa) \tag{5-2}$$

And then, the Young's modulus of this frozen soil is reduced if the stress exceeds the yield stress. The yield stress of the frozen soil was obtained from the long-term strengths of typical soils. The relationship between yield stress and temperature can be expressed as:

$$\sigma_y = 0.127 \cdot e^{0.5|T|} \quad (MPa) \tag{5-3}$$

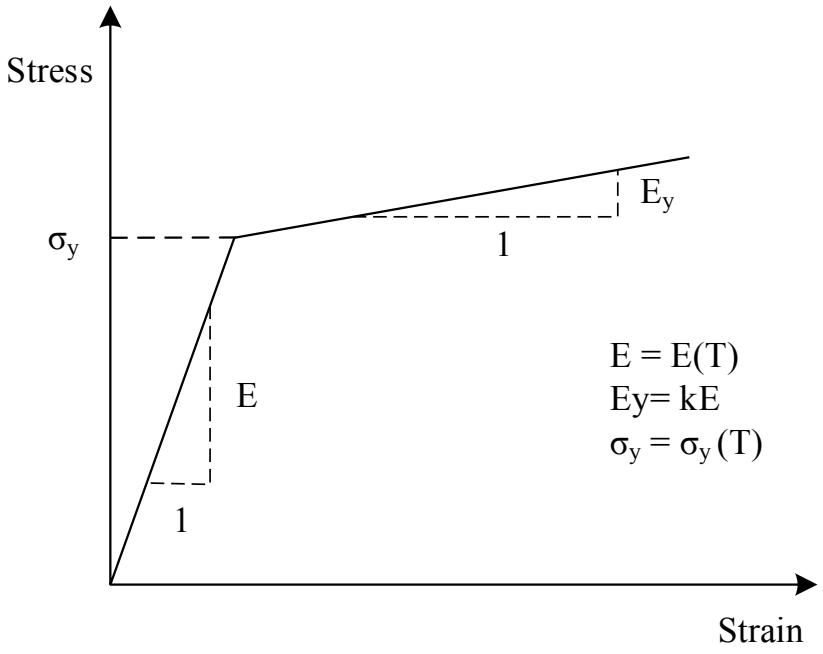



Figure 5-2 Simplified stress-strain relationship of frozen soil.

The slope, $E_y$ of the stress-strain relationship after yielding was assumed to be related to the initial Young's modulus $E$ as:

$$E_y = k \cdot E \tag{5-4}$$

where $k$ is assumed to be smaller than 1. Several values of k were used in the simulations in order to test the effect of different post-yield stress-strain characteristics.

Kim's study (2011) [8] adopted a modified trilinear elastic law to consider the failure conditions. Kim's assumption concerning nonlinear properties is recognized as a modification of and improvement over the previous models. In detail, the relationship between stress and strain is described in three lines, which confirms it as a trilinear model.

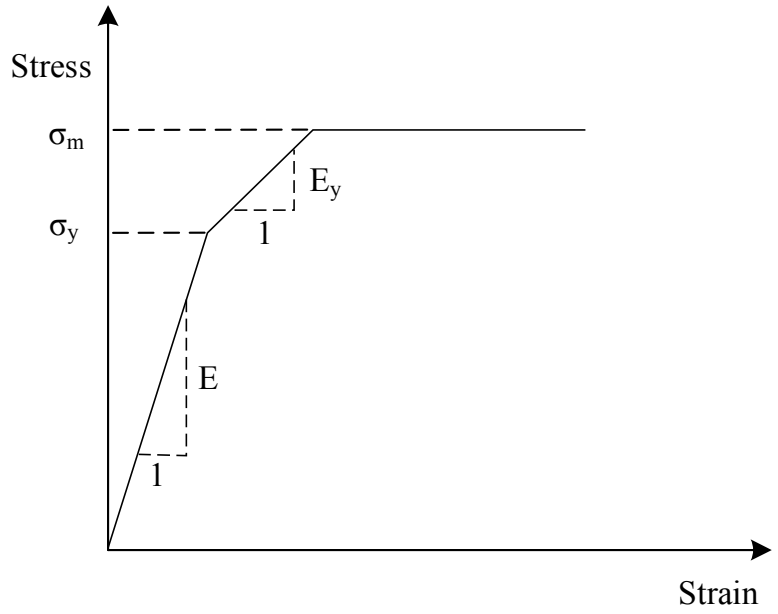



Figure 5-3 Modified bilinear stress-strain relationship for soil mechanical model

In fact, all of these studies concerning the nonlinear properties of frost heave assumed a temperature dependent Young's modulus for frozen status, then a constant Young's modulus for unfrozen stage. However, it is widely accepted that the bearing capacity of the unfrozen soil is closely related to the confining stress and temperature conditions. Hence, in our research, an equation proposed by Duncan and Chang (1963) [28] is used to express the relationship between stress and Young's modulus for unfrozen soil. For frozen soil, we do not adopt a temperature dependent Young's modulus because that there is no widely accepted formula to describe this relationship. The existing formulas are generally obtained by laboratory experiment for specific soil. Only with standard regulation, such method could be applied in a further region. Therefore, an increased Young's modulus is used to represent the increasing soil strength after freezing in this paper. This assumption is very simple but practical. It considers the increased soil strength caused by cold temperature.

Regarding the influence of the nonlinear model, in the normal sense, a nonlinear model will result in smaller stress and larger displacement under the same strain. However, this conclusion becomes complicated when frost heave is considered simultaneously because it is widely accepted that the amount of frost heave is closely related to the constraining stress. A smaller constraining stress would increase the amount of frost heave. Naturally, a large frost heave would produce large frost heave stress. Hence, it is a paradox. We cannot easily predict the differences in frost heave and stress changes for linear and nonlinear models. The constraint condition and soil strength strongly affect frost heave and stress distribution.

$$[K]\{u\} = \{F\} + \{F_t\} \tag{5-5}$$

where [$K$] is the stiffness matrix, $\{u\}$is the displacement, $\{F\}$ is the external force, and $\{F_t\}$ is the force caused by freezing. The stiffness matrix [$K$], is related to the Young's modulus. In this research, the following assumptions are adopted to describe the complicated temperature and stress-dependent Young's modulus: We assume that when $T \geqslant T_S$ (unless described otherwise, $T_S$ is −0.5°C in this study), which means that the soil is unfrozen; $E$ is closely related to stress condition. Duncan and Chang's equation is applied to calculate the Young's modulus. In Duncan and Chang's equation, stress is the dominant factor for unfrozen Young's modulus. When $T < T_S$, the soil strength is dominated by temperature (Konrad, 2002). However, in this paper for simplification, we assume a constant $E$ ($E$ = 5 00 MPa in this study) for frozen soil and sand; this constant value of frozen soil far outweighs that of unfrozen soil.

Concerning Duncan and Chang's equation, Kondner (1963) first proposed the hyperbolic relationship between stress and strain, as shown in Figure 5-4. Based on this relationship, Duncan and Chang (1963) derived the equation for Young's modulus, shown as Equation (5-6). This equation describes the relationship between Young's modulus of unfrozen soil and differential stress ($\sigma_1 - \sigma_3$), which is convenient for numerical application.

$$E = \left(1 - R_f \frac{(1-\sin\phi)(\sigma_1 - \sigma_3)}{2C_u \cos\phi + 2\sigma_3 \sin\phi}\right) \cdot E_i \tag{5-6}$$

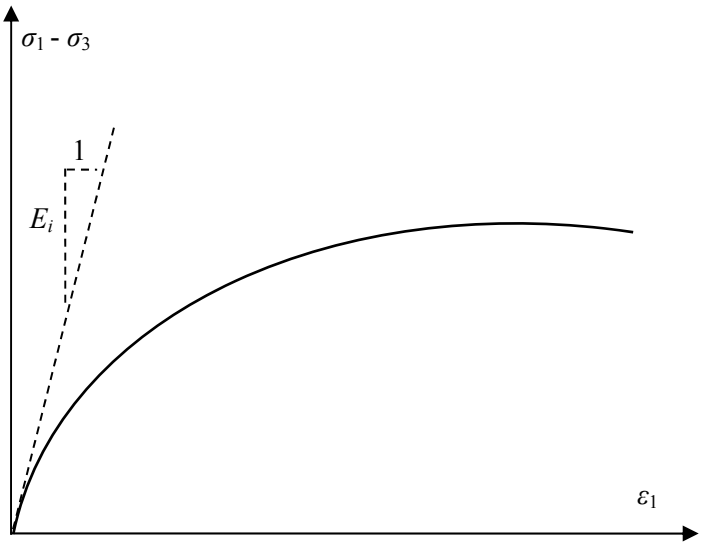



Figure 5-4 Relationship between stress and strain for unfrozen soil.

In which $C_u$ and $\phi$ are the cohesion intercept and the friction angle, respectively. For theoretical clay, the friction angle is very small; hence, in our study, $\phi$ is assumed to be 0 for simplification. $E_i$ is the initial Young's modulus, and $R_f$ is the failure ratio. The failure ratio relates the stress intensity range ($\sigma_1 - \sigma_3$) for the ultimate failure. The typical range is 0.75 to 1, but values between 0 and 1 (inclusive) are acceptable. In this study, 1 is assigned to $R_f$. Here $\sigma_1$and $\sigma_3$ are the major and minor principal stresses and $\varepsilon_1$ is the strain corresponding with major principal stress.

## 5.2 DISCUSSION OF NONLINEAR INFLUENCE

In this section, some examples are provided to discuss the influence caused by nonlinear property.

### 5.2.1 1D Nonlinear Example

In this section, based on our verified simulation program, linear and nonlinear models are compared to confirm the influence of the nonlinear properties. First, a 1D model is used to confirm the simplest configuration of nonlinear properties. The size and mesh of the numerical model are the same as in Figure 4-4, but the boundary and temperature conditions are different. In this numerical example, displacements at all the boundaries are forbidden (Figure 5-5). The initial temperature is set at 2°C and −5°C is applied from the top surface to freeze the sample. Side boundaries are thermally insulated and the initial temperature of 2°C is maintained at the bottom. Based on this numerical model, we compare the vertical direction stress and Young's modulus in the red colored element for the linear and nonlinear models.

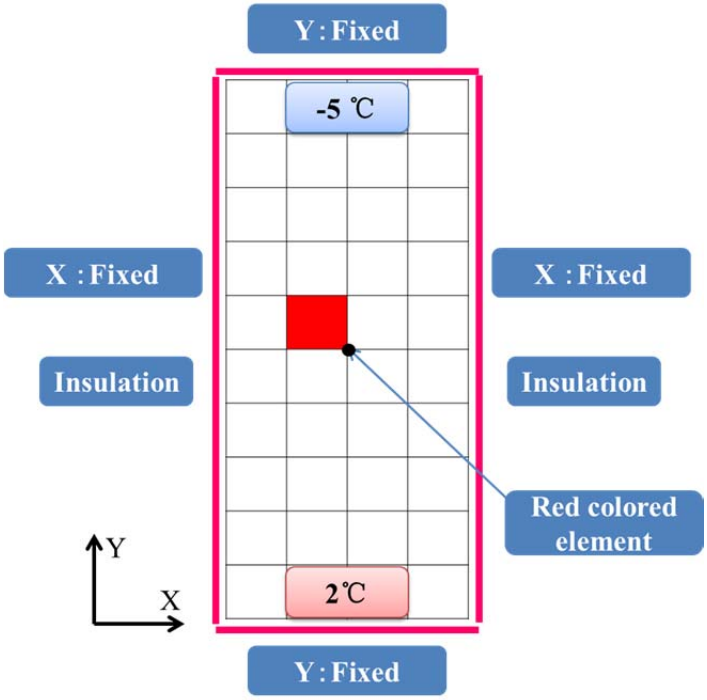



Figure 5-5 Meshing and boundary conditions for linear and nonlinear numerical models.

When we examine the vertical stress caused by freezing, we find that for both the linear and nonlinear models, the trends of stress development are very similar. However, the stress value of the nonlinear model is obviously smaller than that of the linear model, according to Figure 5-6. For such a simple 1D freezing model, it is very easy to understand that in the nonlinear model, the Young's modulus is temperature and stress-dependent. Additionally, the frozen soil causes some frost heaving, which may compress unfrozen areas. According to Duncan and Chang's equation, the strength of the unfrozen soil decreases, which naturally relaxes the compression stress. This is a possible and reasonable explanation for such a reduction in vertical stress.

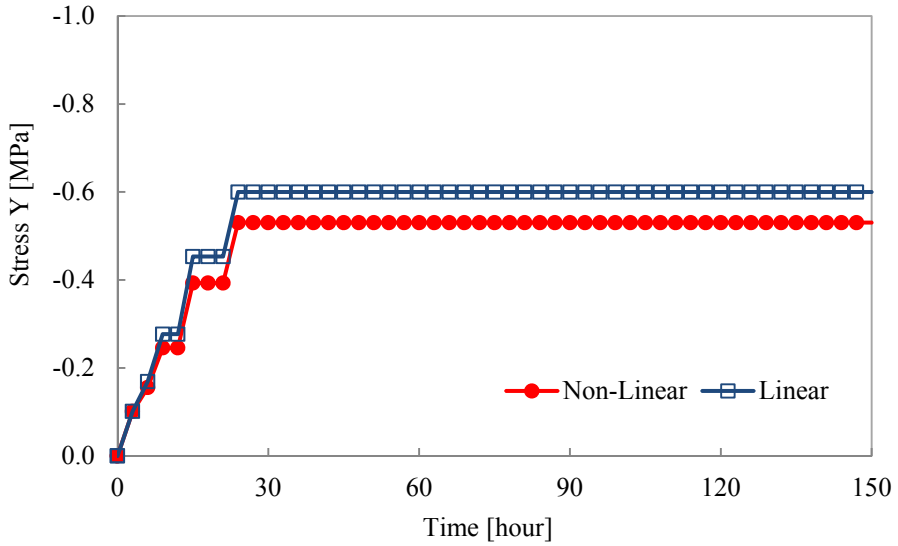



Figure 5-6 Vertical stress of the red colored element for linear and nonlinear models.

Another issue is that we assume the Young's modulus to be temperature and stress-dependent. In the following, the changing history of the Young's modulus is shown to provide a clear and direct image to clarify this assumption. Figure 5-7 shows that the Young's modulus of the linear model is always constant for unfrozen situation. After the element is frozen, a large value of Young's modulus is adopted for this frozen soil. However, in the nonlinear model, the Young's modulus changes drastically. In the first stage, owing to the increment of $(\sigma_1 - \sigma_3)$, $E$ decreases quickly for unfrozen soil. After the element is frozen, the soil strength is increased to a large and constant value for frozen soil. This value does not increase further although the temperature decreases further. This changing trend of the Young's modulus agrees with our thermal analysis. There is a direct relationship between temperature and Young's modulus in Figure 5-7.

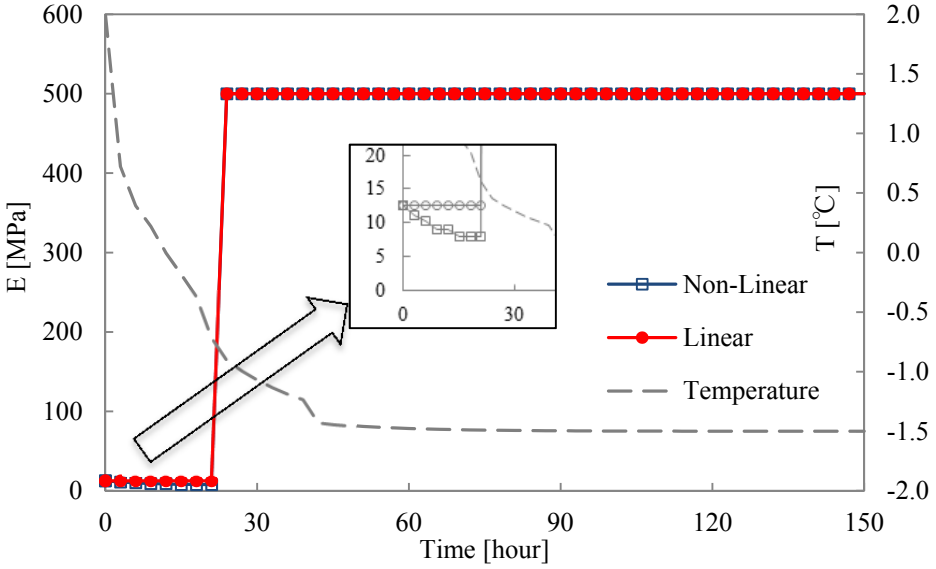



Figure 5-7 Young's modulus of red colored element and temperature.

### 5.2.2 2D Nonlinear Example

In this section, a 2D indoor experiment is used to confirm the influence of the nonlinear properties. This experiment intended to simulate the uplifting process of a freezing pipeline. A chilled gas pipe is buried under unfrozen soil. After the chilled gas is circulated in the pipe, soil surrounding the pipe would be frozen and then frost heave would occur which leading to an uplift of the pipeline. Unfortunately, in this indoor experiment, only temperature and displacement were monitored; the stress data were never obtained. Thus, we cannot discuss the influence of the nonlinear properties on stress. The numerical model and experimental equipment are shown in Figure 5-8. The size of each part is given in the figure; the diameter of the pipe is 75 mm and the thickness of the aluminum pipe is approximately 3 mm. Frost-susceptible soil which is a mixture of 25% pyrophyllite clay and 75% sand is used for the soil layer and there is a 50-mm standard sand layer on the surface, and no external load is applied on the surface. The experiment period was approximately 120 h. The temperature change inside the pipe is completed by a flowing antifreeze fluid. In this experiment, during the first 87.5 h, the temperature of the pipe was changed from −0.5°C to −4°C, which is shown in Figure 5-9.

Table 5-1 Material parameters for 2D indoor experiment.

| Parameters | Soil | Buried pipe | Sand |
|---|---|---|---|
| $E$ [N m$^{-2}$] | $2.80 \times 10^{7}$ | $7.00 \times 10^{10}$ | $2.80 \times 10^{6}$ |
| ν | 0.2 | 0.33 | 0.2 |
| $\rho$ [kg m$^{-3}$] | 1930 | 2700 | 1550 |
| $c$ [J kg$^{-1}$ K$^{-1}$] | 1005 | 913 | 1005 |
| $\lambda$ [J s$^{-1}$ m$^{-1}$ K$^{-1}$] | 1.00 | 2.56※ | 1.0 |
| $\theta$ | 0.5 | 0 | 0.25 |
| $\xi_0$ | 0.025 | 0 | 0.0279 |
| $U_0$ [m s$^{-1}$] | $6.90 \times 10^{-8}$ | 0 | 0.000 |
| $\sigma_0$ [N m$^{-2}$] | 800 | 0 | 0.000 |
| $\beta$ | 0 | 0 | 0 |
| $R_f$ | 1 | / | 1 |
| $C_u$ [N m$^{-2}$] | $6.00 \times 10^{5}$ | / | $6.00 \times 10^{5}$ |

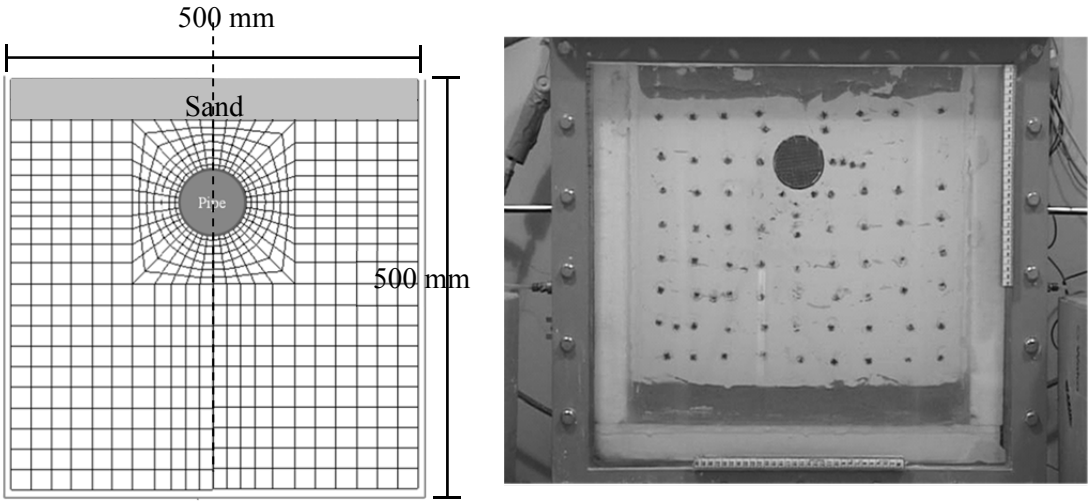



Figure 5-8 Numerical mesh and experimental equipment for 2D indoor experiment.

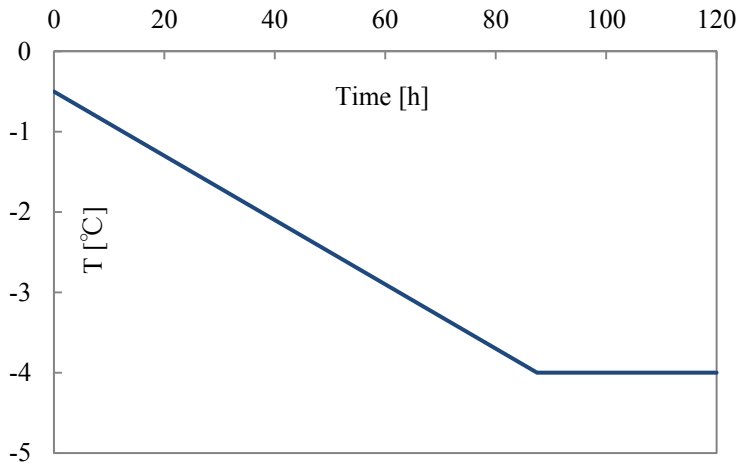



Figure 5-9 Temperature change inside the buried pipe.

For the numerical simulation, only the right half of the model is calculated because of its symmetrical property. There are 399 nodes and 352 elements in this model. The calculation period is 120 h and in order to meet the limit of the Courant number, the size of the time step is only 6 s. At each time step, the temperature of pipe is changed, as shown in Figure 5-9. In this example, the pipe is always treated as a linear material. The boundary conditions are as follows: the top surface, right side, and bottom are in contact with room air, the temperature of which is maintained at approximately 2°C; the middle side of the broken line is thermal insulation. There is no horizontal displacement to the right or middle sides; and no vertical displacement on the bottom. The top surface is totally free for displacement and not overburdened. The initial temperature of the sample is 2°C.

According to the size of the frost bulb in the experiment and the thermal analysis of the numerical simulation (Figure 5-10), we find that $T_S$ in this example equals −0.5°C results in a similar size of frost bulb with experiment. All of the material parameters are listed in Table 5-1. Considering the limit of the Courant number, the thermal conductivity of aluminum pipes is too large (256 W m-1 K-1); hence, we assume that it is only one percent of the real value, because the thickness of the pipe is only 3 mm, and we believe that it does not obviously affect the final results of the simulation.

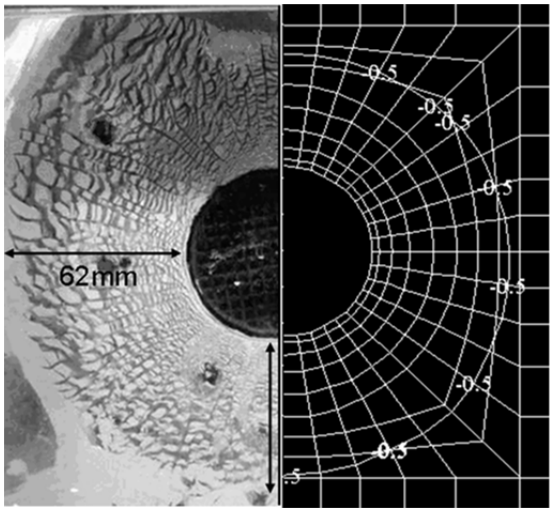



Figure 5-10 Frost bulb comparison between numerical simulation and experiment.

Figure 5-11compares the experimental and simulation results for frost heave 45mm above the pipe. In fact, according to Figure 5-11, linear model overestimates the results of the indoor experiment. Meanwhile, nonlinear model underestimates the amount of frost heave. However, one critical point should not be ignored: Takashi's equation performs well only in the valid stress range (98 – 1470 kPa). Moreover, in our numerical model, the boundary condition for the top surface is totally free and no load is applied from the top. The constraining stress to the frost bulb only results from the self-weight of the soil above the frost bulb. The weight of the soil layer is extremely small, even compared to the minimum valid range of Takashi's equation. If the constraining stress was too small, the frost heave ratio would be infinitely large. Consequently, for this simulation, Takashi's equation would not perform well for predicting the frost heave ratio owing to its limited constraining stress. In fact, in this simulation, Takashi's equation is supposed to overestimate the frost heave ratio because the constraining stress is outside the valid range. As our expectation, for linear model, it is obvious that simulation result calculated by Takashi's equation is larger than the experimental results. However, for nonlinear model, due to the changing Young's modulus, the amount of frost heave is reduced. And in this paper, the estimation of unfrozen soil E and frozen soil E are just assumed value, so the calculation results of nonlinear model can just demonstrate the trend but not the accurate value of frost heave. Discarding the experimental result and Takashi's equation, only considering the influence of the nonlinear properties, we discern that the nonlinear model exhibits a smaller frost heave than the elastic model.

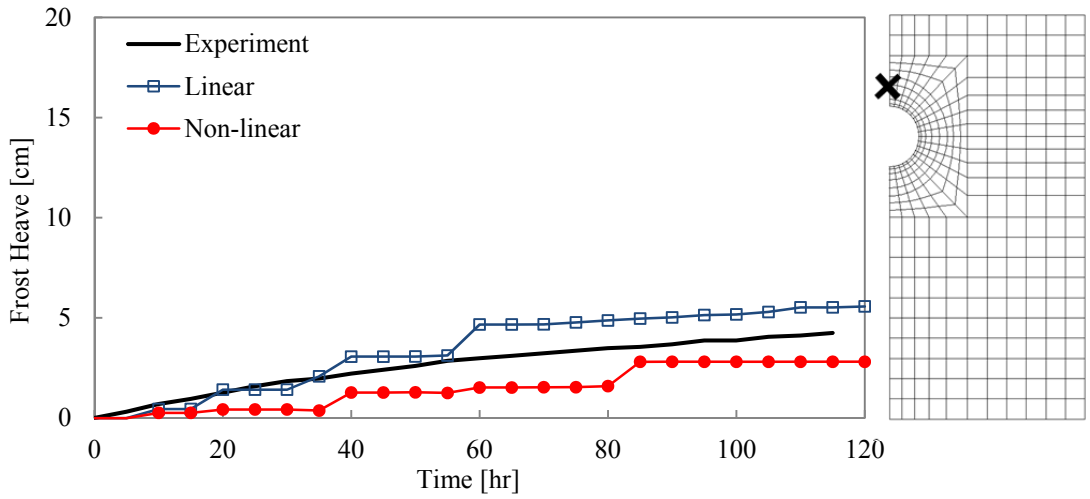



Figure 5-11 Displacement comparison among the experimental, linear and nonlinear models at 45 mm above the pipe.

Some conclusions may be derived from these results. First, although the stress range for Takashi's equation is not a rigid and compulsory requirement for application, it should be carefully considered for satisfactory simulation results. Further research is desired to extend the valid range of Takashi's equation for situations with small constraining stress. Second, the relationships between soil strength, temperature, and stress require more attention. Only accurate constitutive equations may result in satisfactory estimation results. If possible, a specially designed, large, and lengthy experiment is desired to validate the influence of the nonlinear properties, such as the frost heave amount, stress distribution, and even the changes in Young's modulus, for each element under various temperatures. Finally, although there are some differences between the simulated and experimental results, the trends of frost heave development are very similar, and our assumptions concerning to the nonlinear model are demonstrated to be a promising direction for further research.

### 5.2.3 2D Application Nonlinear Example

After comparisons with 1D and 2D indoor experiments, a more practical application example is illustrated. A 2D underground concrete box culvert is used in this example. This structure is frozen by the cold air inside the concrete box culvert and on the top surface. Because this is a symmetrical model, only half of the model is considered, as shown in Figure 5-12. The size of each part is shown in the picture and the boundary and temperature conditions are described as follows: For the concrete and top sections, displacement is free and no constraint is applied. The temperature in the concrete and on top is changed with time according to a sine function which is from 0 °C to −20 °C during 90 days. This is intended to simulate the changes in air temperature during the winter season. For the side boundary, the displacement in the horizontal direction is fixed and no heat flux is allowed; displacement in the vertical direction is forbidden for the bottom, which is assumed as the thermal

insulation boundary.

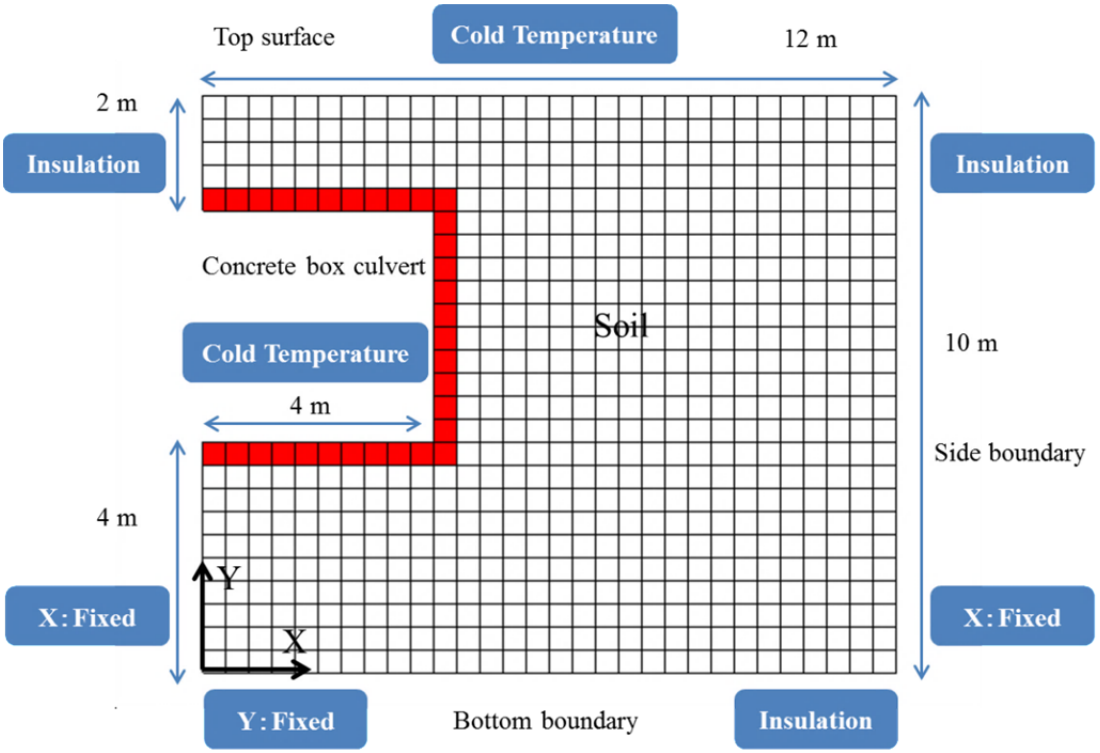



Figure 5-12 Schematic diagram of the concrete culvert example.

Table 5-2 Material parameters for concrete culvert example.

| Parameters | Soil | Concrete |
|---|---|---|
| $E$ [N m$^{-2}$] | $1.26 \times 10^{7}$ | $2.50 \times 10^{10}$ |
| ν | 0.3 | 0.2 |
| $\rho$ [kg m$^{-3}$] | 2000 | 2400 |
| $c$ [J kg$^{-1}$ K$^{-1}$] | 750 | 800 |
| $\lambda$ [J s$^{-1}$ m$^{-1}$ K$^{-1}$] | 1.7 | 1.0 |
| $\theta$ | 0.4 | 0 |
| $\xi_0$ | $6.478 \times 10^{-3}$ | 0 |
| $U_0$ [m s$^{-1}$] | $4.431 \times 10^{-7}$ | 0 |
| $\sigma_0$ [N m$^{-2}$] | 4563 | 0 |
| $\beta$ | 0 | 0 |
| $R_f$ | 1 | / |
| $C_u$ [N m$^{-2}$] | $6.00 \times 10^{5}$ | / |

In this numerical model, there are 716 nodes and 650 elements. The size of each element is 0.4 m × 0.4 m. The total calculation period is 90 days and the size of the time increments is 6 min. The

material parameters used in this model are given in Table 5-2. The initial temperature is 5 °C for soil and concrete. After 90 days of freezing, we can examine the frozen zone based on our numerical simulation results.

Figure 5-13 exhibits the temperature distribution and frozen zone. From the side of concrete culvert, there is an 80-cm frozen layer. Meanwhile, freezing also occurs from the top surface. We may argue that the largest frost heave should appear to the left side of the top surface in a linear model because this represents the largest frozen depth in the vertical direction. Next, the frost heave should decrease gradually from left to right. However, concerning the nonlinear model, this is very difficult to predict without careful calculations by using numerical examples because frost heave is heavily affected by the Young's modulus and stress condition. Furthermore, the value of the Young's modulus is determined by the stress and temperature conditions. The calculation result of the linear model supports our previous prediction. Figure 5-14 confirms that the frost heave distribution of linear model on the top surface is exactly the same as our prediction: The maximum frost heave appears to the left side, and the value of this frost heave is approximately 8.84 cm. However, the frost heave is complicated in the nonlinear model. The deformed nonlinear model after 90 days of freezing is shown in Figure 5-15. The distribution of Young's modulus in the nonlinear model is illustrated by Figure 5-16. According to these simulation results, for the nonlinear model, the maximum frost heave is smaller than that of the linear model. This means that the linear model over predicts the amount of frost heave comparing to nonlinear model. Generally, the trend of frost heave distribution is similar to that in the linear model, in which the maximum frost heave appears to the left side of the top surface. However, in the middle of the top, the trend of frost heave is not totally the same with linear one. We consider the nonlinearity of soil to be the primary reason for this situation. Hence, we examined the Young's modulus' distribution after 90 days, as shown in Figure 5-16, in which the red color represents a large value of Young's modulus and the blue color represents weakened soil. We observe that in the frozen area, the Young's modulus greatly increases (red part in Figure 5-16), but in the unfrozen area, because of stress changes produced by the frost heave expansion, the Young's modulus decreases. In Figure 5-16, the red area around the concrete and surface illustrates that frozen soil is stronger. Further, surrounding the frozen zone, there is a blue layer that indicates weak soil. In the blue layer outside the frozen layer, it appears that the frost heave expansion in the frozen part changes the stress condition, and according to Duncan and Chang's equation, the Young's modulus is reduced. We confirm that this layer has a direct relationship with the frost expansion. Owing to frost heave, the difference increases between $\sigma_1$ and $\sigma_3$, and according to Duncan and Chang's equation, the Young's modulus decreases. This situation agrees well with our theory and prediction.

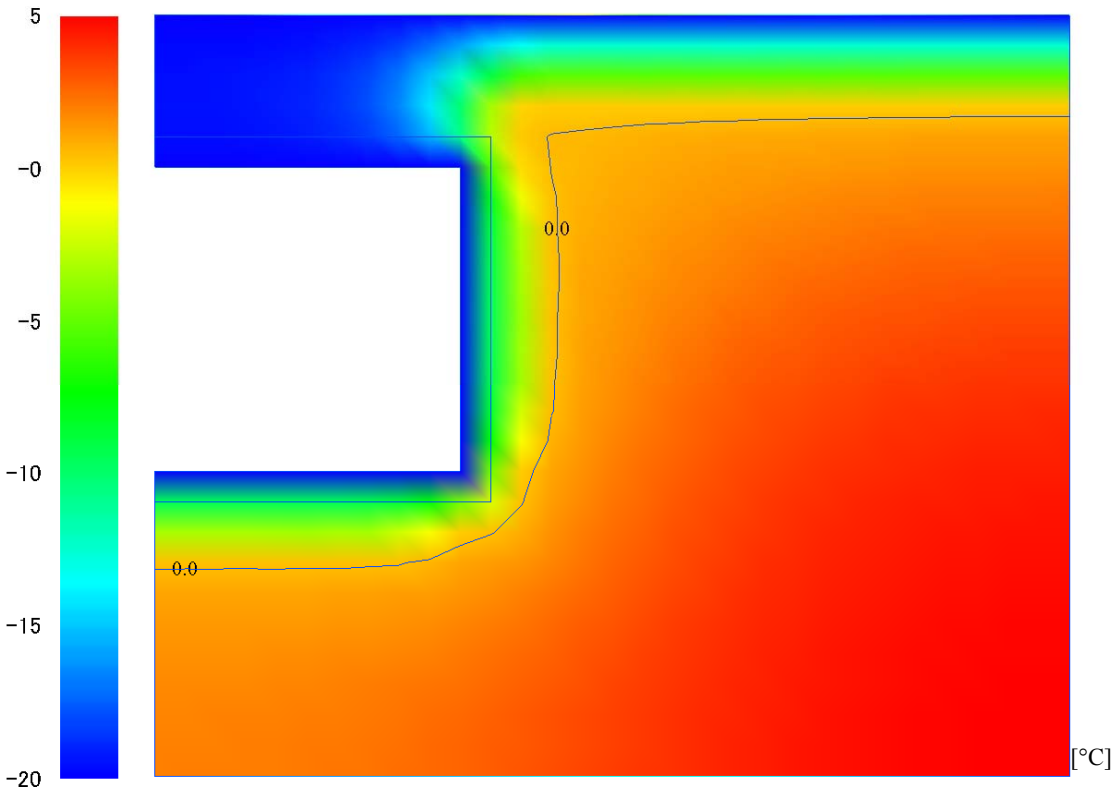



Figure 5-13 Temperature contour of the concrete culvert example after 90 days.

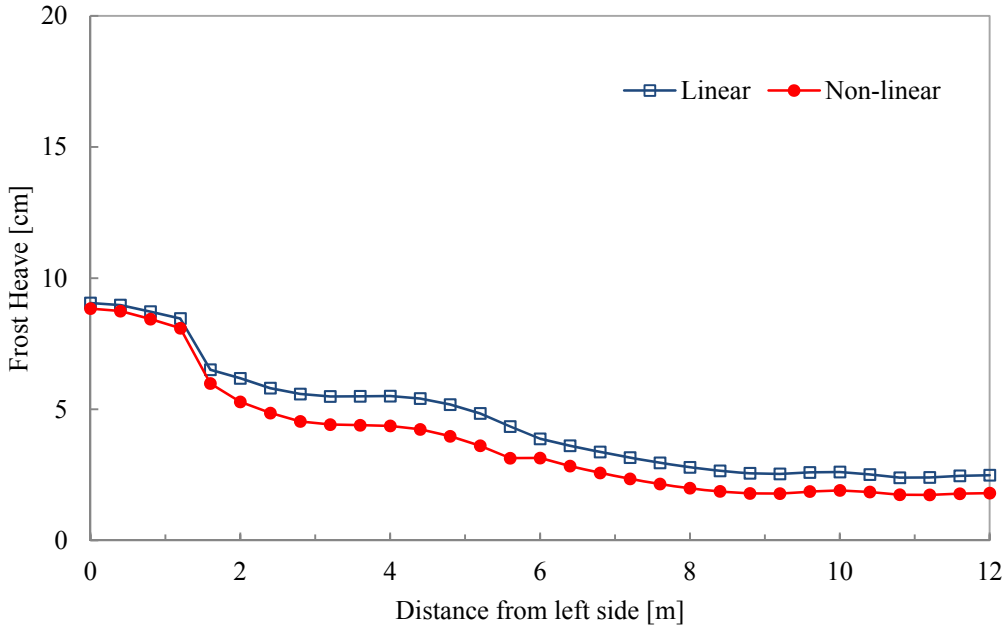



Figure 5-14 Frost heave at the top surface of the concrete culvert example after 90 days

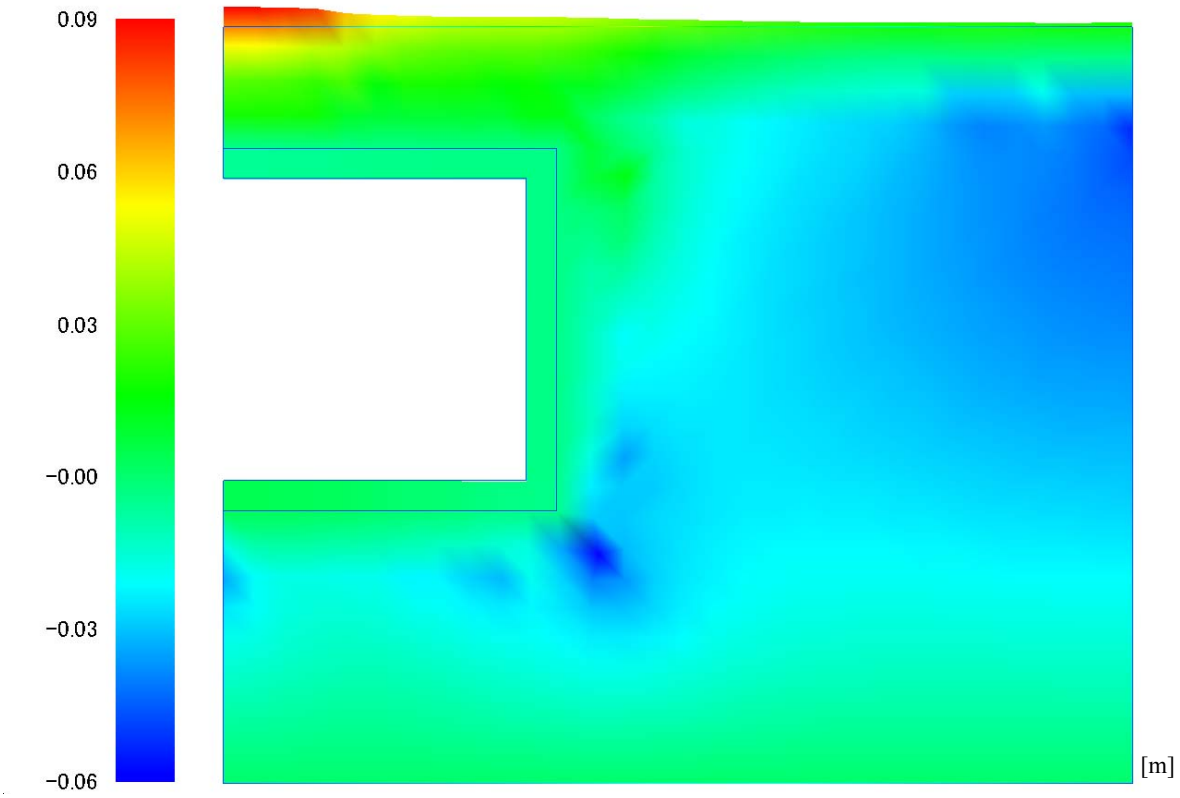



Figure 5-15 Vector displacement distribution of nonlinear model after 90 days (amplification ratio is 3).

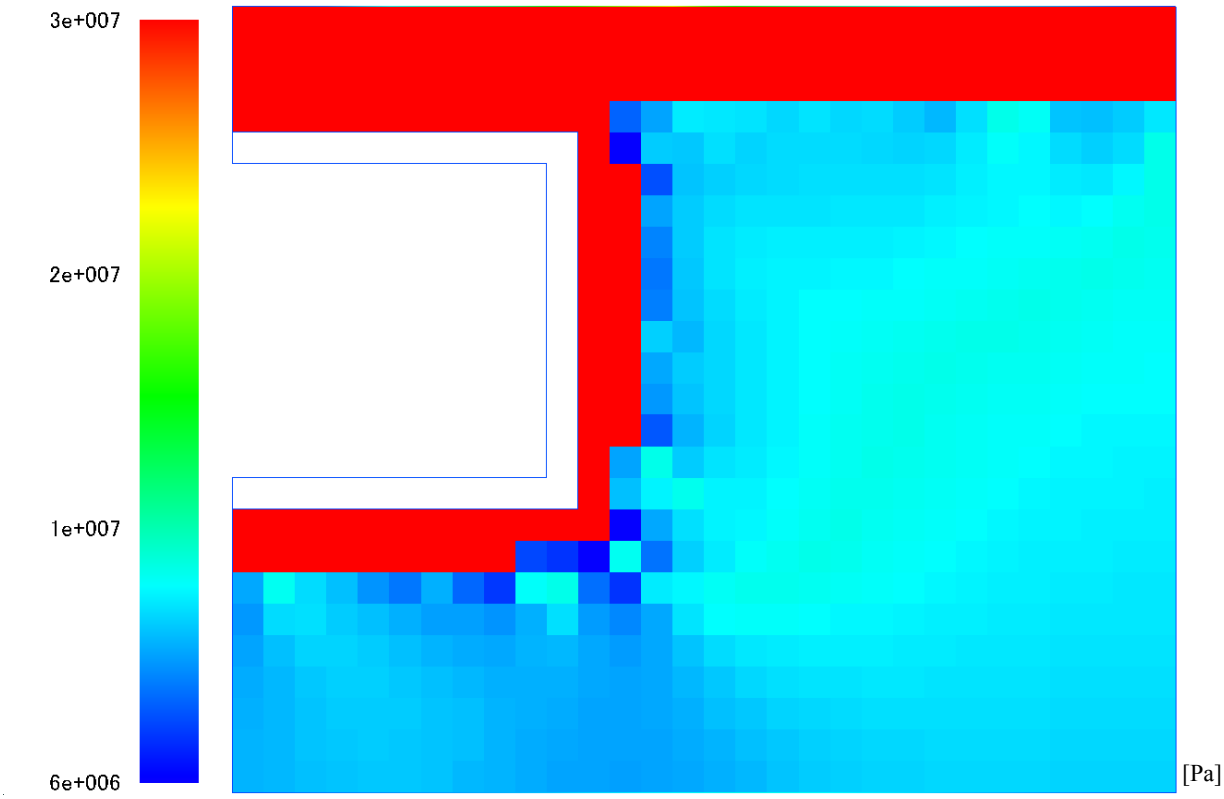



Figure 5-16 Distribution of Young's modulus of soils in nonlinear model for the concrete culvert example after 90 days.

Frost heave is not the only factor we examined for nonlinear properties. In fact, changes in stress field caused by nonlinearity represent another very critical aspect of practical engineering activities. Owing to the complicated distribution of Young's modulus (Figure 5-16) and uneven frost heave (Figure 5-14), the stress distribution of nonlinear models becomes overly complicated. Hence, in this section, we only compare the stress in some critical areas. In the following section, the stress conditions at the bottom and right boundary side of this model are compared for the linear and nonlinear models. The stress distributions around the boundaries are shown in Figure 5-17 and Figure 5-18.

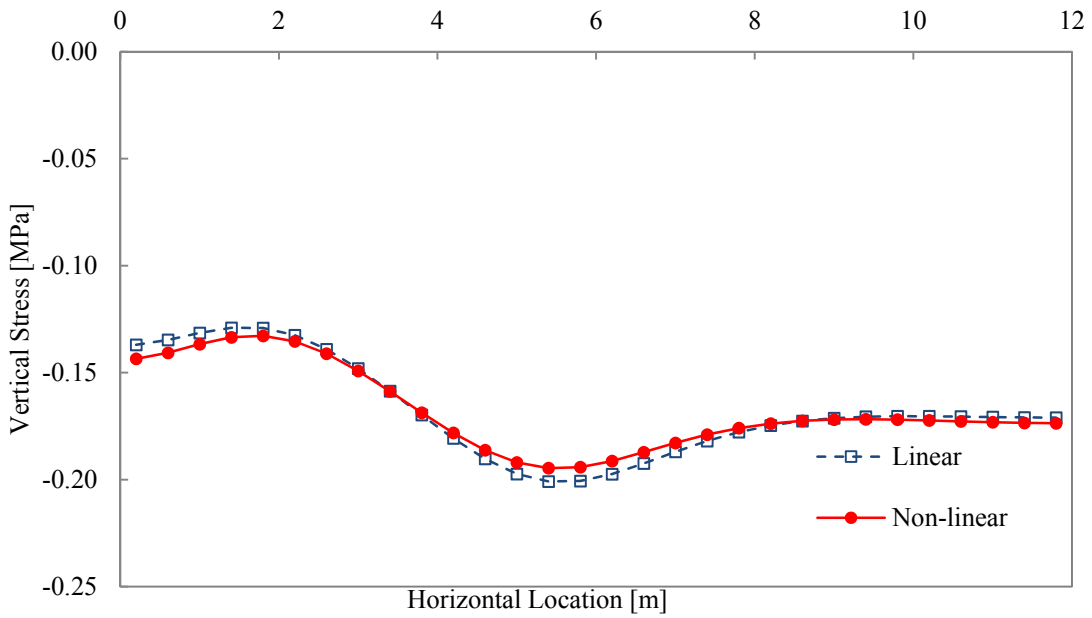



Figure 5-17 Stress ($\sigma_{yy}$) distribution at the bottom of the concrete culvert example after 90 days

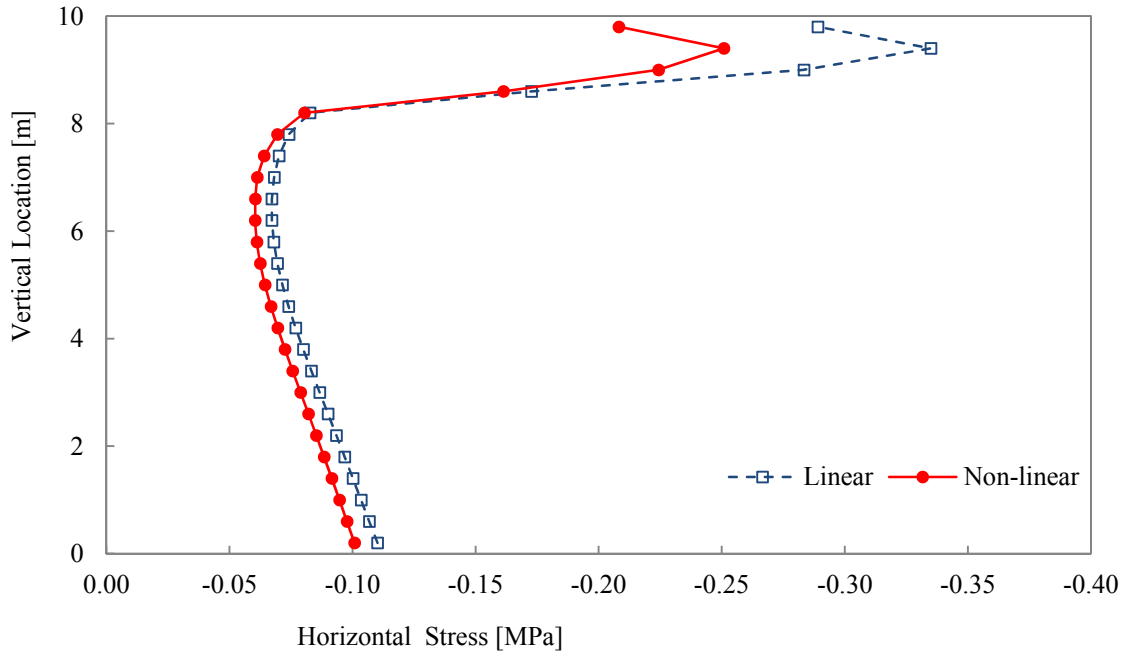



Figure 5-18 Stress ($\sigma_{xx}$) distribution at the right boundary of the concrete culvert example after 90 days

We find that between these two boundaries, the right boundary receives the maximum stress caused by frost heave around the concrete culvert. From the vertical direction, between frozen and unfrozen boundaries the stress fluctuates as a result of frost heave (Figure 5-18). In Figure 5-17, the linear model shows that under the concrete culvert, compression stress occurs. However, for the nonlinear model, owing to the softening process of soil under the concrete culvert, this compression stress is relieved compared to linear one. Additionally, the nonlinear model always displays a smaller absolute value of stress than the linear model, which proves that the linear model may overestimate the stress. And the softened soil always relaxes the stresses. These overestimations of frost heave and stress increase the requirements for structures. Accordingly, the inclusion of nonlinear properties during the estimation of frost heave is essential for both economic and safety purposes. Our model, which combines frost heave analysis and nonlinear properties, is proved to be necessary.

## 6. HYDRAULIC ANALYSIS

In this chapter, thermal influence brought by water flow and unsaturated frost heave are discussed. According to this purpose, water flow governing equation considering both saturated and unsaturated conditions is derived. Then empirical equations for specific capacity of soil and pressure dependent water content are introduced. Further we assume that the unsaturated hydraulic conductivity for unfrozen soil is related to water pressure. For frozen situation, we assume this value to be zero to represent the low hydraulic conductivity. Based on this hydraulic analysis, simple example is used to verify our calculation first and then examples are provided to state the unsaturated frost heave and thermal influence brought by water flow.

### 6.1 GOVERNING EQUATION OF WATER FLOW

In Figure 6-1, 1234 is a very small element. And the time interval is *dt.*

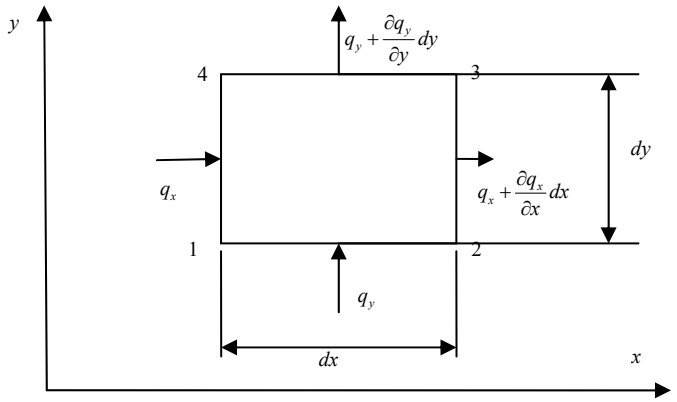



Figure 6-1 The flow balance of two dimension small element

The water transfer in x direction:

$$\left\{ q_x - \left( q_x + \frac{\partial q_x}{\partial x} dx \right) \right\} dydt = -\frac{\partial q_x}{\partial x} dxdydt \tag{6-1}$$

Where $q_x = -k_x \frac{\partial h}{\partial x}$, $k_x$ is the permeability coefficient in *x* direction. $q_x$ is the water flux in *x* direction, and *h* is the total head (hydraulic head), *P* is the pore water pressure head, *z* is the elevation head and *h* = *P*+*z*.

Thus Equation (6-1) can be rewritten as follows:

$$-\frac{\partial q_x}{\partial x} dxdydt = k_x \frac{\partial^2 h}{\partial x^2} dxdydt \tag{6-2}$$

Similarly, water transfer in *y* direction can be written as follows:

$$k_y \frac{\partial^2 h}{\partial y^2} dxdydt \tag{6-3}$$

The sum of water flow into *x* and *y* direction is:

$$k_x \frac{\partial^2 h}{\partial x^2} dxdydt + k_y \frac{\partial^2 h}{\partial y^2} dxdydt \tag{6-4}$$

At the same time, the change of water in this element during *dt* equals to:

1) Saturated situation

$$S_S \frac{\partial h}{\partial t} dxdydt \tag{6-5}$$

$S_S$ is the volumetric specific storage of soil. Volumetric specific storage is the volume of water that an aquifer releases from storage, per volume of aquifer, per unit decline in hydraulic head, and the unit of this parameter is $m^{-1}$.

2) Unsaturated situation

$$C \frac{\partial h}{\partial t} dxdydt \tag{6-6}$$

*C* is the specific capacity of soil and $C = \partial\theta/\partial P$. $\theta$ is the volumetric water content.

And combine these two situations; the change of water during *dt* could be expressed as:

$$(\gamma S_S + C)\frac{\partial h}{\partial t}dxdydt \tag{6-7}$$

For a saturated condition, $\gamma = 1$ and $C = 0$; for an unsaturated condition, $\gamma = 0$ and $C \neq 0$.

With Equation (6-4) and Equation (6-7), the following equation can be obtained:

$$(\gamma S_S + C)\frac{\partial h}{\partial t}dxdydt = k_x \frac{\partial^2 h}{\partial x^2}dxdydt + k_y \frac{\partial^2 h}{\partial y^2}dxdydt \tag{6-8}$$

And if assume $k_x = k_y = k$, the equation can be rewritten:

$$(\gamma S_S + C)\frac{\partial h}{\partial t} = k\left(\frac{\partial^2 h}{\partial x^2} + \frac{\partial^2 h}{\partial y^2}\right) \tag{6-9}$$

This is the governing equation which considers saturated and unsaturated conditions together.

The quantity C = ∂θ/∂P can be determined from the soil–water characteristics. It is computationally convenient to represent the soil–water characteristics as a known or assumed function, relating the pore water pressure and volumetric water content. This can be done by determining point values of θ and P in the laboratory and applying a least squares fitting of an assumed function to their data. Cold Regions Research and Engineering Laboratory (CRREL) carried this out for a large number of soils and found that Gardner's function fits these soils well [29] [30]:

$$\theta = \frac{\theta_o}{A_w |P|^a + 1} \tag{6-10}$$

where $\theta_o$ is the soil porosity. $a$ and $A_w$ are the best fit parameters determined for different soils. This equation is used to obtain the water content in our calculation. Thus, specific capacity $C$ can be expressed as follows:

$$C = \frac{\partial \theta}{\partial P} = \frac{\theta_o a A_w |P|^{a-1}}{\left(A_w |P|^a + 1\right)^2} \tag{6-11}$$

Similarly, it is computationally convenient to represent the hydraulic permeability function for unsaturated soils as a known or assumed function. This function can be obtained from laboratory data by determining point values of k and P for different soils and by applying a least squares fitting of an assumed function to these data. Again, CRREL performed this for a large number of soils and found that Gardner's function also fits these data well [31] [32]:

$$k = \frac{k_s}{A_k \left| P \right|^b + 1} \tag{6-12}$$

where $k_S$ is the saturated hydraulic conductivity and $A_k$ and $b$ are the best fit parameters determined for different soils. Because Equation (6-9) is also applied to thawing or freezing zones, an empirical phenomenological relationship is necessary to adjust the unfrozen coefficient of hydraulic conductivity to represent the frozen hydraulic conductivity $k_f$ where ice may partly block the soil pores, reducing the hydraulic conductivity. For simplification, we neglect the water permeability in frozen soil, thus, $k_f = 0$.

The best method of estimating the freezing pore water pressure head is to compute $P$ from Equation (6-10) by known or assumed parameters, $a$ and $A_w$, and the unfrozen water content factor. Since we rely on Takashi's equation to represent the complicated coupled thermal and hydraulic process during freezing, thus we assume the pore water pressure to be 0 if the soil was completely frozen. Concerning the mechanical analysis, more details could be referred to our previous works [33] [34]. At this point, the computational model for frost heave development, which accompanies the coupled processes of thermal–hydraulic–mechanical, is fully developed. In the subsequent section, this model would be applied in various conditions to illustrate its applicability.

## 6.2 THE APPLICATION OF FEM TO WATER FLOW EQUATION

Based on the Equation (6-9), we assume a $\bar{h}$ first and then we can get the error or residual $R$:

$$R = \left\{ k\left( \frac{\partial^2 \bar{h}}{\partial x^2} + \frac{\partial^2 \bar{h}}{\partial y^2} \right) - (\gamma S_s + C)\frac{\partial \bar{h}}{\partial t} \right\} - \left\{ k\left( \frac{\partial^2 h}{\partial x^2} + \frac{\partial^2 h}{\partial y^2} \right) - (\gamma S_s + C)\frac{\partial h}{\partial t} \right\}$$

$$= k\left( \frac{\partial^2 \bar{h}}{\partial x^2} + \frac{\partial^2 \bar{h}}{\partial y^2} \right) - (\gamma S_s + C)\frac{\partial \bar{h}}{\partial t} \tag{6-13}$$

In an attempt to reduce this error in some overall manner over the whole domain, we attempt to make such an integral:

$$\iint \left\{ k\left( \frac{\partial^2 \bar{h}}{\partial x^2} + \frac{\partial^2 \bar{h}}{\partial y^2} \right) - (\gamma S_s + C)\frac{\partial \bar{h}}{\partial t} \right\} \delta h \, dxdy = 0 \tag{6-14}$$

Then apply the Green's theorem to Equation (6-14), we can see that:

$$\iint k\left( \frac{\partial^2 \bar{h}}{\partial x^2} + \frac{\partial^2 \bar{h}}{\partial y^2} \right) \delta h dxdy$$

$$= \oint_S k \frac{\partial \bar{h}}{\partial x} n_x \delta h ds - \iint k \frac{\partial \delta h}{\partial x} \frac{\partial \bar{h}}{\partial x} dxdy + \oint_S k \frac{\partial \bar{h}}{\partial y} n_y \delta h ds - \iint k \frac{\partial \delta h}{\partial y} \frac{\partial \bar{h}}{\partial y} dxdy$$

$$= -\oint_S q_x n_x \delta h ds - \iint k \frac{\partial \delta h}{\partial x} \frac{\partial \bar{h}}{\partial x} dxdy - \oint_S q_y n_y \delta h ds - \iint k \frac{\partial \delta h}{\partial y} \frac{\partial \bar{h}}{\partial y} dxdy \tag{6-15}$$

$$\iint (\gamma S_s + C)\frac{\partial \bar{h}}{\partial t} \delta h \, dxdy = (\gamma S_s + C) \iint \frac{\partial \bar{h}}{\partial t} \delta h \, dxdy \tag{6-16}$$

Thus Equation (6-14) can be rewritten as:

$$\iint k \frac{\partial \delta h}{\partial x} \frac{\partial \bar{h}}{\partial x} dxdy + \iint k \frac{\partial \delta h}{\partial y} \frac{\partial \bar{h}}{\partial y} dxdy - (\gamma S_S + C) \iint \frac{\partial \bar{h}}{\partial t} \delta h dxdy = -\oint_S q_x n_x \delta h ds - \oint_S q_y n_y \delta h ds \tag{6-17}$$

After that, the temperature can be expressed by shape function as follow:

$$h = \begin{bmatrix} N_1 & N_2 & N_3 & N_4 \end{bmatrix} \begin{Bmatrix} h_1 \\ h_2 \\ h_3 \\ h_4 \end{Bmatrix} = [N]\{h\} \tag{6-18}$$

$$\delta h = [N]\{\delta h\} \quad \frac{\partial h}{\partial x} = \left[\frac{\partial N}{\partial x}\right]\{h\} \quad \frac{\partial \bar{h}}{\partial t} = [N]\left\{\frac{\partial h}{\partial t}\right\} \tag{6-19}$$

Equation (6-17) becomes:

$$\{\delta h\}^T k\left\{\iint\left(\left[\frac{\partial N}{\partial x}\right]^T\left[\frac{\partial N}{\partial x}\right]+\left[\frac{\partial N}{\partial y}\right]^T\left[\frac{\partial N}{\partial y}\right]\right)dxdy\right\}\{h\}$$

$$-\{\delta h\}^T\left\{\oint_S q_x n_x [N]^T ds + \oint_S q_y n_y [N]^T ds\right\}$$

$$(\gamma S_s + C)\iint\frac{\partial \bar{h}}{\partial t}\delta h\, dxdy = \{\delta h\}^T(\gamma S_s + C)\iint[N]^T[N]dxdy\left\{\frac{\partial h}{\partial t}\right\}$$

Finally,

$$k\left\{\iint\left(\left[\frac{\partial N}{\partial x}\right]^T\left[\frac{\partial N}{\partial x}\right]+\left[\frac{\partial N}{\partial y}\right]^T\left[\frac{\partial N}{\partial y}\right]\right)dxdy\right\}\{h\} - (\gamma S_s + C)\iint[N]^T[N]dxdy\left\{\frac{\partial h}{\partial t}\right\} =$$

$$-\oint_S q_x n_x [N]^T ds - \oint_S q_y n_y [N]^T ds \tag{6-20}$$

where,

$$\left[\frac{\partial N}{\partial x}\right]^T\left[\frac{\partial N}{\partial x}\right]+\left[\frac{\partial N}{\partial y}\right]^T\left[\frac{\partial N}{\partial y}\right]$$

$$=\begin{bmatrix}\frac{\partial N_1}{\partial x}\\ \frac{\partial N_2}{\partial x}\\ \frac{\partial N_3}{\partial x}\\ \frac{\partial N_4}{\partial x}\end{bmatrix}\begin{bmatrix}\frac{\partial N_1}{\partial x} & \frac{\partial N_2}{\partial x} & \frac{\partial N_3}{\partial x} & \frac{\partial N_4}{\partial x}\end{bmatrix}+\begin{bmatrix}\frac{\partial N_1}{\partial y}\\ \frac{\partial N_2}{\partial y}\\ \frac{\partial N_3}{\partial y}\\ \frac{\partial N_4}{\partial y}\end{bmatrix}\begin{bmatrix}\frac{\partial N_1}{\partial y} & \frac{\partial N_2}{\partial y} & \frac{\partial N_3}{\partial y} & \frac{\partial N_4}{\partial y}\end{bmatrix}$$

$$=\begin{bmatrix}\frac{\partial N_1}{\partial x} & \frac{\partial N_1}{\partial y}\\ \frac{\partial N_2}{\partial x} & \frac{\partial N_2}{\partial y}\\ \frac{\partial N_3}{\partial x} & \frac{\partial N_3}{\partial y}\\ \frac{\partial N_4}{\partial x} & \frac{\partial N_4}{\partial y}\end{bmatrix}\begin{bmatrix}\frac{\partial N_1}{\partial x} & \frac{\partial N_2}{\partial x} & \frac{\partial N_3}{\partial x} & \frac{\partial N_4}{\partial x}\\ \frac{\partial N_1}{\partial y} & \frac{\partial N_2}{\partial y} & \frac{\partial N_3}{\partial y} & \frac{\partial N_4}{\partial y}\end{bmatrix}=[B]^T[B]$$

Finally Equation (6-20) becomes as below:

$$k\left\{\iint[B]^T[B]dxdy\right\}\{h\}-(\gamma S_s+C)\iint[N]^T[N]dxdy\left\{\frac{\partial h}{\partial t}\right\}=\{f\} \tag{6-21}$$

Here $\{f\}=\oint_S q_x n_x[N]^T ds+\oint_S q_y n_y[N]^T ds$.

This is the idea how we calculate the hydraulic process inside this model. other details of this section are similar with that of thermal analysis, such as the numerical integration and the time domain.

## 6.3 DISCUSSION OF HYDRAULIC INFLUENCE

In section, first our hydraulic analysis is validated by some simple examples and then based on this verified model, more complicated examples are presented to discuss the water influence.

### 6.3.1 Validation Examples

In this section, one-dimensional and two-dimensional water flow models are shown to validate the basic function of this model. Excel calculation is not provided because that the calculation process is totally the same as shown for thermal analysis. First, a one-dimensional model is given to check the

water flow situation. The parameters used in this example are shown by the following Table:

Table 6-1 Parameters for one-dimensional water flow simulation

| Mechanical Parameters | | Hydraulic Parameters | | Thermal Parameters | |
|---|---|---|---|---|---|
| $E$ [N/ m$^2$] | $2.80\times10^{7}$ | $k_s$ [m/s] | $1.16\times10^{-7}$ | $\lambda$ [J/m.K.s] | 1.00 |
| Poisson ratio | 0.3 | $a$ | 0.638 | $c$ [J/kg.K] | 1008 |
| $\theta_o$ | 0.3 | $A_w$ | $1.58\times10^{-2}$ | $\rho$ [kg/ m$^3$] | 1800 |
| $\xi_0$ | $6.478\times10^{-3}$ | $b$ | 2.36 | $c_w$ [J/kg.K] | 4200 |
| $\sigma_0$ [N/m$^2$] | $4.563\times10^{3}$ | $A_k$ | $6.46\times10^{-5}$ | $\rho_w$ [kg/m$^3$] | 1000 |
| $U_0$ [m/s] | $4.431\times10^{-7}$ | $S_s$ [m$^{-1}$] | $3.0\times10^{-4}$ | $\beta$ | 0 |

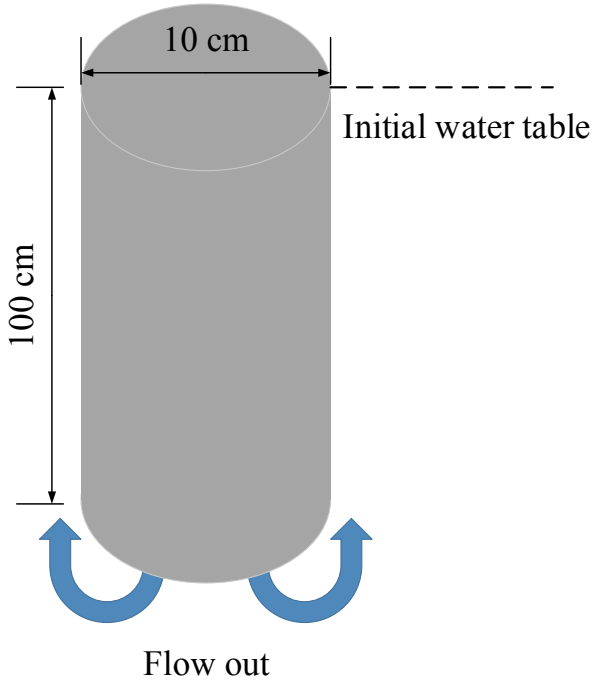



Figure 6-2 The one-dimensional water flow model

Initially, the soil column is assumed fully saturated and water table is at the top surface of this column. After that we let the water flow out from the bottom and we check the water table location change as the time change. The size of each time step is 12 seconds. By the following figure, we can check the water table change. As the time goes, the water flows out gradually.

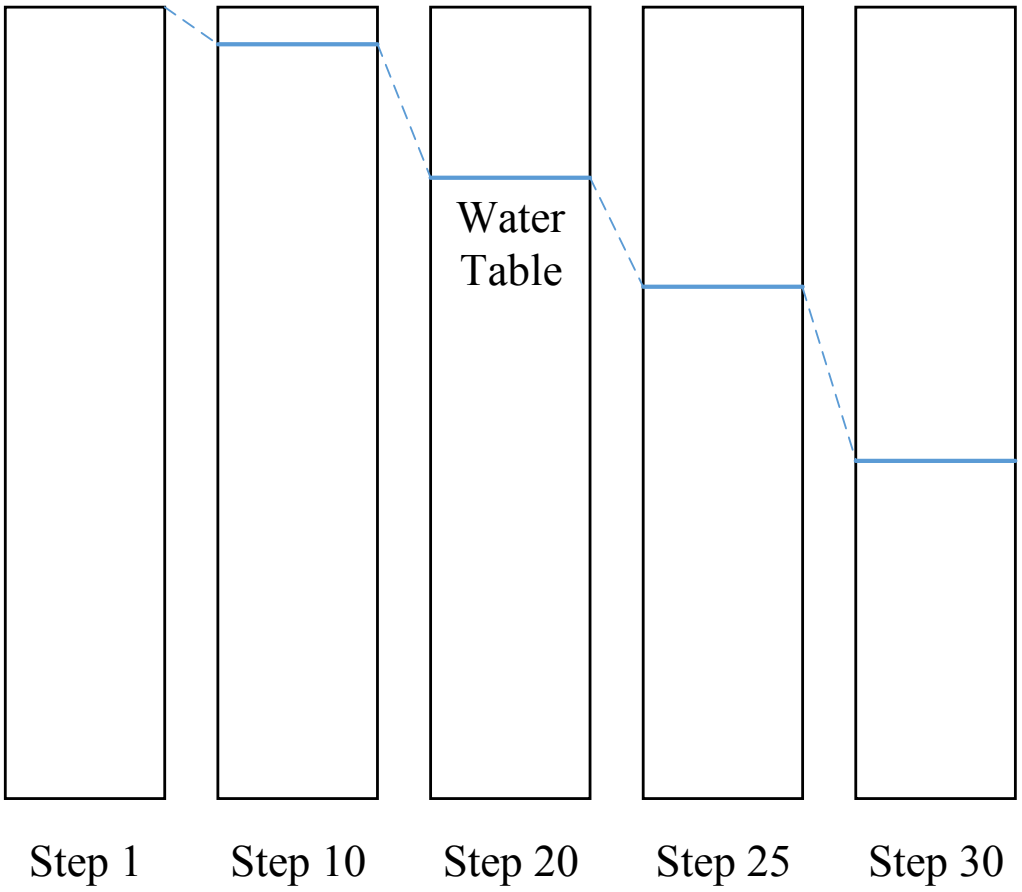



Figure 6-3 The water table location at each time step for one-dimensional model

After one-dimensional water flow simulation, a 2D model is illustrated to give a more complicated and real image of water flow. The size of this 2D model is 1m × 1m.

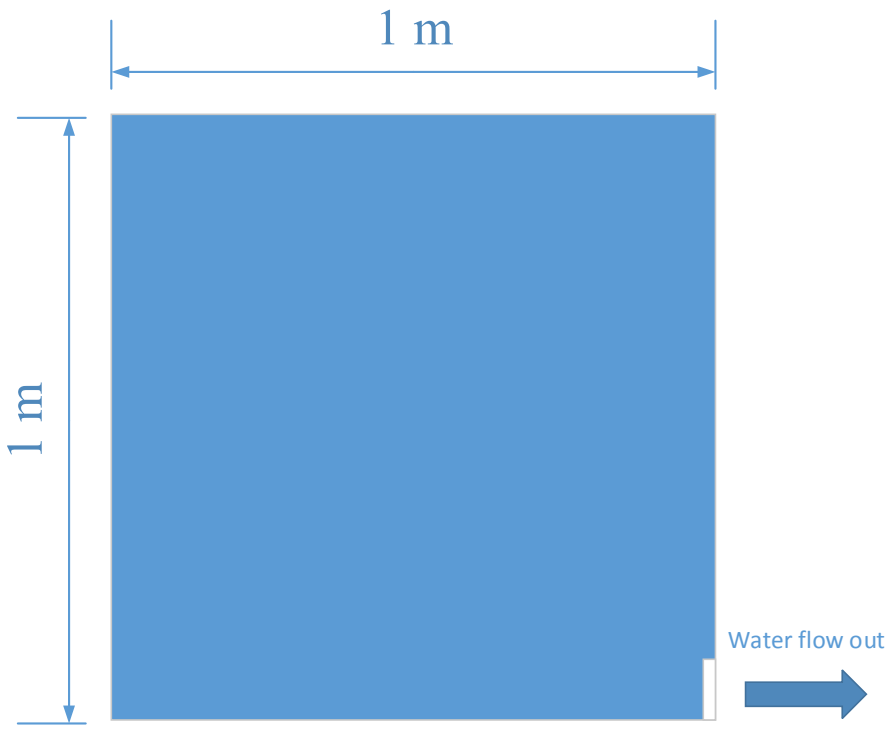



Figure 6-4 The two-dimensional water flow model

Table 6-2 Parameters for one-dimensional water flow simulation

| Mechanical Parameters | | Hydraulic Parameters | | Thermal Parameters | |
|---|---|---|---|---|---|
| $E$ [N/ m$^2$] | $2.80\times10^{7}$ | $k_s$ [m/s] | $5.56\times10^{-6}$ | $\lambda$ [J/m.K.s] | 1.00 |
| Poisson ratio | 0.3 | $a$ | $5.7\times10^{-3}$ | $c$ [J/kg.K] | 1008 |
| $\theta_o$ | 0.3 | $A_w$ | 1.6286 | $\rho$ [kg/ m$^3$] | 1800 |
| $\xi_0$ | $2.5\times10^{-2}$ | $b$ | $7.54\times10^{-2}$ | $c_w$ [J/kg.K] | 4200 |
| $\sigma_0$ [N/m$^2$] | $8.0\times10^{2}$ | $A_k$ | $4.365\times10^{-1}$ | $\rho_w$ [kg/m$^3$] | 1000 |
| $U_0$ [m/s] | $6.9\times10^{-8}$ | $S_s$ [m$^{-1}$] | $2.0\times10^{-2}$ | $\beta$ | 0 |

As the time goes, water will flow out from the bottom hole. In this situation, we can observe the water tables. The size of time step is 6 seconds.

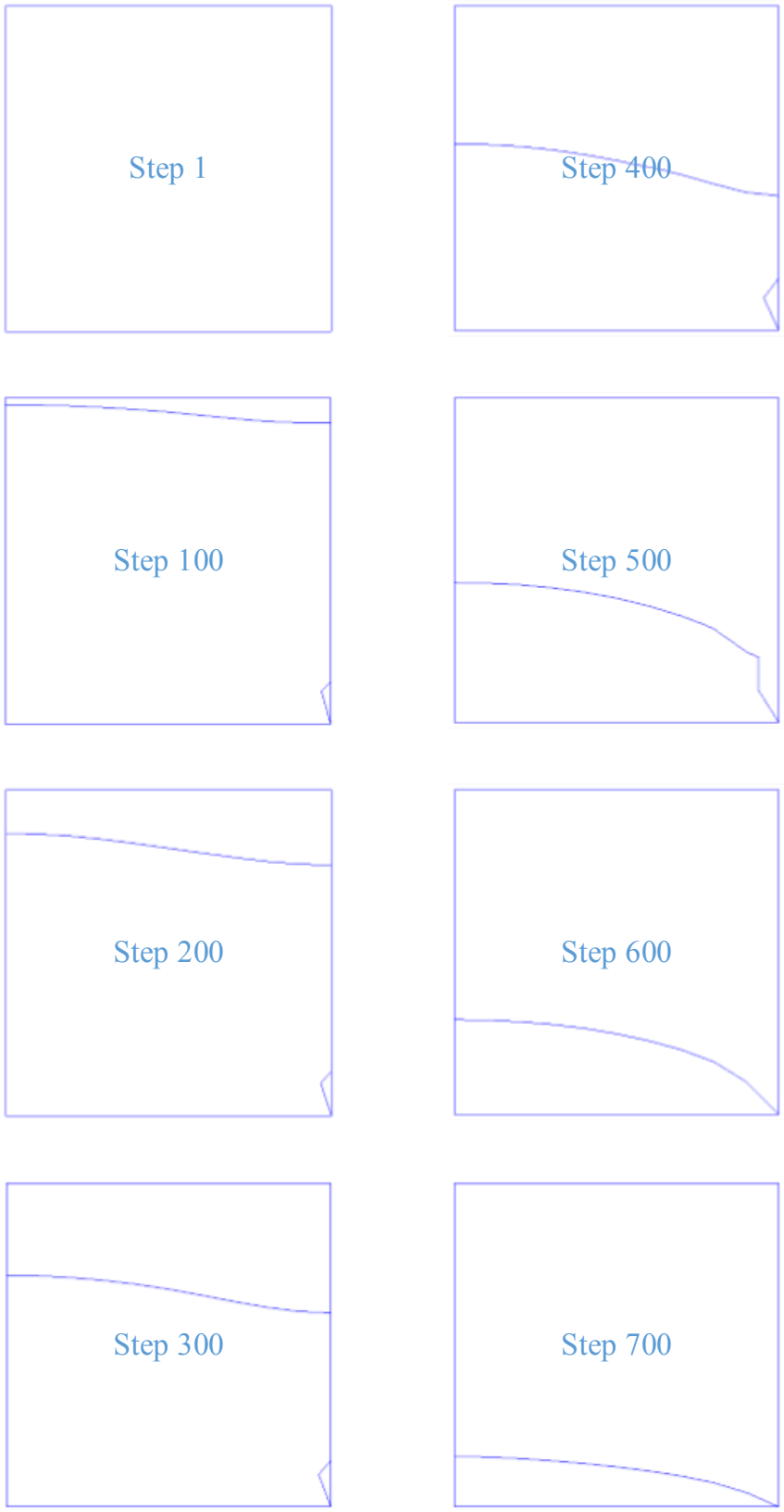



Figure 6-5 The water table location at each time step for two-dimensional model

### 6.3.2 Influence of Hydraulic Condition

The direct purpose of this simple 1D example is to verify that our program works. Here, temperature distribution and frost heave amount are considered. A computational domain of 15 cm in height and 6 cm in width is used for the simulation (Figure 6-6). In the horizontal direction, displacement in X direction is prohibited and heat flow is forbidden at both sides. At the bottom boundary, displacement in Y direction is fixed. For the top surface of this model, displacement is free. The material parameters used in this model are listed in

Table 6-3. Based on this simple model, we compare the temperature distribution and frost heave using an opposite freezing direction. We assume that the initial water table is at 15 cm in height from the bottom which means that the sample is fully saturated at the beginning. Water is supplied from the bottom in order to maintain the saturated situation. As we know, Takashi's equation is only valid for a saturated condition. For an unsaturated situation, only in-situ freezing can occur and there is a 9% volume increment when the water becomes ice.

The initial temperature of this soil sample is kept at 0 °C. The temperatures on the cold side are shown in Figure 6-7. The other side remains constant at 0 °C. The difference is that we apply this cold temperature from different directions: top and bottom. The temperature distribution results of these two calculations after 60 hours are given in Figure 6-8. Frost heave when the freezing direction is from top to bottom is about 11.36 mm. Frost heave when the freezing direction is from bottom to top is about 11.26 mm. These results are shown in Figure 6-9. The shape of frost heave development is step wise. It is because that, our model in vertical direction is divided into 10 elements and in every step we judge each element is frozen or not. If this element was frozen, then frost heave occurs. If the model is divided into more elements in vertical direction, such a step wise situation will be improved or avoided. According to the temperature distribution (Figure 6-8), the entire sample is saturated and 90% of the sample is frozen. Hence, we can use Takashi's equation to estimate the frost heave of this sample. The curves clearly demonstrate our expectation. We can see that though the freezing direction is different, the total frost heave amount is very close. This is easy to understand since regardless of the freezing direction, the total frozen portion is the same, about 90% of the sample. The small difference seems to be the result of the constraining stress in Takashi's equation, not the freezing direction itself. In fact, Takashi's equation cannot consider the influence caused by the different freezing directions. Due to the actual weight of the soil, when the freezing was from the bottom, the constraining stress is slightly larger than when the freezing was from the top. According to Takashi's equation, a larger constraining stress leads to a smaller frost heave ratio, therefore the frost heave when the freezing direction is from bottom to top is smaller. However, in this example, the difference between these different freezing directions is really small, 0.1 mm, hence we can neglect the influence caused by freezing directions.

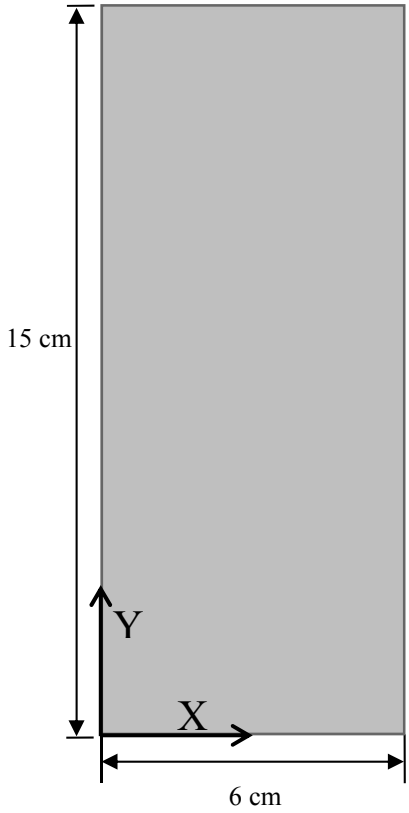



Figure 6-6 Diagram of 1D simulation sample

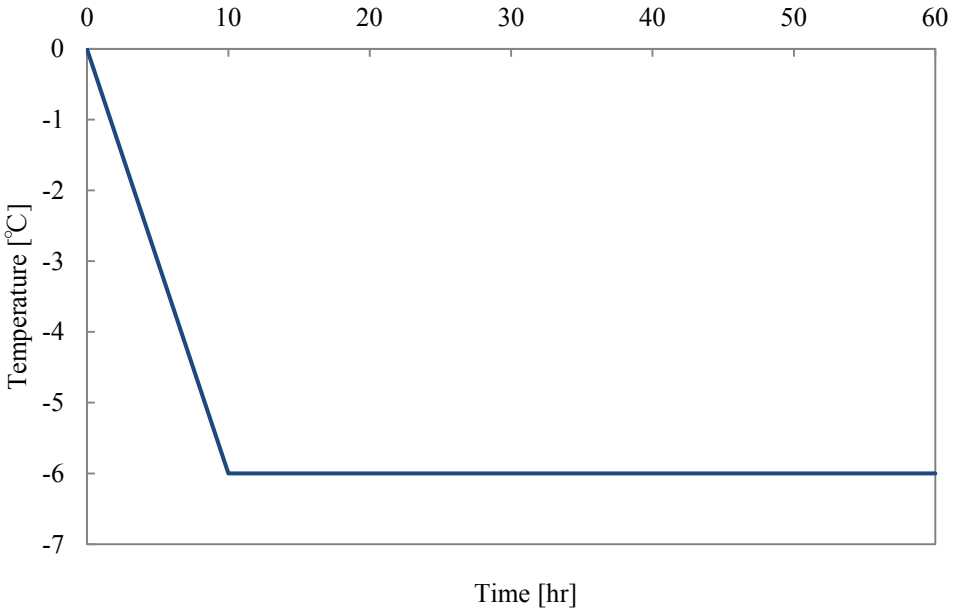



Figure 6-7 Freezing temperatures at cold side

Table 6-3 Soil parameters for 1D simulation.

| Mechanical Parameters | | Hydraulic Parameters | | Thermal Parameters | |
|---|---|---|---|---|---|
| $E$ [N/ m$^2$] | $2.80\times10^{7}$ | $k_s$ [m/s] | $1.16\times10^{-7}$ | $\lambda$ [J/m.K.s] | 1.00 |
| Poisson ratio | 0.3 | $a$ | 0.638 | $c$ [J/kg.K] | 1008 |
| $\theta_o$ | 0.3 | $A_w$ | $1.58\times10^{-2}$ | $\rho$ [kg/ m$^3$] | 1800 |
| $\xi_0$ | $6.478\times10^{-3}$ | $b$ | 2.36 | $c_w$ [J/kg.K] | 4200 |
| $\sigma_0$ [N/m$^2$] | $4.563\times10^{3}$ | $A_k$ | $6.46\times10^{-5}$ | $\rho_w$ [kg/m$^3$] | 1000 |
| $U_0$ [m/s] | $4.431\times10^{-7}$ | $S_s$ [m$^{-1}$] | 0 | $\beta$ | 0 |

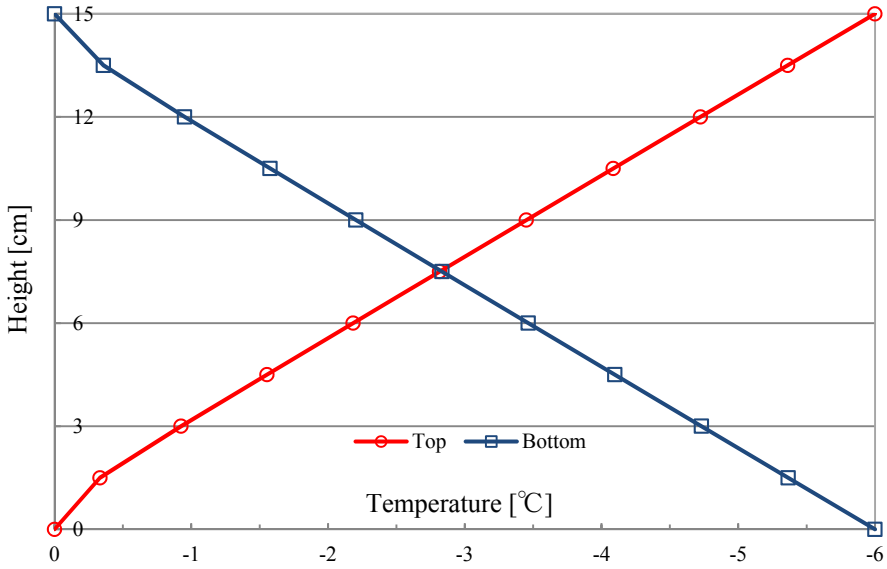



Figure 6-8 Temperature distributions of different freezing directions

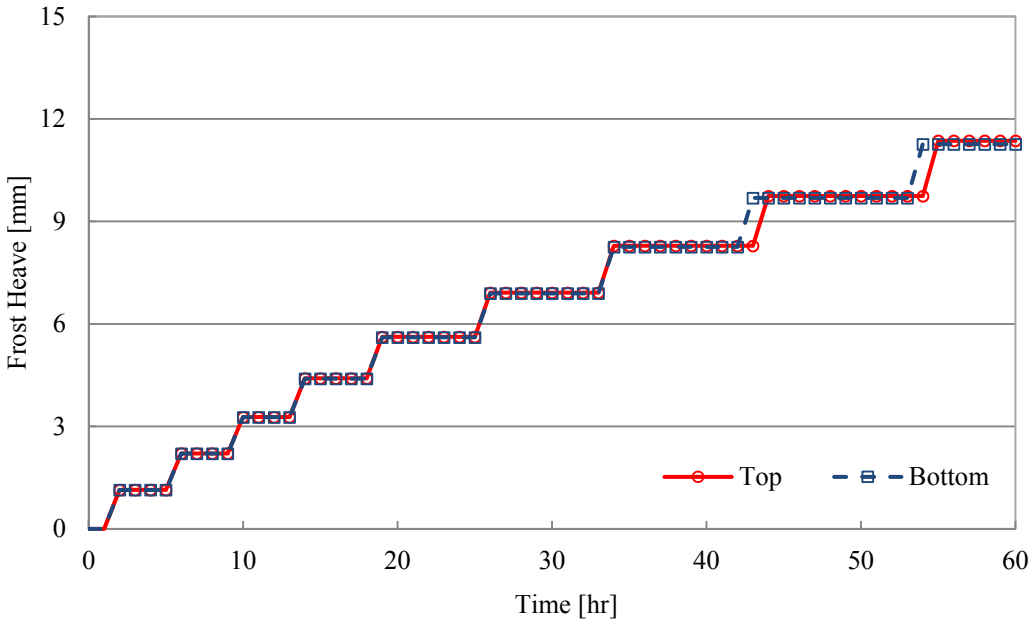



Figure 6-9 Frost heave comparisons of different freezing directions

Following this discussion of freezing directions, we evaluate the influence of the different hydraulic conditions. In order to have a clear and significant comparison, two different water tables are used, 7.5 cm and 15 cm in height from the bottom. That means unsaturated frost heave occurs in this example. And here we assume a very simple assumption to calculate unsaturated frost heave. There is a 9% volume increment when the water becomes ice. If the current water content × 1.09 > the initial porosity, frost heave happens and frost heave ratio= current water content × 1.09 - initial porosity. This assumption may be not good enough, if there is some good theories describing the unsaturated frost heave, I am really glad to adopt that and improve our existing model.

$$\xi_v=1.09\times\theta-\theta_0 \qquad (6\text{-}22)$$

where $\xi_v$ is frost heave ratio; $\theta$ is the current water content and $\theta_0$ is initial soil porosity.

Water is supplied from the bottom to maintain the water table. The freezing direction is from top to bottom, which is generally adopted in laboratory testing. Figure 6-10 plots the time history of the frost heave development. In this graph, when the water table is 15 cm, the total frost heave is 11.36 mm and when the water table is 7.5 cm, the total frost heave is 7.57 mm. This means that when the entire sample is saturated, the total frost heave is slightly smaller than twice of that when only half of the sample is saturated. This phenomenon can be explained by the fact that when the whole sample is saturated, the frost heave is calculated using only Takashi's equation. However, when only half of the sample is saturated, except the saturated half frost heave is calculated by Takashi's equation, there is

also some in-situ frost heave occurring in the unsaturated half of sample. The in-situ frost heave is always smaller than that calculated by Takashi's equation. Thus, the frost heave when water table is 15 cm is not twice of that when the water table is 7.5 cm.

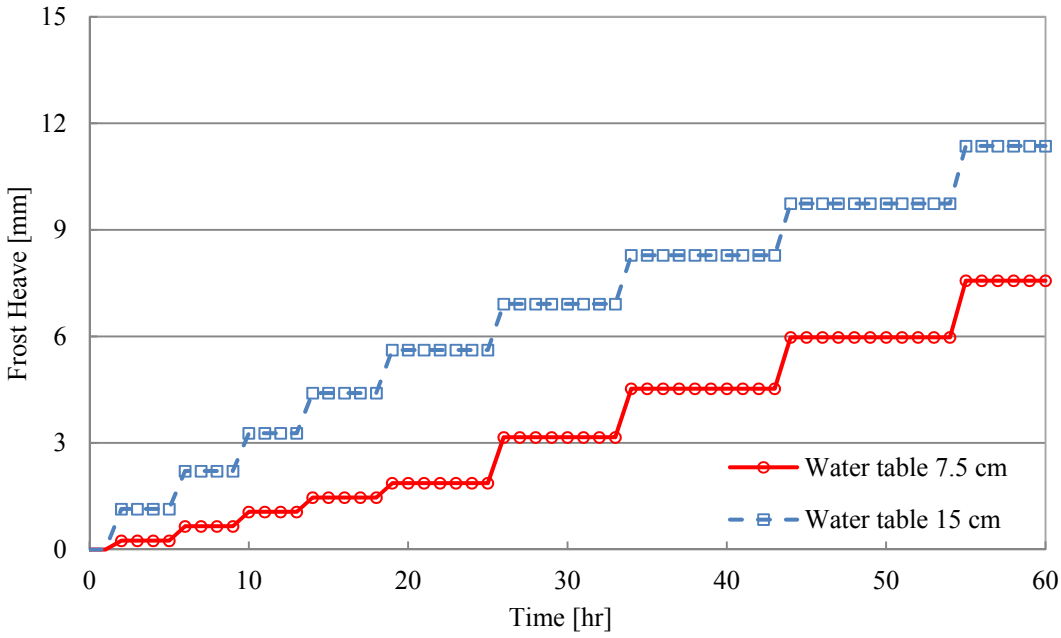



Figure 6-10 Frost heave comparisons of different water tables

According to this simple 1D example, which simulates the frost heave test in the laboratory, we confirm that our model and program works well and are reliable. More complicated examples could be evaluated by this verified model.

### 6.3.3 Influence of Water Flow

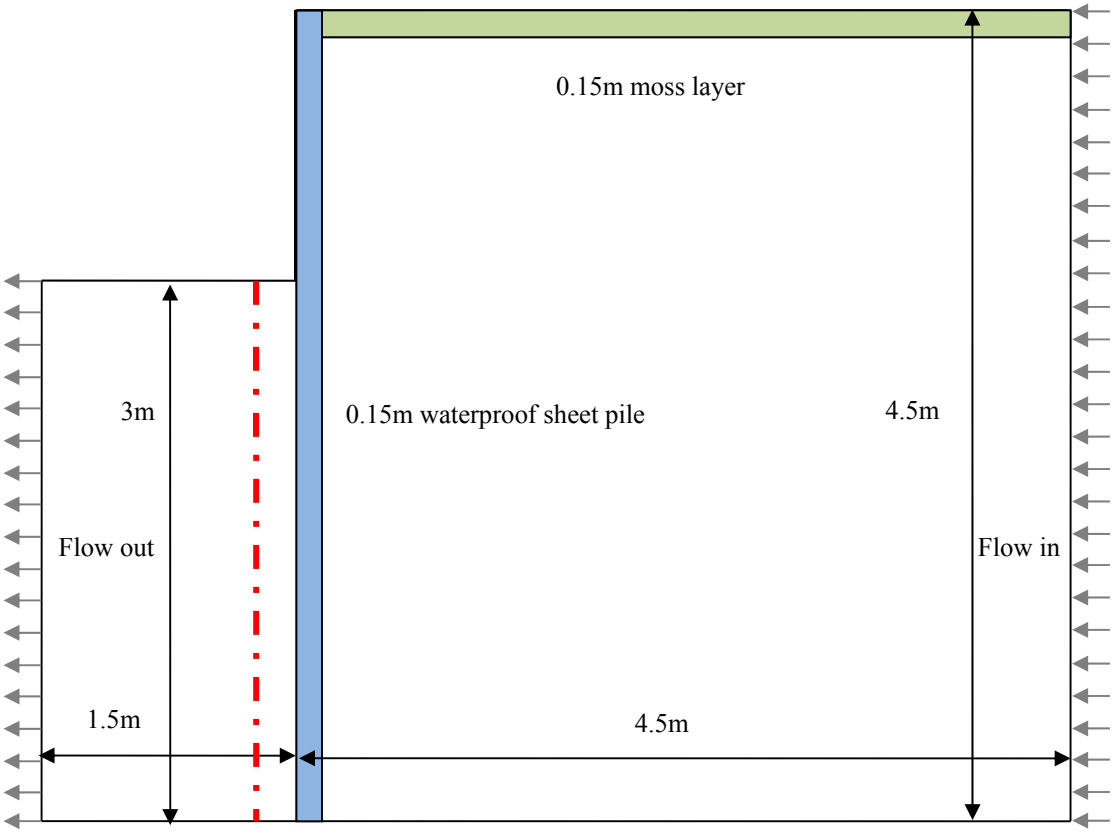



Figure 6-11 Diagram of 2D excavation example

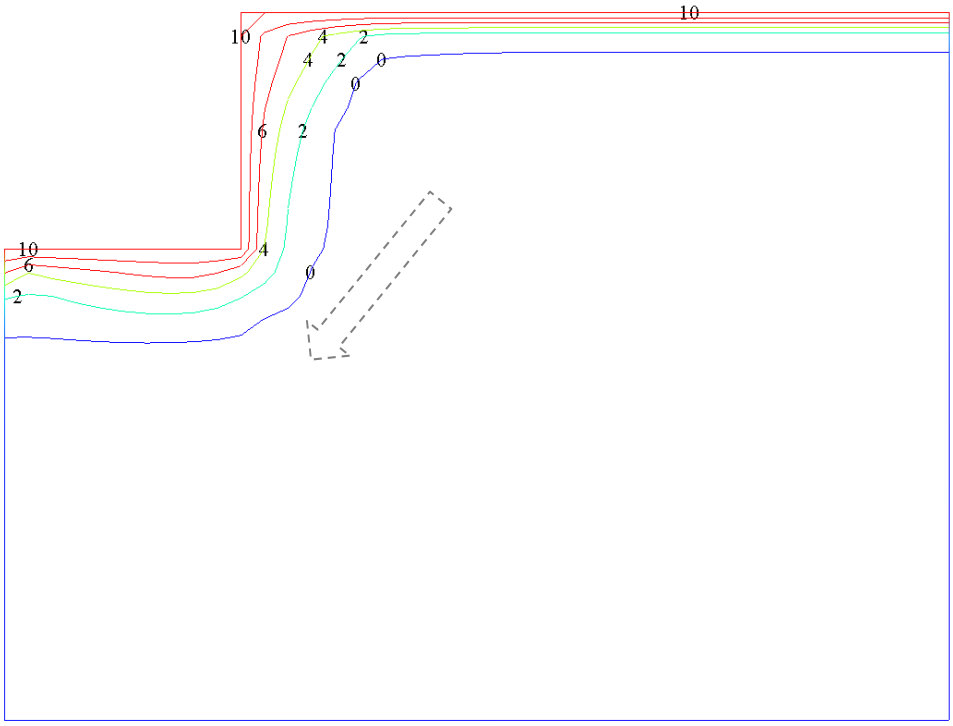



Figure 6-12 Temperature distribution of excavation example without waterproof sheet pile after 40 days

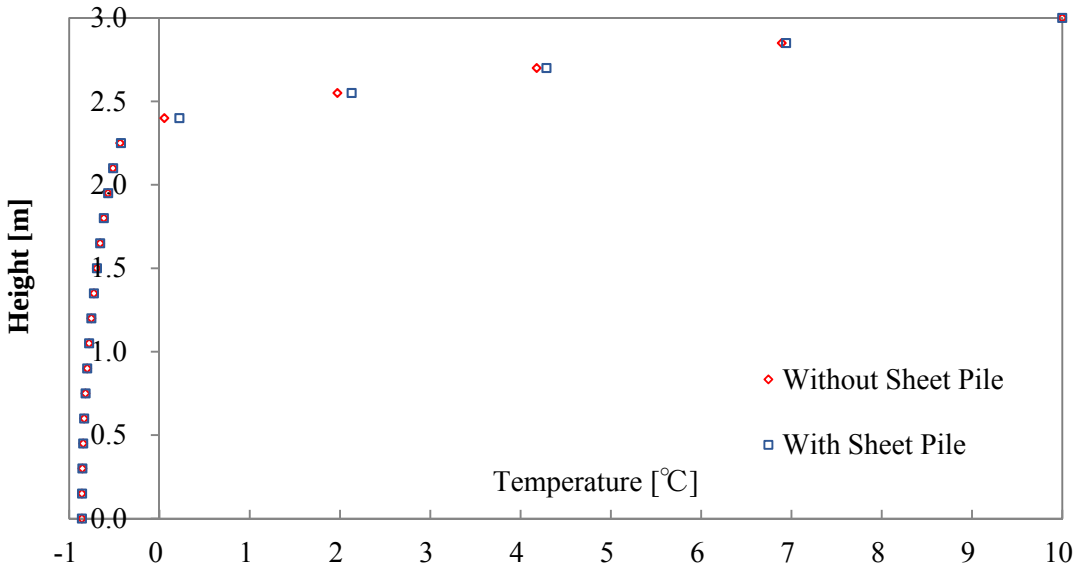



Figure 6-13 Temperature comparisons with and without waterproof sheet pile after 40 days

Table 6-4 Additional material parameters for excavation example

| $Ss$ [$m^{-1}$] | $k_s$ for soil [m/s] | $k_s$ for sheet pile [m/s] | $\lambda$ for moss layer [J/m.K.s] |
|---|---|---|---|
| $2.0\times10^{-2}$ | $1.16\times10^{-6}$ | $1.16\times10^{-9}$ | 0.1 |

The purpose of this example is to evaluate the temperature difference caused by water flow. This 2D example simulates an excavation process in a cold region as shown in Figure 6-11. In this example, due to the construction of a foundation, part of the original soil is removed and the top moss layer which is always considered as the protective layer for permafrost is also destroyed. The size of each layer is shown in the figure. For simplification, the same material parameters of the 1D example are used. Additional material parameters used in this example are listed in Table 6-4. At the right side of the top surface, a 15 cm moss layer is assumed. Here we use one-tenth of the soil thermal conductivity to represent the different thermal characteristic of the moss layer which has a slow heat transfer speed. In this example, a larger permeability of soil is adopted in order to include the obvious influence of the water flow. In order to observe the influence of water flow, a 15 cm thick waterproof sheet pile is installed at the boundary of the excavation. The thermal conductivity of this sheet pile is the same as the soil. The boundary conditions are set as impermeable and heat insulation for the bottom boundary. For the vertical and horizontal surface of excavation part, water flow is forbidden and temperature is fixed at 10 °C. The only outlet for water is the left boundary without heat flow, meanwhile water can flow in from the right boundary and no heat flux is allowed. The temperature of surface including the excavation surface is set at 10 °C and the initial temperature of this soil body is assumed as −1 °C (soil is in a frozen status). In real situation, the initial temperature profile is complicated and change with

depth. However, the purpose of this example is to justify the influence brought by water flow. A simplified temperature profile is adopted. There is no horizontal displacement at the side boundaries. The bottom is fixed from vertical displacement. Top surface is free for deformation. After 40 days, the temperature distribution without the waterproof sheet pile is shown in Figure 6-12. Then, the temperature distributions along the dashed line shown in Figure 6-11 are compared by Figure 6-13. From Figure 6-12 and Figure 6-13, we make the following observations: 1) The location of the 0 °C isotherm of the example without the waterproof sheet pile is about 60 cm under the excavation surface. 2) The comparison between the temperatures shows that after the sheet pile was installed at the boundary, the temperature is higher than without the sheet pile. Further, the difference only appears in the top 60 cm, which agrees with the 0 °C isotherm. This phenomenon indicates that during thawing process, water flows from the cold area and lowers the temperature. 3) At the right side of this model, the isotherm is much shallower which indicates a low temperature. This is caused by the surface moss layer, which effectively slows the heat transfer process.

### 6.3.4 Sewage Tank Example

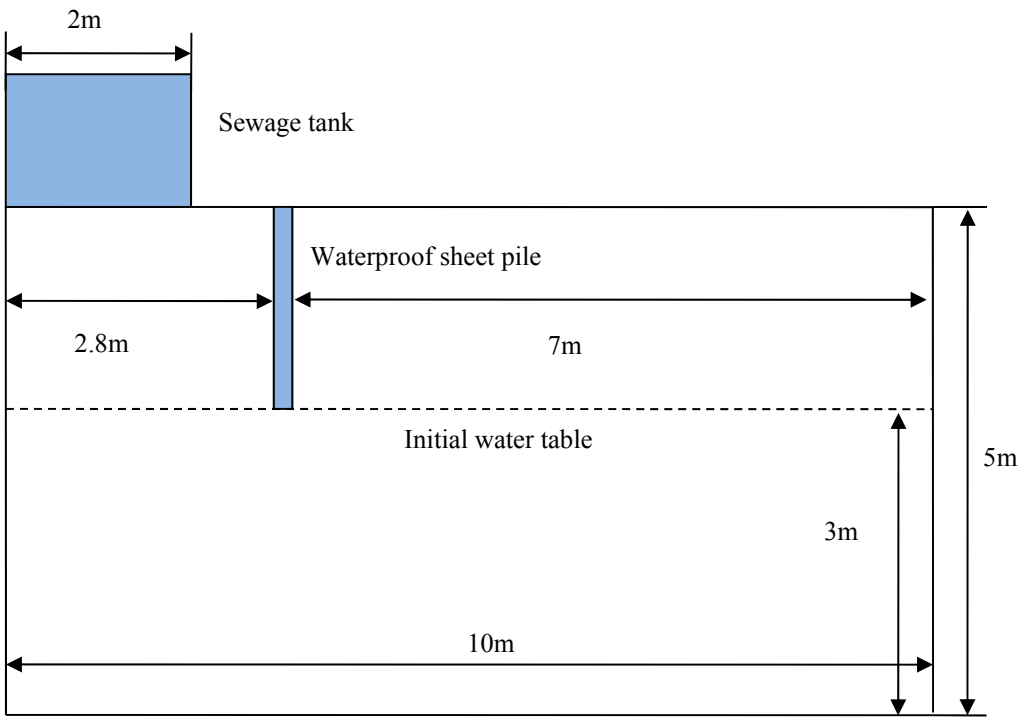



Figure 6-14 Diagram of 2D sewage tank example

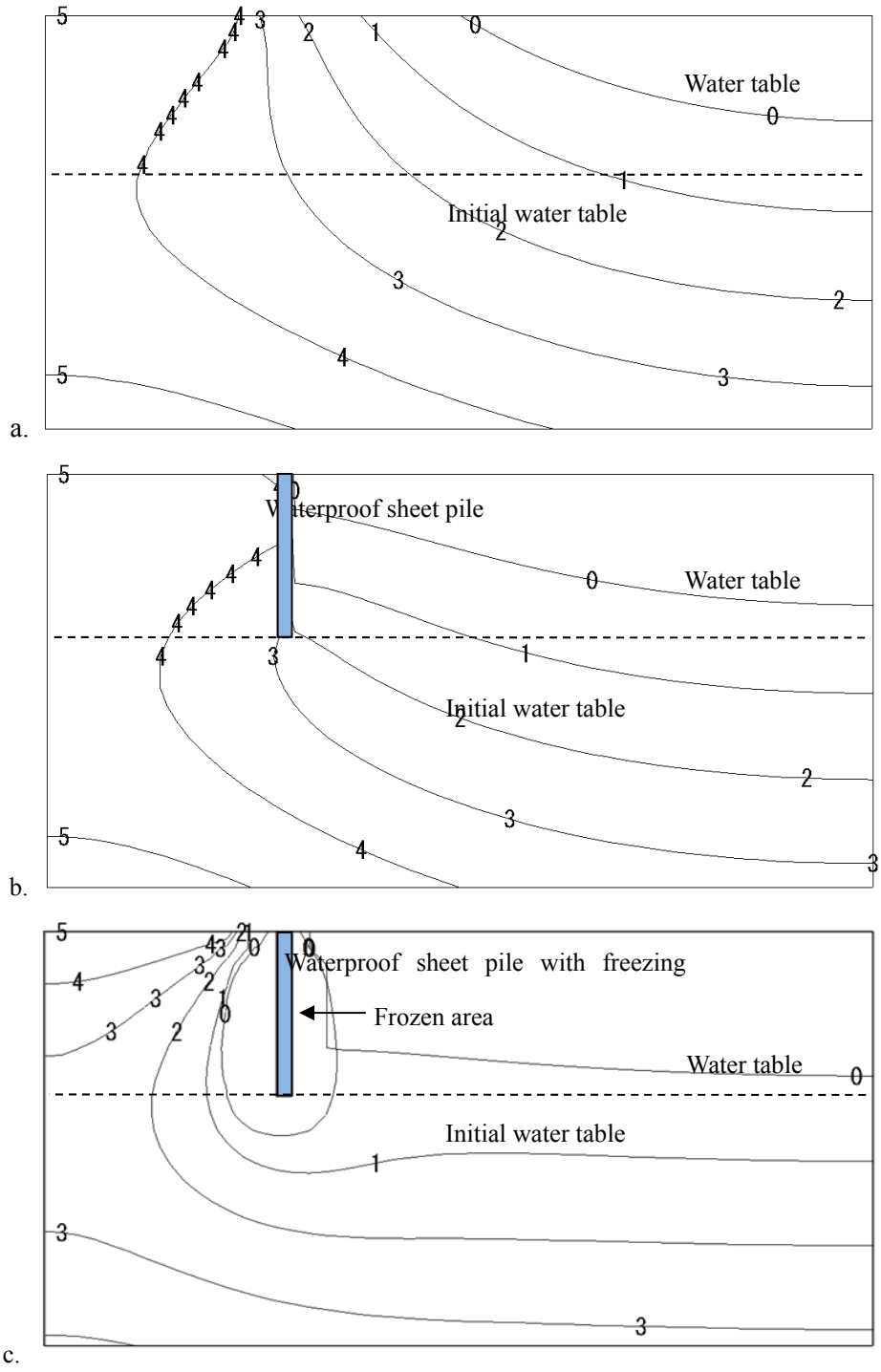



Figure 6-15 Calculation results after 20 days. a) Pore water pressure head for case 1; b) Pore water pressure head for case 2; c) Pore water pressure head and frozen area for case 3.

Table 6-5 Additional material parameters for sewage tank example

| $Ss$ [$m^{-1}$] | $k_s$ for soil [m/s] | $k_s$ for sheet pile [m/s] |
|---|---|---|
| $2.0\times10^{-2}$ | $1.16\times10^{-7}$ | $1.16\times10^{-9}$ |

We present another 2D model, shown in Figure 6-14, in order to discuss the relationship between freezing temperature and water head. The size of this model is 10 m × 5 m. At the left surface there is a sewage tank with a leak at the bottom and sewage flowing into the ground (the water head at the bottom of the tank is kept constant at 10 m for simplification). The temperature of the ground surface including the bottom of sewage tank is set at 10 °C. Additional material parameters are shown in Table 6-5. The other parameters are the same as the first example. For the left and right boundaries, no horizontal displacement is allowed. And the vertical displacement is forbidden at the bottom. The top surface is totally free. Regarding to the left, bottom and right boundaries, they are watertight and thermal insulation. The initial temperature of this example is set as 1 °C which means the soil is unfrozen and water can flow freely. And the initial water table is 3 m from the bottom. We apply three different conditions for this model and then compare the results, water table and frozen area after 20 days. Case 1: Nothing is done (control group), just let sewage leak into the ground. Case 2: Insert a waterproof sheet pile that has a very small hydraulic conductivity to prevent the sewage from polluting the underground water, but having the same thermal conductivity as the soil. Case 3: The same waterproof sheet pile is used as in Case 2, but we install a freezing unit inside the sheet pile which provides a −8 °C to freeze the surrounding soil. After 20 days, we check the water table location and frozen area. If the location of water table has not changed, we consider that the polluted water is blocked and controlled. The results are shown in Figure 6-15. We find that, compared to Case 1 and Case 2, Case 3 has the best efforts of impeding the sewage. The freezing sheet pile successfully freezes the surrounding soil and blocks the polluted water from the water tank. The water table in the unfrozen part is not increased a lot. Case 2 also has obvious effects of reducing the water flow compared to Case 1. However, Case 2 does not perform as well as Case 3 which a freezing temperature is applied inside the waterproof sheet pile. In Case 3, before application, if careful design and calculation are carried out, an optimal solution could be obtained that would suggest the best location and freezing temperature for the freezing sheet pile to reduce the damage of frost heave and enhance the effects of stopping the water flow from the tank.

These 2D models are not aimed to describe a perfect solution for a practical engineering project, but rather to prove that our model can effectively address the complicated thermal–hydraulic–mechanical situation in the real world. Thus, examples and parameters used in this paper are assumed, just intending to demonstrate the promising application filed for this thermal-hydraulic-mechanical model.

## 7. CONCLUSIONS

In this research, numerous frost heave models are discussed. The basic mechanism of frost heave is introduced. Then based on the comparisons and considerations, Takashi's equation is adopted to predict frost heave ratio. Further, this one-dimensional experiment based equation is expanded into two-dimensional problem by an anisotropic parameter. For the parameters used in Takashi's equation, thermal and mechanical analyses are necessary. In this research, the latent heat is included by the equivalent heat capacity method for an accurate result of temperature distribution. Concerning the mechanical analysis of soil, we adopt the Duncan-Chang model to express the relationship between stress and strain for unfrozen soil. For frozen soil, a simplified assumption is used. We assume a constant value for Young's modulus of frozen soil and do not change with temperature. In fact, a temperature dependent relationship is easy to complete in our numerical model, however, the accurate relationship between temperature and Young's module is unclear. Therefore, a simplified assumption may be a better solution. In addition, considering the fact that Takashi's equation including the water transfer process happened during freezing process, but it cannot evaluate the water flow for unfrozen situation. We introduce the hydraulic analysis in this model. In the hydraulic analysis part, we consider the pore water pressure and temperature dependent hydraulic conductivity. At the same time, the heat energy brought by flow water is taken into account. The water flow process during thawing situation is the foundation for the further estimation of thawing settlement.

In this model, the interactive relationships are seriously considered (Figure 7-1). Takashi's equation is the core of our model which is used to predict frost heave ratio. Thermal and mechanical analyses provide basic information for this estimation equation, and then hydraulic analysis is added to complete this model for unfrozen and unsaturated situation. The interactive influences between these factors are described as follows. Thermal analysis can affect hydraulic analysis and mechanical analysis: Freezing range affects the water flow and content. Temperature also affects the soil mechanical property, for example, frozen soil has a larger Young's modulus to represent the increased soil strength after frozen. Hydraulic analysis can influence the mechanical process too: We adopt the effective constraining stress in freezing direction for Takashi's equation. This effective stress equals total stress from mechanical analysis minus the pore water pressure obtained by hydraulic analysis. And the consolidation caused by the increase of effective stress is not considered. Moreover, hydraulic analysis impacts the thermal calculation: water content influences the latent heat during thermal analysis and finally will lead to different frost heave amount. These are the complicated interactive behaviors among these three aspects.

However, it is not the whole story. Takashi's equation is also included in such coupling process. Thermal analysis acts on the frost heave calculation through freezing rate. Frost heave amount will impact the stress analysis. On the contrary, stress will react to the frost heave calculation by Takashi's equation where small constraining stress will result in a larger frost heave ratio. All these interactions

are considered simultaneously in this model.

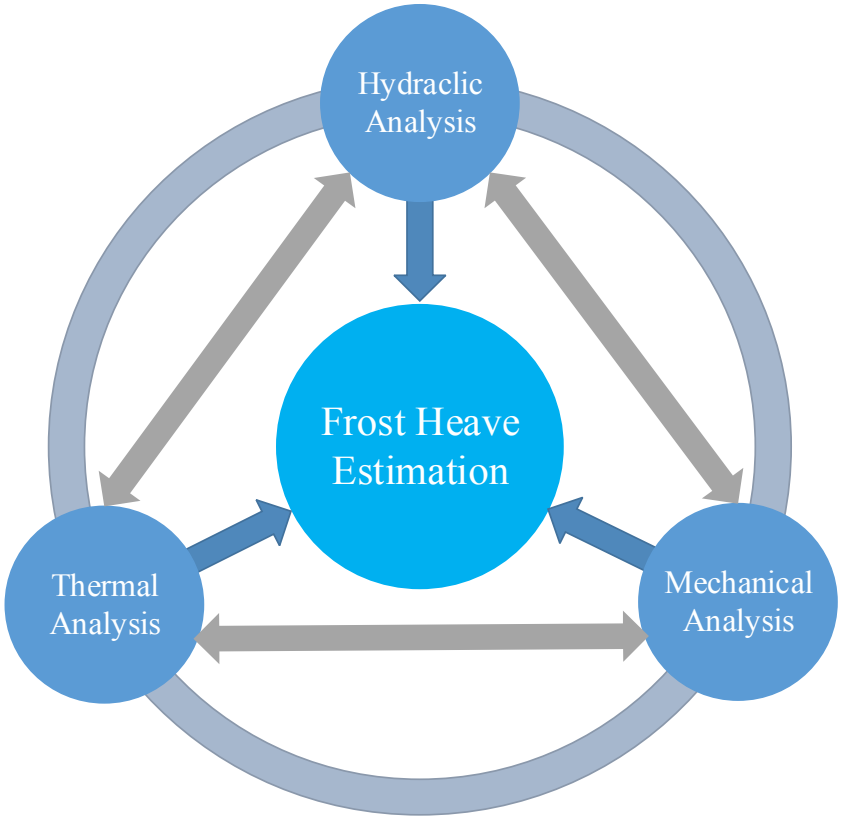



Figure 7-1 The interactive relationship inside the thermal-hydraulic-mechanical frost heave model

Including so many details, this numerical simulation model which combines thermal-hydraulic and mechanical analysis is built by this research. And through this numerical model, a lot of calculations and comparisons are made. By such analyses, the following conclusions could be obtained:

1. Although Takashi's equation is derived from one-dimensional indoor frost heave experiment, we can expand this equation into two-dimensional issues easily. The calculation results prove our assumption. With suitable anisotropic parameter, an accurate estimation of frost heave could be obtained. The suitable anisotropic parameter could be obtained from three-dimensional indoor frost heave test. However, if we want to expand this equation into three-dimensional situation with the same idea, it will become difficult. In the 3D situation, we can fix the freezing direction easily. But how to fix the direction perpendicular to the freezing direction and then project the frost heave ratio in these directions into the X, Y and Z coordinate axis, it is not so clear and we need more discussions and assumptions concerning this issue.

2. In our model, water head (or water content), frost depth, the amount of frost heave and even the stress could be evaluated. These are critical aspects for the design and safety evaluation of structures in cold regions. With adequate and accurate calibration of this model and parameters, we can apply it to practical engineering projects. We believe that the basic structure of the thermal–hydraulic–mechanical analysis model has been built in this paper and the model proves its promising ability to deal with complicated situations occurring in cold regions.
3. Hydraulic and thermal conditions are coupled and they influence each other significantly. Temperature and frost heave distribution predictions, after considering the coupling process, become sophisticated that a qualitative analysis based on common sense seems difficult. This point should be noted seriously in real engineering.
4. In our model, the temperature and stress-dependent Young's modulus is adopted, and the simulation result is compared to a 1D indoor experiment. The simulation results agree well with experimental results, which verify the reliability of our model. The expansion of Takashi's equation and the application of nonlinear properties are verified.
5. A simple 1D example is constructed to confirm the influence of the nonlinear model. The calculation results confirm that our nonlinear assumption is rigorously executed and that the linear model would result in an overestimated stress level.
6. The simulation results of both linear and nonlinear models are compared by using a 2D indoor experiment. The results indicate that the stress range for Takashi's equation should be obeyed and that accurate soil strength is necessary for precise simulation. Further research is necessary to enlarge the application field of Takashi's equation, particularly for the situation involving small constraining stress.
7. A concrete culvert example is given in this paper. In this example, the influence of nonlinearity is obvious for both the amount of frost heave and the stress distribution. This influence is caused by the changing Young's modulus. The results indicate that for the analysis of frost heave and related stress problems, nonlinear properties cannot be omitted if an accurate result is desired. The nonlinear model reduces the maximum values of stress and frost heave. Thus, careful calculation is necessary for this complicated engineering situation.
8. For the accurate simulation and analysis of nonlinear properties, much more attention should be given to the detailed relationships of temperature, stress, and soil strength. Only a precise understanding of nonlinear relationships can result in accurate estimation of stress and frost heave.

Future topics:

1. The most urgent topic is the three-dimensional indoor frost heave experiment. Only based on such experiment, accurate and widely applicable 3D frost heave estimation could be obtained. The new equation should consider the freezing rate and stress condition simultaneously. The difficulties of this 3D frost heave test is that how to control the stress and temperature condition accurately and

how to measure the displacement in each direction precisely. Our research group now is designing a new experiment system in order to achieve such a requirement. In future, based on numerous 3D frost heave experiment data, we can have a better prediction equation.

2. The nonlinear property of soil. For the unfrozen soil, the relationship between stress and strain is described by the classic Duncan-Chang equation. And a lot of researches and experiments have been done for unfrozen soil. However, concerning the frozen soil, the temperature and stress dependent Young's modulus is still unclear. Though, in some research, a temperature dependent Young's modulus is adopted. However, this kind of relationship is not demonstrated by widely experiment. And also the stress influence is not considered. We hope such a relationship could be obtained: temperature and stress condition are considered; could be applied for wide kinds of soil, and not so complicated.
3. The thawing settlement estimation. For this objective, there are two different directions. The first one is to estimate thawing settlement by water flow situation. This method estimates thawing settlement from the real reason itself. The ice becomes water and then flow out from the soil which will reduce the volume of soil sample. This idea is reasonable and viable because that in our model the water flow during unfrozen situation is already considered. The second idea is to build a practical equation to describe the thawing settlement relationship. In this situation, the thawing rate (if the thawing rate is too fast, extra water cannot drain out in time), boundary condition (close system or open system) and stress are critical parameters for this equation. This method will simplify the numerical model greatly and make this model easy for application.
4. The last point is about the latent heat calculation. In the existing model, we use equivalent heat capacity method to modify the temperature if we confirm that phase change occurs. However, by this method, if the time step is large, the accuracy will decrease. We need a more accurate method which can divide the time step into small size and then find the accurate where phase change happens. Then based on this temperature, recalculate the influence of latent heat. In fact, the research concerning this point has already starts.

In this paper, for the discussion of each factor, we control all other factors to be same and then discuss only one factor each time. In fact, our model owns the ability to analyze the comprehensive situation and discuss interactive influences simultaneously. However, there is no such comprehensive experiment that monitors so many parameters accurately at the same time. That means we do not have a good experiment example to compare with our numerical simulation. The accurate experiment technology concerning frost heave is desired and would play a critical role for further understanding of frost heave mechanism.

**REFERENCE:**


[1]. Society, T.J.G., *JGS 0171-2003*, in *Test Method for Frost Heave Prediction of Soils*. 2003. p. 6.

[2]. Black, P.B. and M.J. Hardenberg, *Historical Perspectives in Frost Heave Research. The Early Works of S. Taber and G.Beskow*. 1991. p. 167.

[3]. Taber, S., *The mechanics of frost heaving.* The Journal of Geology, 1930: p. 15.

[4]. S.Henry, K., *A Review of the Thermodynamics of Frost Heave*. 2000. p. 26.

[5]. Edlefsen, N.E. and A.B.C. Anderson., *Thermodynamics of Soil Moisture*. 1943.

[6]. Miyata, Y., *A Thermodynamic Study of Liquid Transportation in Freezing Porous Media.* JSME international journal. Series B, fluids and thermal engineering, 1998. **41**(3): p. 9.

[7]. Miyata, Y. and S. Akagawa, *An Experimental Study of Dynamic Solid-Liquid Phase Equilibrium in a Poroius Medium.* JSME international journal. Series B, fluids and thermal engineering, 1998. **41**(3): p. 11.

[8]. Kim, K., *Multi-Dimensional Frost Heave Modeling with SP Porosity Growth Function*, in *Civil and Environmental Engineering*. 2011, University of Alaska Fairbanks. p. 254.

[9]. Peppin, S.S.L. and R.W. Style, *The Physics of Frost Heave and Ice-Lens Growth.* Vadose Zone Journal, 2013. **12**(1): p. 35.

[10]. Williams, P.J., *Unfrozen Water Content of Frozen Soils and Soil Moisture Suction.* Géotechnique, 1964. **14**(3): p. 16.

[11]. Miller, R.D., *Freezing and Heaving of Saturated and Unsaturated Soils.* Highway Research Record, 1972. **393**.

[12]. Miller, R.D. *Frost heaving in non-colloidal soils*. in *In Proceedings of the 3rd International Conference on Permafrost*. 1978.

[13]. Konrad, J.M. and N.R. Morgenstern, *The Segregation Potential of a Freezing Soil.* Canadian Geotechnical Journal 1981. **18**(4): p. 10.

[14]. Konrad, J.M. and N.R. Morgenstern, *Frost Heave Prediction of Chilled Pipelines Buried in Unfrozen Soils.* Canadian Geotechnical Journal, 1984. **21**(1): p. 16.

[15]. Groenevelt, P.H. and C.D. Grant, *Heave and Heaving Pressure in Freezing Soils: A Unifying Theory.* Vadose Zone Journal, 2013. **12**(1): p. 11.

[16]. Takashi, T., et al., *Effect of Penetration Rate of Freezing and Confining Stress on the Frost Heave Ratio of Soil*, in *Permafrost, 3rd International Conference*. 1978. p. 6.

[17]. Takashi, T., et al., *Upper Limit of Heaving Pressure Derived by Pore-Water Pressure Measurements of Partially Frozen Soil.* Engineering Geology, 1981. **18**(1): p. 13.

[18]. 英夫, 高.勤.益.稔.山., *凍土に及ぼす未凍結土内の動水抵抗の影響（特に応力の小さい場合）*. 雪氷, 1976. **38**(1): p. 10.

[19]. Carlson, L.E., et al. *Field Test Results of Operating a Chilled, buried Pipeline in Unfrozen Ground*. in *Proceedings of the 4th Canadian Permafrost Conference*. 1982. Calgary, Alta.

[20]. Slusarchuk, W., et al. *Field Test Results of A Chilled Pipeline Buried in Unfrozen Ground*. in

*In: Proceedings. 3rd. International Conference Permafrost* 1978.

[21]. Northwest Alaskan Pipeline Company, I., *Performance Predictions for Fairbanks Frost Heave Test Facility*. 1980. p. 123.

[22]. Huang, S.L., et al., *Field Investigation of Soil Heave by a Large Diameter Chilled Gas Pipeline Experiment, Fairbanks, Alaska.* Journal of Cold Regions Engineering, 2004. **18**(1): p. 33.

[23]. Kim, K., W. Zhoub, and S.L. Huangc, *Frost Heave Predictions of Buried Chilled Gas Pipelines with the Effect of Permafrost.* Cold Regions Science and Technology, 2008. **53**(3): p. 15.

[24]. Kim, K., W. Zhou, and S.L. Huangc, *Frost Heave Predictions of Buried Chilled Gas Pipelines with Effect of Permafrost.* Cold Regions Science and Technology, 2008. **53**(3): p. 15.

[25]. Mu, S. and B. Ladanyi, *Modelling of Coupled Heat, Moisture and Stress Field in Freezing Soil.* Cold Regions Science and Technology, 1987. **14**(3): p. 10.

[26]. Ladanyi, B. and M. Shen. *Freezing Pressure Development on a Buried Chilled Pipeline*. in *Proceedings of 2nd International Symposium on Frost in Geotechnical Engineering*. 1993. Anchorage, AK.

[27]. Konrad, J.M. and M. Shen, *2-D Frost Action Modeling Using the Segregation Potential of Soil.* Cold Regions Science and Technology, 1996. **24**(3): p. 16.

[28]. Duncan, J.M. and C.Y. Chang, *Nonlinear Analysis of Stress and Strain in Soils.* Journal of Soil Mechanics and Foundations Division, 1963. **96**(SM5).

[29]. Guymon, G.L., T.V.H. II, and R.L. Berg, *Two-Dimensional Model of Coupled Heat and Moisture Transport in Frost-Heaving Soils.* Journal of energy resources technology, 1984. **106**(3): p. 8.

[30]. Guymon, G.L., R.L. Berg, and T.V. Hromadka., *Mathematical Model of Frost Heave and Thaw Settlement in Pavements*. 1993, COLD REGIONS RESEARCH AND ENGINEERING LAB HANOVER NH. p. 130.

[31]. Berg, R.L., G.L. Guymon, and T.C. Johnson, *Mathematical Model to Correlate Frost Heave of Pavements with Laboratory Predictions*. 1980, Cold Regions Research and Engineering Lab Hanover, NH.

[32]. Guymon, G.L., T.V.H. II, and R.L. Berg, *A One Dimensional Frost Heave Model Based upon Simulation of Simultaneous Heat and Water Flux.* Cold Regions Science and Technology, 1980. **3**(2-3): p. 10.

[33]. Kanie, S., et al. *Estimation Method of Frost Heaving for Chilled Gas Pipeline Buried in Frost Susceptible Soil*. in *Proceedings of 13th International Conference on Cold Regions Engineering*. 2006.

[34]. Kanie, S., et al. *A Practical Method for Three-Dimensional Frost Heave Simulation Based on Takashi's Equation*. in *Cold Regions Engineering 2012*. 2012. Quebec City, Canada.